3.4 Cooperative Phenomena in Complex Macroscopic Systems

Effects of cavitation on soundwaves

Yuta ASANO, Hiroshi WATANABE, and Hiroshi NOGUCHI

Institute for Materials Research, Tohoku University Katahira, Aoba-ku, Sendai, Miyagi 980-8577

Department of Applied Physics and Physico-Informatics,

Keio University, Hiyoshi, Kohoku-ku, Yokohama, Kanagawa 233-8522

Institute for Solid State Physics,

The University of Tokyo, Kashiwa-no-ha, Kashiwa, Chiba 277-8581

Cavitation is a flow phenomenon involving the formation of bubbles, caused by local pressure-drop in a liquid. Cavitation causes performance degradation, noise, vibration, and erosion in fluid machinery such as ship propellers and turbomachinery. On the other hand, the shock waves and localized high-temperature and -pressure fields generated by the bubble collapse are applied to a wide range of applications, including cleaning, processing, chemical reaction acceleration, and medicine. Therefore, it is vital to understand the cavitation mechanisms for many fields using liquid-gas multi-phase flows. In particular, understanding the effects of cavitation on sound waves is essential for the development of applied technology, such as the realization of highly efficient chemical reactors. However, cavitation is an extremely complex phenomenon in which a tremendous number of bubbles repeatedly generate, grow, split and coalesce, and disappear, making its analysis a challenging problem. Despite numerous experiments and numerical calculations, the mechanism remains thoroughly understood. In this project, we investigate the effect of phase transitions on sound waves by molecular dynamics (MD) simulations [1]. In particular, we clarify the differences in the effects of first- and second-order phase transitions on sound waves.

The fluids are modeled by a monoatomic molecule whose interaction is defined by the smoothed-cutoff Lennard-Jones potential. The system is a rectangular parallelepiped, and the periodic boundary conditions are applied to *y*- and *z*-directions. In *x*-direction, the oscillating and stationary walls are placed at both ends. The total number of particles is about 10 million. We investigate the differences in the waveform change by approaching the phase transition temperature for the liquid near the first-order transition region and supercritical fluid near the critical point. These waveforms are compared with the numerical solution of Burgers' equation.

In the first-order transition region, the waveform varies continuously until just above the phase transition point, in good agreement with the Burgers' equation. When the phase transition occurs, the waveform changes discontinuously due to the appearance of the gas phase, and the Burgers' equation is not applicable. On the other hand, in the continuous transition region, no discontinuous changes occur. Soundwave decay due to the density fluctuations are significant near the critical point. However, the Burgers' equation is applicable even for such large density fluctuations.

Finally, we investigated the bubble effects on the soundwaves by using 60 million particles. We observed a bubble generation and growth near the oscillating wall, movement in the soundwave propagation direction, and then disappearance. Bubbles repeat this long time (about 30-million-time steps) cycle. We found that the bubble motion affects the pressure wave.

The present computational scale could only treat the interaction between a single bubble and sound wave. The bubble generation causes a drastic change in soundwave, known as a change in sound speed, which is caused by the appearance of many bubbles. In order to reveal the peculiar phenomena, it is necessary to perform calculations for much larger systems.

References

[1] Y. Asano, H. Watanabe, and H. Noguchi, arXiv:2112.07139.

Coarse-Grained Molecular Dynamics Study of Biomolecular Assemblies and Nanocolloids

Wataru SHINODA

Research Institute for Interdisciplinary Science,

Okayama University, 3-1-1 Tsushima-naka, Kita-ku, Okayama 700-8530

We have extended the molecular library within the SPICA coarse-grained (CG) force field (FF), which was originally developed for lipids and surfactants. In this year, we have added a new class of lipids, proteins, and nucleic acids to the library. Especially, we improved the CG protein model to facilitate molecular dynamics (MD) simulation with a reproduction of multiple properties from both experiments and all-atom (AA) simulations.[1] The side chain analogs reproduced the transfer free energy profiles across the lipid membrane and showed reasonable association free energy (potential of mean force) in water compared to those from AA-MD. The CG-MD study of the adsorption or penetration of about 150 peptides/proteins into the membrane gave correct predictions of the penetration depth and inclination angle of peptides/proteins at the membrane periphery and transmembrane regions, consistent with the OPM (Orientation of protein in membrane) database. The dimerization free energies of some transmembrane helices in the lipid bilayer were found to be comparable to those obtained from experimental estimates. Application studies on a series of membrane protein assemblies, scramblases, and poliovirus capsids demonstrated the good performance of SPICA FF.

A series of MD simulations of Hepatitis B virus (HBV) capsid have also been carried out at AA and CG resolutions.[2] In this year, we have constructed a molecular model of the entire HBV virion particle including the envelope. The interaction between the membrane protein within the envelope and the capsid spike protein plays an important role in a strong anchoring of envelopes around the capsid. Due to a significant amount of membrane proteins in the envelope reduces the lipid diffusion within the envelope, which is supposed to help increasing the stability of virion particle.

We also analyzed the role of surfactants in the colloidal stability of nanoparticles in oil by CG-MD.[3] Again, SPICA FF was used to observe the molecular-level details of nanoparticle aggregation through simulation. A free energy pathway of aggregation is determined for different surfactant types and system configurations. The deformation of the

surfactant layer surrounding the nanoparticle was shown to be the major source of colloid stabilization. This is evidenced by the surprising result that as the packing density of the surfactants is reduced, the role of the surfactant is reversed from stabilizer to nucleation agent.

References

[1] S. Kawamoto, H. Liu, Y. Miyazaki, S. Seo, M. Dixit, R. DeVane, C. MacDarmaid, G. Fiorin, M. L. Klein, W. Shinoda: *J. Chem. Theory Comput.* DOI:10.1021/acs.jctc.1c01207.

[2] K. Fujimoto, Y. Yamaguchi, R. Urano, W. Shinoda, T. Ishikawa, K. Omagari, Y. Tanaka, A. Nakagawa, S. Okazaki: *J. Chem. Phys.* **155** (2021) 145101.

[3] M. Griffiths and W. Shinoda: *J. Phys. Chem. B* **125** (2021) 6315. [cover title]

Finite temperature properties of generalized Kitaev models

Tsuyoshi OKUBO
Institute for Physics of Intelligence, The University of Tokyo
7-3-1 Hongo, Bunkyo-ku, Tokyo 133-0033

The Kitaev model on the honeycomb lattice has been widely investigated as a fundamental model to investigate the nature of the quantum spin liquid in two dimension[1, 2]. In the Kitaev model, the interactions are Ising type, $S_i^\gamma S_j^\gamma$, and the spin component $\gamma = x, y, z$ is determined from the direction to the neighboring site. The ground state is known to be a gapless spin liquid state, in which the nature is described by Majorana fermions[1]. When we apply a magnetic field to the Kitaev system, the excitation spectrum described by the mobile Majorana fermions opens a gap, and the ground state changes to a topological spin liquid, where a half-integer thermal Hall conductivity emerges in the low-temperature limit [1]. In the recent experiment on α-$RuCl_3$ under a moderate magnetic field, a similar half-integer thermal Hall conductivity was observed at a finite temperature [3], although its ground state seems to be a magnetically ordered state at zero magnetic field due to off-diagonal and (long-range) Heisenberg interactions.

In this year's project, we investigated a finite temperature properties of the Kitaev model with off-diagonal interactions, in paticular concerning the possible thermal Hall conductivity at a finite temperature. The model Hamiltonian is given as

$$\mathcal{H} = \sum_{\gamma \in x,y,z} \mathcal{H}_\gamma - \vec{h} \cdot \sum_i \vec{S}_i, \qquad (1)$$

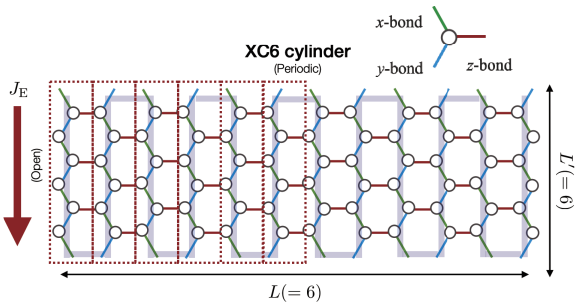

Figure 1: A typical lattice setup and a mappting to a one-dimensional matrix product operator.

where for $\gamma = z$,

$$\mathcal{H}_z = \sum_{\langle i,j \rangle_z} [K S_i^z S_j^z + \Gamma(S_i^x S_j^y + S_i^y S_j^x) + \Gamma'(S_i^z(S_j^x + S_j^y) + (S_i^x + S_i^y)S_j^z)]. \qquad (2)$$

In the cases of $\gamma = x, y$, we consider similar interactions with cyclic rotation of x, y, z components. To numerically calculate the thermal Hall conductivities at a finite temperature, we consider several finite-size clusters with open edges and represent their density matrix as a matrix product operator (MPO), as shown in Fig. 1.

The MPO representing a density matrix at a given temperature was obtained by the exponential tensor renormalization grope (XTRG) algorith [4], where we calculate the density matrix at an inverse temperature β, $\rho(\beta)$, through the relationship $\rho(\beta) = \rho(\beta/2)\rho(\beta/2)$ with the initial condition $\rho(\beta_0) = \exp(-\beta_0 \mathcal{H}) \simeq 1 - \beta_0 \mathcal{H}$

for the sufficiently small β_0. Thus, when we have an MPO representation of the Hamiltonian, a stadard compression algorithm for the tensor network can be used. When the bond dimension of the MPO is D, both of the computation cost and the memory consumption of XTRG algorithm scale $O(D^4)$.

By such an MPO representation of the density matrix, we have successfully calculated the thermal Hall conductivity for various magnetic fields and temperatures up to $N = 72$ spins (see Fig. 1) with a typical bond-dimension $D = 500$. Our calculation showed that the thermal Hall conductivity typically has a peak as a function of the temperature, and it overshoots the half quantized value expected in the zero-temperature limit. Such an overshooting is consistent with the experimental observation [3].

We also investigated Γ and Γ' dependence of the thermal Hall conductivity. We found that depending on the sign of Γ and Γ', the thermal Hall conductivity is largely modified from that of the pure Kitaev model. Some of them could be explained by the increase of the gap, previously calculated through the perturbation theory [5], while overall finite temperature behaviors might not be explained only by Majorana fermion pictures.

A part of this work has been done in collaboration with J. Nasu, T. Misawa, and Y. Motome.

References

[1] A. Kitaev, Ann. Phys. **321** (2006) 2.

[2] Y. Motome and J. Nasu, J. Phys. Soc. Jpn. **89** (2020) 012002.

[3] Y. Kasahara, T. Ohnishi, Y. Mizukami, *et al.*, Nature **559** (2018) 227.

[4] H. Li, D.-W. Qu, H.-K. Zhang, *et al.* Phys. Rev. Research **2** (2020) 043015.

[5] D. Takikawa and S. Fujimoto, Phys. Rev. B **102** (2019) 174414.

Membrane shape deformation by binding of curvature-inducing proteins

Hiroshi NOGUCHI
Institute for Solid State Physics, University of Tokyo

In living cells, biomembrane shapes are controlled by curvature-inducing proteins. We have studied the binding of these proteins using mean-field theories and compared their results with simulation results. Clathrin and coat protein complexes bend membranes in a laterally isotropic manner and generate spherical buds. In contrast, Bin/Amphiphysin/Rvs (BAR) superfamily proteins bend the membrane anisotropically and generate cylindrical membrane tubes. The former and latter proteins can be modeled as laterally isotropic objects and anisotropic objects of a banana or crescent shape, respectively.

For isotropic proteins, we derived the free energy including the Gaussian curvature and area expansion by the protein insertion [1]. Then, we investigated the formation of spherical buds [1] and binding onto a tethered vesicle [2]. A narrow membrane tube (tether) is elongated from a spherical vesicle by an external force imposed by a micropipette and optical tweezers. A first-order transition occurs between a small number of large buds and a large number of small buds with increasing chemical potential of protein binding [1]. For the tethered vesicle, interestingly, a first-order transition occurs twice between low and high protein densities in the tube. The force-dependence curves of the protein density in the membrane tube and the tube curvature are reflection symmetric and point symmetric, respectively, from the force point, in which the tube curvature matches the protein (sensing) curvature [2]. This theory reproduces the meshless membrane simulation results of the homogeneous phases very well. In addition, beaded-necklace-like tubes with microphase separation are formed in the simulation.

For anisotropic proteins, an orientational-dependent excluded volume interaction is included in the free energy. We studied binding onto membrane tubes [3]. The proteins exhibit a second-order or first-order nematic transition with increasing protein density for intermediate and small radii of the membrane tube, respectively. The tube curvatures for the maximum protein binding (sensing) and orientational order are differently varied by the protein density and rigidity. As the external force along with the tube axis increases, a first-order transition from a large tube radius with low protein density to a small radius with high density occurs once, and subsequently, the protein orientation tilts to the tube-axis direction. The density-dependent sensing curvature and the number of transitions are characteristics due to the anisotropic bending energy. Each isotropic protein has a constant sensing curvature. This density-dependent sensing curvature has been measured in the experiment of BAR proteins. This theory quantitatively reproduces the results of meshless membrane simulation for short proteins. For long proteins, the formation of protein clusters generates a quantitative deviation from the theory, although qualitative agreements still hold.

References

[1] H. Noguchi, *Phys. Rev. E* **104**, 014410 (2021).

[2] H. Noguchi, *Soft Matter* **17**, 10469 (2021).

[3] H. Noguchi, C. Tozzi, and M. Arroyo, *Soft Matter* (2022) DOI:10.1039/D2SM00274D.

Development of Thermal Functional Materials Based on First-principles Simulations

Junichiro SHIOMI

Department of Mechanical Engineering,

The University of Tokyo, Hongo 7-3-1, Bunkyo-ku, Tokyo 113-8656, Japan

We have studied thermal functional materials using massive parallel computer system. This year, we focused on the thermoelectric performance of a ternary alloy system and a nanostructured multiphase material.

The main content of these two studies is briefly introduced as below. For the ternary alloys, lattice structures were predicted by Monte Carlo simulation, then thermoelectric properties and the compositional dependence of ternary alloys were studied by first-principle calculation. Fig. 1 shows the predicted energy by cluster expansion and ZT of alloy of a composition. For the multiphase material, the grain size dependence of thermoelectric properties was studied by first-principle calculation for two phases to enhance thermoelectric performance by nanostructure engineering. Fig. 2 shows the nanostructured

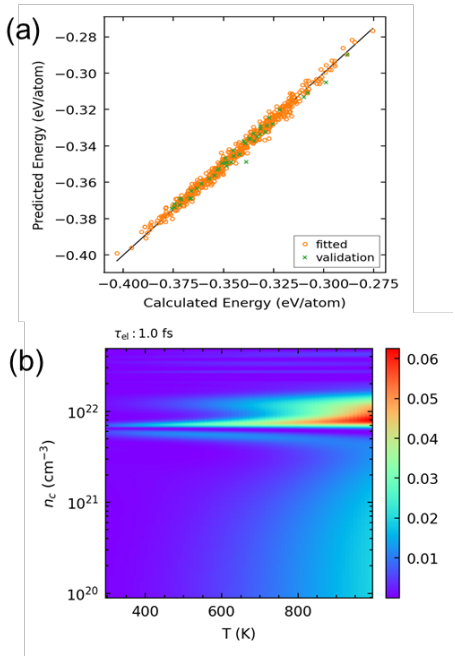

Fig. 1: (a) Formation energies from cluster expansion; (b) ZT of one of the alloys.

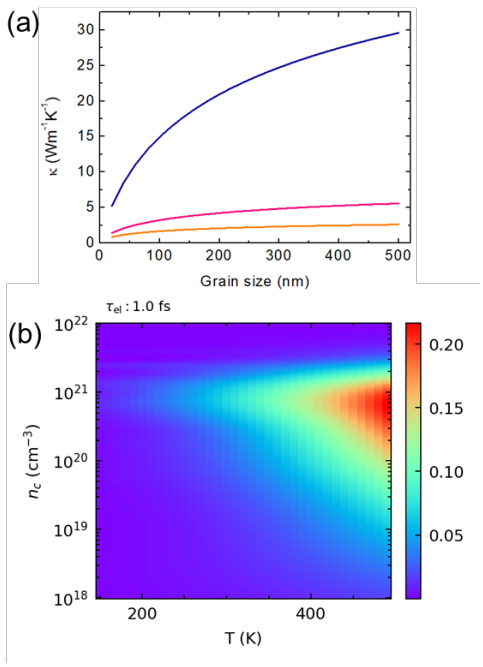

Fig. 2: (a) Thermal conductivity versus grain size; (b) ZT of a nanostructured material.

thermal conductivity at room temperature and ZT of a nanostructured phase.

To conduct these studies, the usage of supercomputer system was described as following. ICET package [1] was employed to predict lattice structures through performing Monte Carlo simulation and cluster expansion based on element substitution and formation energy prediction. BoltzTrap2 package [2] was carried out to calculate electrical transport properties by solving semiclassical linearized Boltzmann transport equation. ALAMODE package [3] was used to fit interatomic force constants by atomic displacements and forces from first-principle calculation, as well as calculate phonon thermal conductivity by relaxation time approximation method. VASP [4] was carried out to perform first-principle calculation for formation energy, band structure and atomic forces. By running our own python script, thermoelectric properties were calculated from phonon thermal conductivity and electrical properties.

References

[1] M. Ångqvist, W. A. Muñoz, J. M. Rahm, E. Fransson, C. Durniak, P. Rozyczko, T. H. Rod, and P. Erhart: Adv. Theor. Simul. 2 (2019) 1900015.

[2] G. K. H. Madsen, J. Carrete, and M. J. Verstraete: Comput. Phys. Commun. 231 (2018) 140.

[3] T. Tadano, Y. Gohda, and S. Tsuneyuki: J. Phys.-Condens. Mat. 26 (2014) 225402.

[4] G. Kresse and J. Furthmüller: Comp. Mater. Sci. 6 (1996) 15.

Feasibility study of Kitaev quantum spin liquid by functional renormalization approach

Kiyu FUKUI and Yusuke KATO
Department of Applied Physics, University of Tokyo, Bunkyo, Tokyo 113-8656
Department of Basic Science, University of Tokyo, Meguro, Tokyo 153-8902

The Kitaev model is an $S = 1/2$ quantum spin model defined on the honeycomb lattice [1]. In spite of its strong frustration due to the bond-dependent interaction, this model is exactly solvable, and its ground state is a quantum spin liquid state. Here we address the feasibility of the Kitaev quantum spin liquid (KQSL) for two extensions of the model, by using the pseudofermion functional renormalization group (PFFRG) method [2].

The first one is for ultracold polar molecules trapped in an optical lattice. While experimentally accessible implementation of the Kitaev-type interaction was proposed in 2013 [3], the stability of the KQSL has not been investigated so far. In this proposal, the bond-dependent anisotropic interactions are mimicked by angle-dependent dipole interactions between molecules. However, the interactions are long ranged with a spatial decay of r^{-3}, where r is the distance between the molecules, it is left as an open question whether the KQSL can survive against such long-range interactions. We studied the ground state of a quantum spin model with long-range angle-dependent Kitaev-type interactions, which was proposed as an implementation of the Kitaev model in ultracold polar molecules, by using the PFFRG method. We clarified that, regardless of the spatial anisotropy of the interactions, the ground state is magnetically ordered in both FM and AFM cases: we found magnetic instabilities toward the FM and zigzag ordered states in the FM and AFM models, respectively. By calculation of the anisotropy parameter dependence of the critical cutoff scale, we concluded that the system is most frustrated and closest to the realization of the KQSL when the interaction is isotropic in both cases. Our findings indicate that the QSL ground state arising from the nearest-neighbor bond-dependent anisotropic interactions in the Kitaev model is destroyed by the long-range interactions. By varying the range of the interactions, we unraveled that the KQSL is unstable even for the third-neighbor interactions. This is the first time that the stability of the KQSL within the above proposal has been revealed.

The other is the extension to higher-spin systems. Although the Kitaev model was originally introduced for the $S = 1/2$ moments, its higher-spin generalization has also attracted attention. While candidate materials with $S = 1$ [4] and $3/2$ [5] have begun to be proposed in recent years, the stability of the KQSL has not been systematically clarified for general spin S in the presence of non-Kitaev interactions, which are inevitably present in the candidate materials. In this study, we present our numerical results on the ground state of higher-spin generalization of the Kitaev model including the Heisenberg interaction, the spin-S Kitaev-Heisenberg model, which we consider to be one of the minimal models for the higher-spin candidate materials, by using an extension of the PFFRG method [6]. Performing the calculations for the models with $S = 1$, $3/2$, 2, $5/2$, and 50 in addition to $S = 1/2$, we elucidate

the ground-state phase diagram by systematically changing the ratio between the Kitaev and Heisenberg interactions and S. We found four magnetically ordered phases: Néel AFM, zigzag AFM, FM, and stripy AFM for all S, and the phase boundaries between these ordered phases are consistent with the previous studies for $S = 1/2$, 1, and ∞. Our results indicated that the ground state is short-range QSL for arbitrary S at the ferromagnetic and antiferromagnetic Kitaev points. It is consistent with an analytical result in the previous study [7]. We clarified that the QSL regions near these Kitaev points are quickly shrunk by increasing S, namely, the KQSL is fragile against the Heisenberg interaction for $S \geq 2$. However, we find the KQSL remains stable for $S \leq 3/2$ around the both Kitaev points. Our findings will provide the search and design of the candidate materials with $S > 1/2$.

References

[1] A. Kitaev, Ann. Phys. **321**, 2 (2006).

[2] J. Reuther and P. Wölfle, Phys. Rev. B **81**, 144410 (2010).

[3] S. R. Manmana *et al.*, Phys. Rev. B **87**, 081106 (2013); A. V. Gorshkov, K. R. Hazzard, and A. M. Rey, Mol. Phys. **111**, 1908 (2013).

[4] P. P. Stavropoulos, D. Pereira, and H.-Y. Kee, Phys. Rev. Lett. **123**, 037203 (2019); A. M. Samarakoon *et al.*, Phys. Rev. B **104**, 184415 (2021).

[5] C. Xu *et al.*, npj Comput. Mater. **4**, 57 (2018); M. Kim *et al.*, Nat. Electron. **2**, 457 (2019); I. Lee *et al.*, Phys. Rev. Lett. **124**, 017201 (2020); C. Xu *et al.*, *ibidem*, 087205 (2020).

[6] M. L. Baez and J. Reuther, Phys. Rev. B **96**, 045144 (2017).

[7] G. Baskaran, D. Sen, and R. Shankar, Phys. Rev. B **78**, 115116 (2008).

Quantum effects on chiral magnets

SOHEI KODAMA and YUSUKE KATO

Department of Basic Science, the University of Tokyo, Tokyo 153-8902, Japan,

We consider the ground state of quantum spin chain of monoaxial chiral ferromagnet. The Hamiltonian is given by

$$H = \sum_i \left[-J\hat{\boldsymbol{S}}_i \cdot \hat{\boldsymbol{S}}_{i+1} - D\left(\hat{\boldsymbol{S}}_i \times \hat{\boldsymbol{S}}_{i+1}\right)_y - H\hat{S}_i^z + K\left(\hat{S}_i^y\right)^2 \right],$$

where, J, D, H, and K, respectively, denote exchange interaction, Dzyaloshinskii-Moriya (DM) interaction, the magnetic field perpendicular to the chiral axis (y -axis) and single ion anisotropy.

The magnetization curves for finite-sized systems obtained by *exact diagonalization* are distinctly different between half-odd-integer and integer spins; The level crossings occur for S=1/2,3/2, accompanied by π shift of the crystal momentum k while the magnetization process is continuous and k is always zero for S=1,2. These behaviors are commonly observed for arbitrary values of J/D. We argue that in the limit J=0 with D finite, single soliton has the minimum energy for k=π (k=0) for half-odd integer (integer) S, based on the Perron-Frobenius theorem within the subspace spanned by a single soliton basis. Our approach [1] is complementary to earlier studies on quantum effects on Ising domain wall [2] and skyrmions [3] based on semiclassical treatment of quantum spin taking account of the Berry phase term.

References

[1] S. Kodama, A. Tanaka, and Y. Kato, in preparation.

[2] H. B. Braun, Adv. Phys. **61**, 1 (2012).

[3] R. Takashima, H. Ishizuka, and L. Balents, Phys. Rev. B **94**, 134415 (2016).

New scaling analysis for graph percolations

Y. Ozeki and K. Hagiwara v

Graduate School of Informatics and Engineering, The University of Electro-Communications

We investigate the transition point and the critical exponent β for graph percolations. A new size-independent scaling analysis is proposed, which enables us to analyze numerical data without finite-size effects. This means that the results are equivalent to those in the infinite system. Such a scaling analysis has been applied as dynamical scaling analysis in the nonequilibrium relaxation method [1] for phase transitions and critical phenomena.

In graph percolations, a number of vertices are prepared instead of a lattice. Each edge between two of these vertices is considered to be connected or not. In the Erdős-Rényi (ER) model, a classical graph percolation, a new edge is connected to a graph at random. The probability of a vertex belonging to the infinite cluster, which is denoted by $P(r)$, is recognized as the order parameter, where r is the average number of edges per vertex. The function $P(r)$ can be written as [2]

$$P(r) \equiv 1 - \sum_s s n_s, \tag{1}$$

where n_s is the number of clusters with size s divided by N. $P(r)$ is expected to behave algebraically as

$$P(r) = a|r - r_{\rm c}|^{\beta}, \tag{2}$$

where β is referred to as a critical exponent. In the present study, we define a new function $P(x, r)$ by extending $P(r)$,and introduce a new parameter x representing the maximum cluster size:

$$P(x, r) \equiv 1 - \sum_{s<x} s n_s. \tag{3}$$

This function $P(x, r)$ represents the probability that a randomly selected vertex belongs to a cluster greater than or equal to x. We expect the following asymptotic ($x \to \infty$) behaviors for every r case:

$$P(x, r) \sim \begin{cases} A \exp(-x/\xi) & (r < r_{\rm c}) \\ x^{-\lambda_P} & (r = r_{\rm c}) \\ p_\infty + A' \exp(-x/\xi) & (r > r_{\rm c}) \end{cases} \tag{4}$$

where we introduce a function ξ depending on r as $\xi = \xi(r)$ and exponent λ_P. The asymptotic behavior of ξ is expected to be

$$\xi(t) = b|r - r_{\rm c}|^{-\nu}, \tag{5}$$

where we define a new exponent ν satisfying the relation

$$\lambda_P = \beta/\nu. \tag{6}$$

In the asymptotic regime in $r \sim r_{\rm c}$, $P(x, r)$ is expected to satisfy the following scaling form:

$$P(x, r) = \xi^{-\lambda_P} \Psi(x/\xi). \tag{7}$$

The transition point $r_{\rm c}$ and critical exponent β can be estimated from the behavior of $P(x, t)$. Appropriate values of $r_{\rm c}$ and β as well as a, b, ν in Eqs. (2) and (5) should be chosen such that $\xi^{\lambda_P} P(x, t)$ is fitted as a function of $x/\xi(r)$ on a scaling function Ψ. In order to carry out such a scaling plot efficiently, we apply the method introduced for the dynamical scaling, in which the Bayesian inference and the kernel method are used [3].

Here, we demonstrate the above scaling analysis to the ER model, for which the analytic solution is known; $r_{\rm c} = 1/2, \beta = 1$. For precise analysis, we need to check the size dependence. We have found that, for $x \leq 3000$, no size dependence appears in the data for the system with $N = 1 \times 10^8$ or larger. The simulation is performed using these parameters, and 2240 independent samples were used for averaging. The results for $P(x, r)$ are plotted in Fig. 3, and the resultant scaling plot is shown in Fig. 4. The transition points and the critical exponent are evaluated as $r_{\rm c} = 0.49978(7)$ and $\beta = 1.010(9)$, respectively, where the error bars are estimated by the bootstrap method [3]. The deviations from the analytic values $r_{\rm c} = 1/2, \beta = 1$ are approximately 0.044% and 1.0%, respectively, demonstrating that the present analysis is reliable.

We apply the above scaling method to the dCDGM model [4], in which a vertex is selected from randomly chosen m vertices so that the size of the connected cluster is smallest and the new edge connects two vertices selected twice with the aforementioned process; the integer value m is fixed and distinguishes the model as the dCDGM(m) model. We investigate the dCDGM($m = 2$) model. The same analysis was performed. It is confirmed that the simulation for the system with $N = 1 \times 10^8$ to $x \leq 3000$ is sufficiently large. The simulation is performed using these parameters, and 4480 inde-

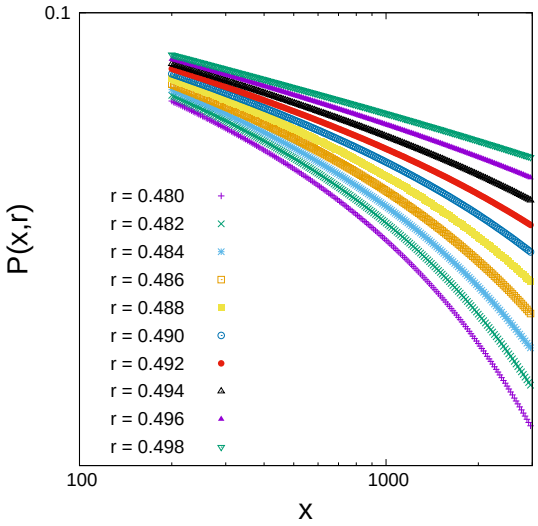

Figure 1: Results of $P(x, r)$ for the ER model.

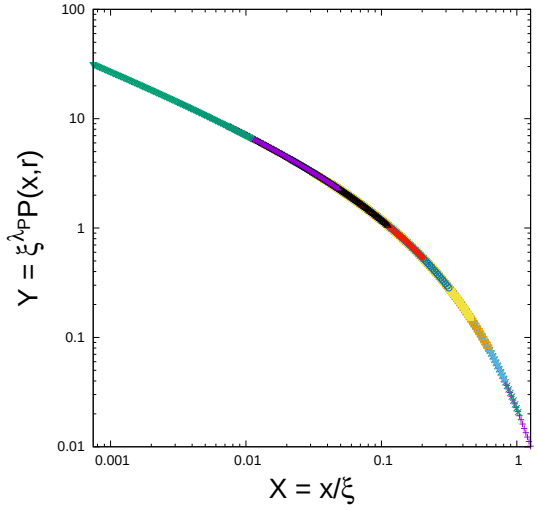

Figure 2: Scaling plot of $P(x, r)$ for the ER model.

pendent samples are used for averaging. The transition points and the critical exponent are evaluated as $r_c = 0.923211(5)$ and $\beta = 0.056(1)$, respectively, which are consistent with those of Da Costa ($r_c = 0.923207509297(2)$ and $\beta = 0.05557108(1)$) [4].

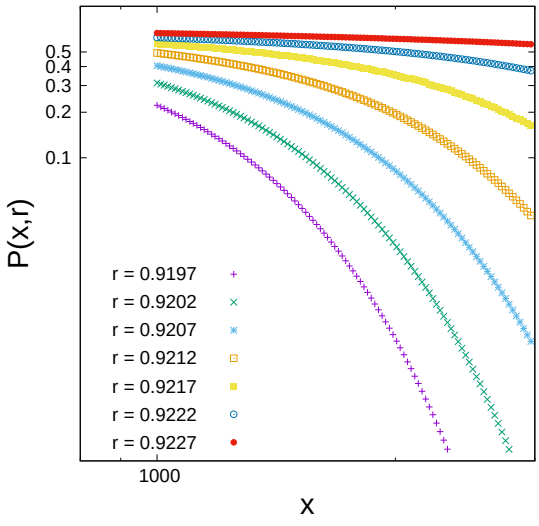

Figure 3: Results of $P(x, r)$ for the dCDGM(2) model.

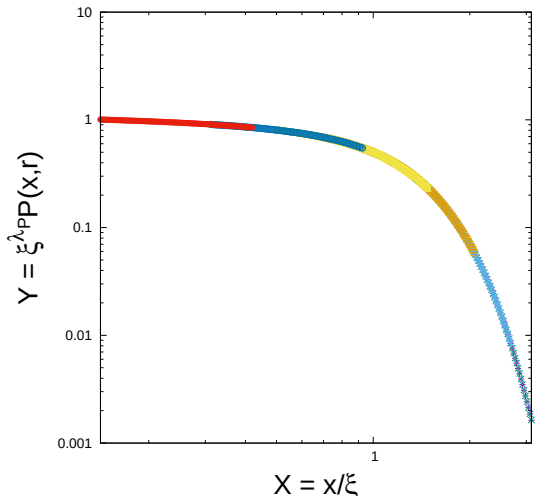

Figure 4: Scaling plot of $P(x, r)$ for the dCDGM(2) model.

References

[1] Y. Ozeki and N. Ito, *J. Phys.: Math. Theor.* **40** R149 (2007).

[2] D. Stauffer and A. Aharony, "Introduction to percolation theory", (Taylor & Francis,1994)

[3] Y. Echinaka and Y. Ozeki, *Phys. Rev.* E**94** 043312 (2016).

[4] R. A. Da Costa, S. N.Dorogovtsev, A. V. Goltsev, and J. F. F. Mendes, *Phys. Rev.* E**89** 042148 (2014); *Phys. Rev.* E**90** 022145 (2014).

Computational design of proteins useful for medical and industrial applications

Masataka YOSHIMURA[1], Sairi MATSUMOTO[1], Mizuki TERANISHI[1],
Hirotaro SHIMAMURA[2], Rina AOYAMA[1], Koji OOKA[2], Shino MASUOKA[1],
Shunji SUETAKA[1], Nao SATO[1], Yuuki HAYASHI[1], and Munehito ARAI[1,2]
[1]*Department of Life Sciences, Graduate School of Arts and Sciences, and*
[2]*Department of Physics, Graduate School of Science,*
The University of Tokyo, Komaba, Meguro, Tokyo 153-8902

Proteins have been widely used as therapeutics for various diseases and as enzymes for industrial production of useful substances. Recently, theoretical design of proteins has attracted much attention; however, it is still difficult to theoretically design useful proteins. To solve this problem, we have designed various useful proteins using the Rosetta 3.13 suite [1] and have experimentally checked the validity of the computational design.

Magnets are optogenetic tools for manipulating protein-protein interactions (PPIs) [2]. They consist of pMag and nMag, which heterodimerize upon exposure to blue light. However, improvement of their binding affinity has been demanded. Here we computationally designed the Magnets mutants with higher pMag/nMag affinity than the original ones by theoretical mutagenesis using Rosetta. Experiments confirmed that the mutants enhanced the dimer affinity. Thus, these Magnets mutants may be useful for *in vivo* manipulation of PPIs.

Severe acute respiratory syndrome (SARS) coronavirus 2 (SARS-CoV-2) is an emerging virus that causes the pandemic of the coronavirus disease 2019 (COVID-19). Since the viral infection is caused by the binding of the receptor binding domain (RBD) of the spike protein of SARS-CoV-2 to the human angiotensin-converting enzyme 2 (ACE2) [3], we computationally designed a single-chain variable fragment (scFv) of an antibody against the SARS-CoV-2 RBD using the scFv against the SARS-CoV RBD as a template. Experiments showed that the designed antibody has a high affinity to SARS-CoV-2 RBD comparable to that of the antibody medicines for SARS-CoV-2.

Formation of a ternary complex by interleukin-33 (IL-33), interleukin-1 receptor accessary protein (IL-1RAcP), and the ST2 receptor of type 2 innate lymphoid cells is responsible for allergic asthma [4]. To develop a therapeutic agent for the disease, we are trying to computationally design a protein that tightly binds ST2 but does not bind IL-1RAcP using IL-

33 as a template. We have finished designing a protein that tightly binds to ST2. Further design of the IL-33 mutant that abolishes the binding with IL-1RAcP is under way.

The interaction between the programmed cell death protein 1 (PD-1) and the programmed death-ligand 1 (PD-L1) is important in suppressing T-cell inflammatory activity [5]. To develop an inhibitor of the T-cell activity, we computationally designed the mutants of a PD-L1 fragment that tightly bind PD-1. Experiments confirmed that some mutants have improved affinity with PD-1. We are trying to further improve the affinity by multiple mutations.

Alkane biosynthesis has attracted much attention as a promising way of producing carbon-neutral bioenergy. A key enzyme for cyanobacterial alkane biosynthesis is aldehyde deformylating oxygenase (ADO) [6]. We computationally designed ~10 mutants of ADO that are expected to have high activity. The experimental test of the ADO activity is ongoing.

Understanding protein dynamics is essential for improving catalytic activity of enzymes. We performed molecular dynamics simulations of ADO using the Gromacs 2021.4 program package [7]. An initial structure was constructed using the AmberTools21 package. The force fields for the substrate (aldehyde) and the product (alkane) were obtained using Antechamber module. The simulations were performed for ~800 ns each for the apo form, holo (iron-bound) form, substrate-bound form, and product-bound form of ADO. We found that the product has higher flexibility than the substrate inside the protein molecule, thereby facilitating the product release.

Finally, to predict the folding processes of proteins, we calculated free energy landscapes of multi-domain proteins using the Wako-Saitô-Muñoz-Eaton model, which is an Ising-like, structure-based statistical mechanical model [8]. By introducing modifications to the model, we succeeded in obtaining the folding pathways and intermediates that are fully consistent with experimental results. Thus, our method may pave the way for solving the folding mechanisms of multi-domain proteins that are abundant in proteomes.

References

[1] J. K. Leman, et al.: Nat Methods, **17** (2020) 665-680.

[2] F. Kawano, et al.: Nat Commun. **6** (2015) 6256.

[3] J. Shang, et al.: Nature, **581** (2020) 221-224.

[4] X. Liu, et al.: Proc Natl Acad Sci USA. **110** (2013) 14918-14923.

[5] C. N. Bryan, et al.: Proc Natl Acad Sci USA. **118** (2021) e2102164118.

[6] M. Arai, et al.: Adv Exp Med Biol. **1080** (2018) 119-154.

[7] M. J. Abraham, et al.: SoftwareX, **1-2** (2015) 19-25.

[8] M. Sasai, et al.: Biophys Physicobiol. **13** (2016) 281-293.

Topological order and quantum operation in quantum many-body systems

Synge TODO
Department of Physics, University of Tokyo, Tokyo, 113-0033
Institute for Solid State Physics, University of Tokyo, Kashiwa, 277-8581

We developed novel numerical methods by combining quantum Monte Carlo methods, tensor-network algorithms, and other optimization techniques and investigated topological quantum phase transitions in strongly correlated many-body systems and optimization of quantum operations in quantum computing.

Phase transition in quantum dimer model: Based on the idea of stochastic series expansion, we implemented a Monte Carlo algorithm for investigating the phase transition of the quantum dimer model in an efficient way to simulate with shorter CPU time and extended it to simulation on larger Hilbert space, including monomer-dimer and monomer-monomer interaction. We obtained the phase-transition temperature between the critical and columnar phases by different order parameters by simulations at finite temperatures. We found it vanishes at around Rohksar-Kivelson (RK) point, while the classical limit merges smoothly to the value obtained by the classical Monte Carlo.

Tensor-network Markov-chain Monte Carlo: We developed a novel *quantum-inspired* method that combines the tensor-network representation of weight function and the sampling scheme based on the Markov-chain Monte Carlo method. We can remove the systematic bias due to the finiteness of the bond dimension in tensor network representation from the Markov-chain sampling. Furthermore, the statistical error of the sampling reduces exponentially as increasing bond dimension, and we can avoid the negative-sign problem in quantum lattice models by adopting a high-precision tensor network renormalization scheme.

Many-body localization in random spin chain: We study the many-body localization of the random-field Heisenberg chain using the nested shift-invert Lanczos method with an iterative linear solver. We use the minimum residual method (MINRES) inside each Lanczos iteration. As a probe of many-body localization transition, we propose a unitary operator called the twist operator, which has a straightforward interpretation in the real space. We estimate the transition point of the random-field Heisenberg chain precisely [1].

Decomposition of multi-qubit gate: We obtain efficient decompositions of CCZ and CCCZ gates, typical multi-qubit gates, under several qubit connectivities, using the sequential quantum-circuit optimization algorithm. We can construct the CCZ gate with only four CZ-depth when the qubit is square-shaped, including one auxiliary qubit. In T-shaped qubit connectivity, which has no closed loop, we can decompose the CCCZ gate with 17 CZ gates [2].

References

[1] T. Kutsuzawa and S. Todo, preprint: arXiv:2203.09732.

[2] K. M. Nakanishi, T. Satoh and S. Todo, preprint: arXiv:2109.13223.

O(N) algorithm for the Monte Carlo simulation of the Kitaev model

Masahiko G. YAMADA[1]
Yutaka AKAGI[2]
Masafumi UDAGAWA[3]
[1]*Department of Materials Engineering Science, Osaka University*
Machikaneyama-cho, Toyonaka, Osaka 560-8531
[2]*Department of Physics, University of Tokyo*
Hongo, Bunkyo-ku, Tokyo 113-0033
[3]*Department of Physics, Gakushuin University*
Mejiro, Toshima-ku, Tokyo 171-8588

The thermodynamics of the Kitaev model is of great interest, especially after the characteristic specific heat behavior called a double peak has been discovered by the Monte Carlo simulation [1].

We extend their simulation using a new $O(N)$ calculation method for the Kitaev model Monte Carlo [2]. We newly employed the infinite product expansion (iPE) method instead of the previous Trotter decomposition method. By this iPE method, we succeeded in reducing the calculation cost of the Kitaev model drastically from $O(N^4)$ to $O(N)$. As a benchmark, we did a simulation for the Kitaev model on the honeycomb lattice and computed the heat capacity and its double-peak structure. Using the new algorithm and a supermassive parallelization in the ISSP supercomputer, we succeeded in reproducing the results in [1] within the errorbar (see Fig. 1). Though currently the calculation is limited up to the 54-site cluster with an open boundary, we will eventually extend this to the large-scale Monte Carlo simulation up to $O(1000)$-site simulations. If we also extend the calculation to three dimensions, we can potentially discuss the thermodynamic properties of the vaporization transition in the three-dimensional Kitaev model, which was suggested in Ref. [1].

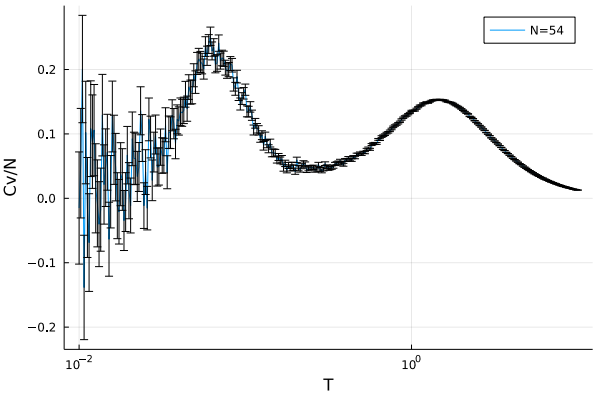

Figure 1: Specific heat data for the $N = 54$ cluster simulation.

References

[1] J. Nasu, M. Udagawa, and Y. Motome: Phys. Rev. Lett. **113** (2014) 197205.

[2] M. G. Yamada, Y. Akagi, and M. Udagawa: to appear.

DMRG algorithm with a full SU(N) implementation

Masahiko G. YAMADA
Department of Materials Engineering Science, Osaka University
Machikaneyama-cho, Toyonaka, Osaka 560-8531

The density matrix renormalization group (DMRG) is one of the most powerful numerical methods for strongly correlated condensed matter systems. Following the previous work, we extended DMRG to the case with the SU(N) symmetry with $N > 2$, even for two-dimensional systems. As a killer application, we simulated the ground state of the SU(4) Heisenberg model on the honeycomb lattice, which can potentially be realized in cold atomic systems and solid state systems like α-$ZrCl_3$ [2]. We keep up to 12800 SU(4) states equivalent to more than a million U(1) states. This supermassive DMRG simulation reveals the quantum spin-orbital liquid ground state, which has dubiously been expected for more than a decade. The methodology developed here can be extended to any classical Lie groups, paving the way to a next-generation DMRG with a full symmetry implementation [3].

References

[1] P. Nataf, and F. Mila: Phys. Rev. B **97** (2018) 134420.

[2] M. G. Yamada, M. Oshikawa, and G. Jackeli: Phys. Rev. Lett. **121** (2018) 097201.

[3] M. G. Yamada, K. Penc, and F. Pollmann: to appear.

Efficient Sampling Simulation of the Soft Modes Significantly Contribute to Protein Properties

K. TAKEMURA, D. TRAN, M.M. SOBEH, Y. MIYAZAWA, R. KIUCHI, T.N. WIJAYA, T. OGAWA, Y. TAIRA, R. MISU, R. Osawa, M. Yoshioka, H. NAKAYA and A. KITAO

School of Life Science and Technology, Tokyo Institute of Technology

Ookayama, Meguro, Tokyo 152-8550

Previously, we developed parallel cascade selection molecular dynamics (PaCS-MD) as an enhanced sampling strategy that uses cycles of multiple independent MD simulations done in parallel to improve the chance of biologically rare events occurring without external perturbation [1]. PaCS-MD consists of cycles of several independent parallel short all-atom MD simulations followed by selecting initial structures for the next cycle according to a specified quantity. We conducted the dissociation simulation of the p53 DNA binding domain (p53DNA) from DNA [2]. We used the inter-center of mass distance (inter-COM distance, d) between p53-DBD and DNA as a quantity for ranking the snapshots generated in each cycle. By repeating a series of cycles for the selected top-ranked snapshots (top 10 snapshots), dissociation PaCS-MD generates structures with larger inter-COM distances than those found in the previous cycle, which significantly enhances the probability of transitions from the bound to unbound states. Finally, we repeated the cycles until d = 70 Å to complete the dissociation, as we can see in the PaCS-MD flowchart in Fig. 1

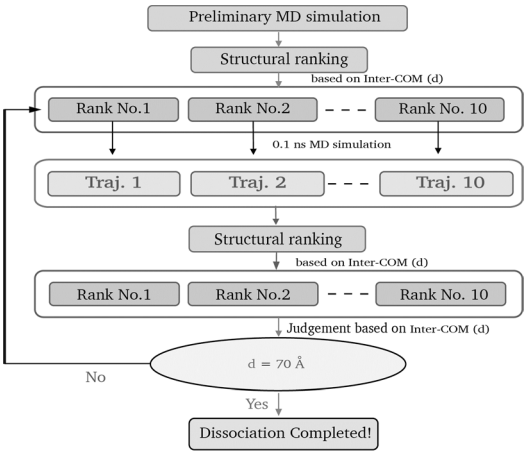

Fig. 1 The flowchart of PaCS-MD

We successfully generated 75 different dissociation pathways of p53-DBD from DNA. We used the COM positions of the p53-DBD interface residues relative to those of DNA to visualize the dissociation pathways, as shown in Fig. 2. Inspection of the dissociation pathways indicates that the

sampled space formed a cone-like shape around the DNA. Around 93% of the sampling pathways (70 pathways) dissociated along the +X and −Y directions (namely, the −Y directions), while the other pathways moved along +X and +Y directions, which only occupy 7% (5 pathways), hereafter called the +Y directions.

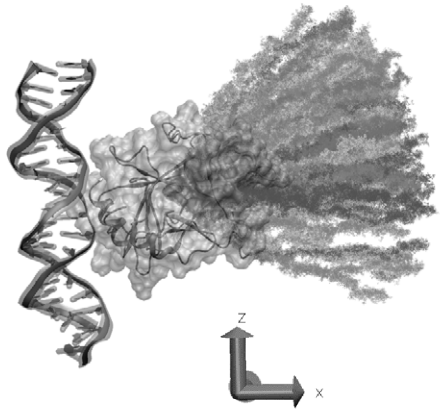

Fig. 2 Dissociation pathways of 75 PaCS-MD trials of p53-DBD from DNA.

Using the Markov state model (MSM), We obtained the free energy profile of p53-DBD dissociation from DNA and showed the projections onto the XY planes, as shown in Fig. 3. The global minimum of this profile represents the bound state. As discussed above, dissociation mainly (93%) occurred along the −Y directions on the XY-plane, and other dissociations (7%) occurred along the +Y directions. As we can see in Figure 4, during the dissociation process, the PMF increased at a higher rate in the bound state to achieve convergence (became flat) in the unbound region (d ≥ 45 Å). We calculated the binding free energy (ΔG°) for this system predicted at 11.8 kcal/ mol. This value is very close to the binding free energy of p53-DBD (residues 94−312) with the consensus DNA sequence of −11.1 kcal/ mol measured by isothermal titration calorimetry, suggesting that the calculated free energy profile is reasonable.

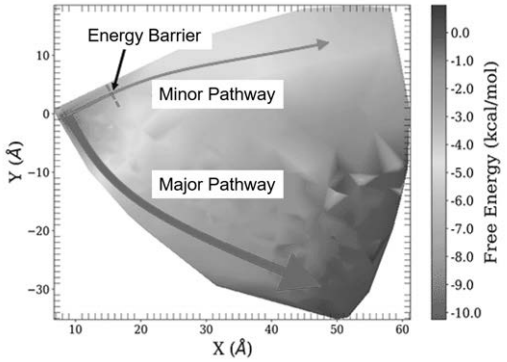

Fig. 3 Free energy profile mapped onto the XY-plane

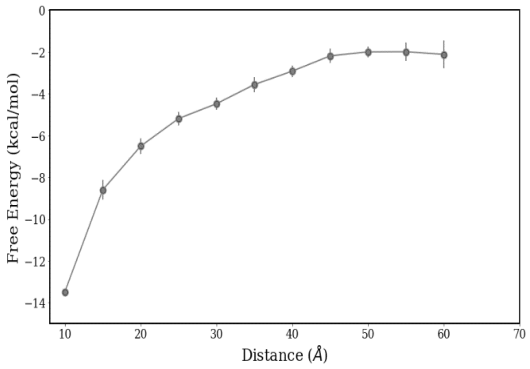

Fig.4 PMF as a function of X coordinate.

References

[1] R. Harada and A. Kitao. J Chem Phys 139, 035103 (2013).

[2] M.M. Sobeh and A. Kitao J. Chem. Inf. Model, 62, 1294–1307 (2022).

Molecular dynamics simulations for assembly and disassembly of protein aggregates

Hisashi Okumura

Exploratory Research Center on Life and Living Systems, Institute for Molecular Science, Okazaki, Aichi 444-8585

Proteins are normally folded correctly and perform functions that are necessary to sustain life. However, when the concentration of proteins increases due to aging or other reasons, they can aggregate and cause a variety of diseases. For example, Alzheimer's disease, which is one type of dementia, is caused by amyloid-β (Aβ) peptides, which aggregate into spherical oligomers or amyloid fibrils. Molecular dynamics (MD) is nowadays a standard tool to investigate these systems. However, once a conformation gets trapped in a local-minimum free-energy state, it is hard to escape from there within the time scale of the simulation.

The replica-exchange method (REM), is widely used to overcome this difficulty because of its convenience. Recently, we proposed the replica-permutation method (RPM) and the replica sub-permutation method (RSPM) to improve the transition ratio of replicas in the temperature space. However, the RPM and RSPM are not available for general users because these methods are implemented only in our own molecular simulation programs and not in open-source packages. We implemented the RPM and RSPM into LAMMPS [1]. LAMMPS is an open-source classical MD simulation package that can be applied from material to biomolecular systems. We used the supercomputer at the Supercomputer Center, the Institute for Solid State Physics, the University of Tokyo to perform benchmark calculations for this program.

In addition, continuing from the last year, we performed non-equilibrium MD simulations of the destruction process of amyloid fibrils by an infrared laser. We first revealed the disruption process of Aβ amyloid fibrils [2]. We are now performing MD simulations of poly-alanine amyloid fibrils. We found that poly-alanine amyloid fibril is less easily destroyed by infrared laser than Aβ amyloid fibrils. We will try to clarify this difference.

References

[1] M. Yamauchi, G. La Penna, S. G. Itoh, and H. Okumura, Comput. Phys. Commun. **276**, 108362 (2022).

[2] H. Okumura, S. G. Itoh, K. Nakamura, and T. Kawasaki, J. Phys. Chem. B **125**, 4964–4976 (2021).

Critical phenomena in novel Anderson transitions

TOMI OHTSUKI[1]
TOHRU KAWARABAYASHI[2]
KEITH SLEVIN[3]
1) Dept. Phys., Sophia University, Chiyoda-ku, Tokyo 102-8554, Japan
2) Dept. Phys., Toho University, Miyama 2-2-1, Funabashi 274-8510, Japan
3) Dept. Phys., Osaka University, Toyonaka, Osaka 560-0043, Japan

Random quantum systems have no translational/rotational symmetries, but can have time reversal, spin rotation, chiral and particle-hole symmetries. According to these symmetries, the random quantum systems are classified to 10 symmetry classes. The three of them, the so-called Wigner-Dyson classes, were discovered in 1950's and 1960's and have been well studied. Recent experimental discoveries of topological insulators and Weyl semimetal (WSM) have inspired extensive research of random systems other than Wigner-Dyson classes. These 7 new classes contain discrete chiral or particle-hole symmetries.

Here we have introduced a set of Hamiltonians for these new classes, where the high accuracy numerical studies of the three dimensional Anderson transition is possible [1]. We have also studied the novel two dimensional systems, corresponding to a topological superconductor, both analytically [2] and numerically [3]. We especially focused on the critical behaviors near the tricritical point, where ordinary insulator, topological insulator and thermal metal phases meet.

When we introduce the non-Hermiticity to the Hamiltonian, the classification is extended and the systems are categorized to 38 classes. We have shown that adding the non-Hermiticity changes the universality class [4], and show that the transfer matrix method widely used in the Anderson transitions also works for non-Hermitian systems [5]. We have further shown that the critical behaviors of 38 classes are mapped to universality classes for the 10 Hermitian symmetry classes [6].

Machine learning is now widely used in condensed matter physics. We have studied the various quantum phase transitions by analyzing the wave functions via convolutional neural network (CNN). The method is adopted to classify wave functions obtained via density functional theory, which is applied to study the metal-insulator transitions in doped semiconductors [7]. In addition, using the long-short term memory network (LSTM), we have analyzed the time series of diffusion motion of quantum particles in kicked rotors. The model is equivalent to the Anderson model, where the dimensions of the Anderson transition is controlled by the modulation of the kick strength. We have drawn the phase diagram of higher dimensional Anderson transitions by LSTM [8].

References

1. T. Wang, T. Ohtsuki, and R. Shindou, Physical Review B **104**, 014206 (2021).
2. Z. Pan, T. Wang, T. Ohtsuki, and R. Shindou,, Physical Review B **104**, 174205 (2021).
3. T. Wang, Z. Pan, T. Ohtsuki, I.A. Gruzberg, and R Shindou, Physical Review B **104**, 184201 (2021).
4. X. Luo, T. Ohtsuki, R. Shindou, Physical Review Letters **126**, 090402 (2021).
5. X. Luo, T. Ohtsuki, and R. Shindou, Physical Review B **104**, 104203 (2021).
6. X. Luo, Z. Xiao, K. Kawabata, T. Ohtsuki, and R. Shindou, arXiv:2105.02514
7. Y. Harashima, T. Mano, K. Slevin, and T. Ohtsuki, Journal of the Physical Society of Japan **90**, 094001 (2021).
8. T. Mano, and T. Ohtsuki, Annals of Physics **435**, 168500 (2021).

Non-equilibrium relaxation analysis on the $J_1 - J_2$ frustrated Ising model

Keisuke Iikura and Hiroshi WATANABE
Department of Applied Physics and Physico-Informatics, Keio University
Yokohama, Kanagawa 223-8522, Japan

We consider frustrated J_1-J_2 Ising model on the square lattice which Hamiltonian is given by

$$H = J_1 \sum_{\langle i,j \rangle} \sigma_i \sigma_j + J_2 \sum_{\langle\langle i,j \rangle\rangle} \sigma_i \sigma_j,$$

where $\langle i,j \rangle$ and $\langle\langle i,j \rangle\rangle$ denote the summation over the nearest and the next-nearest neighbor pairs, respectively. Spins are Ising-like variable, $\sigma_i = \pm 1$ and $J_1 < 0$ and $J_2 > 0$ denote ferromagnetic and antiferromagnetic interactions, respectively. The parameter of the system is given by $g = J_2/|J_1|$. This model exhibits criticality with varying exponents as the parameter g changes. This behavior is believed to be Ashkin-Teller (AT) universality class. The AT-like behavior will end at some points g^*, and the phase transition becomes the first-order for $1/2 < g < g^*$. The end-point is predicted to be 4-state Potts universality class. However, the localtion of the end-point g^* varies from study to study. Furthermore, whether the phase transition in the range $1/2 < g < g^*$ is a first-order transition or a continuous transition is under debate [1]. Since the interactions of this model involves frustration, the cluster algorithm cannot be applied. Therefore, we apply non-equilibrium relaxation (NER) method to analize the criticality of this model.

We first observe the non-equilibrium relaxation of the order parameter. The stripe order of this system is defined as follows,

$$m_x \equiv \frac{1}{N} \sum_i (-1)^{x_i} \sigma_i, \quad m_y \equiv \frac{1}{N} \sum_i (-1)^{y_i} \sigma_i,$$

where (x_i, y_i) are the coordinates of the i-th spin on the lattice. Then the magnetizaiton is given by $m^2 = m_x^2 + m_y^2$. The order parameter decays exponentially in the disordered phase, converges to a constant in the ordered state, and exhibits power-law decay at the critical point. Then we can identify the critical point from the non-equilibrium behavior of the parameter. We determine the critical exponents from the non-equilibrium fluctuation of obervables [2]. The location of Potts point is determined to be $g^* \sim 0.58$. From the numerical analysis, the phase transition is continuous for $1/2 < g < g^*$ and we did not find any signs of the first order transition. We are currently analyzing the behavior of ordered structure under the fields, and we confirm the existence of a nematic phase. The identification of the nature of the phase transition is a subject for future work.

References

[1] S. Jin, A. Sen, and A. W. Sandvik, Phys. Rev. Lett. **108**, 045702 (2012).

[2] Y. Ozeki and N. Ito, J. Phys. A: Math. Theor. **40**, R149 (2007).

Structure and mechanical properties of crystalline polymers absorbing water molecules

Yuji HIGUCHI
Institute for Solid State Physics, University of Tokyo
Kashiwa-no-ha, Kashiwa, Chiba 277-8581
Research Institute for Information Technology, Kyushu University
Motooka Nishi-ku, Fukuoka 819-0395

We have studied soft matter by molecular simulations and revealed the fracture processes of semicrystalline polymers [1] for the improvement of the toughness and dynamics of lipid bilayers [2] as a model system for biological membranes.

This year, self-assembly processes of amphiphilic molecules were studied by dissipative particle dynamics (DPD) [3] simulations on systems B and C using the LAMMPS program [4]. We revealed that two different molecules were self-sorted or mixed and the processes depended on the hydrophobic length [5].

Furthermore, we studied the adsorption and absorption processes of water molecules to crystalline polymers by coarse-grained molecular dynamics simulation. Water molecules are represented as a sphere in the simulation. The attractive interaction between water and polymer spheres is sufficiently strong to treat polymers as hydrophilic. Figure 1 shows a snapshot at 10 ns and the number of adsorbed water molecules to polymers along the cell axis. Water molecules selectively attach to and absorb into amorphous layers. The tendency is the same as that in the different surfaces, where the water sphere selectively absorbs into amorphous parts. In the hydrophilic semicrystalline polymers, the absorption of water into amorphous parts leads to the gain of attractive interaction compared to that into crystal parts.

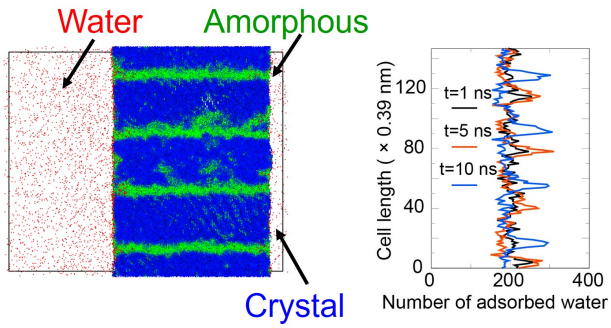

Figure 1: Adsorption and absorption processes of water molecules to polymers. Number of adsorbed water molecules to polymers along the cell axis.

References

[1] Y. Higuchi: Phys. Rev. E **103** (2021) 042502.

[2] Y. Higuchi, Y. Asano, T. Kuwahara, and M. Hishida: Langmuir **37** (2021) 5329.

[3] R. D. Groot and P. B. Warren, J. Chem. Phys. **107** (1997) 4423.

[4] S. Plimpton: J. Comput. Phys. **117** (1995) 1.

[5] R. Wakabayashi, R. Imatani, M. Katsuya, Y. Higuchi, H. Noguchi, N. Kamiya, and M. Goto: Chem. Commun. **58** (2022) 585.

Majorana-mediated spin transport in Kitaev model

Akihisa Koga
Department of Physics, Tokyo Institute of Technology, Meguro, Tokyo 152-8551

Spin transport has recently attracted much interest. One of the interesting examples is the spin transport in the Kitaev model [1]. In the model, quantum spins are fractionalized into itinerant Majorana fermions and local fluxes due to quantum many-body effects. Due to the existence of the local conserved quantities, spin moments never appear in the ground state. Nevertheless, the itinerant Majorana fermions carry the spin excitations and the spin transport is realized without spin oscillations. Since Majorana and flux excitations have distinct energy scales, it is highly desired to clarify how stable such a Majorana-mediated spin transport is against thermal fluctuations.

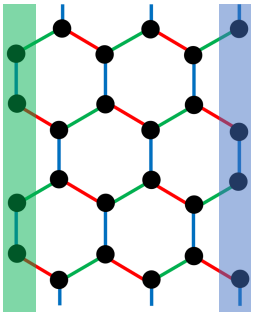

Figure 1: Kitaev model with armchair edges. Green, red, and blue lines indicate x-, y-, and z-bonds, respectively. The static magnetic field h_R is applied in the right region, and no magnetic field is applied in the middle region. Time-dependent pulsed magnetic field is introduced in the left region.

Motivated by this, we deal with the Kitaev model with armchair edges, which is shown in Fig. 1, and consider the spin transport at finite temperatures. Applying the thermal pure quantum state method to the 28-site cluster, we examine the dynamics of the system after the magnetic pulse is introduced at the left edges. When $T \sim T_L$, where T_L corresponds to an energy scale of local flux, larger oscillations in the spin moments are induced in the other edge, compared to the results at the ground state. At higher temperatures, excited Z_2 fluxes disturb the coherent motion of the itinerant Majorana fermions, which suppresses the spin propagation. Our results demonstrate a crucial role of thermal fluctuations in the Majorana-mediated spin transport [2].

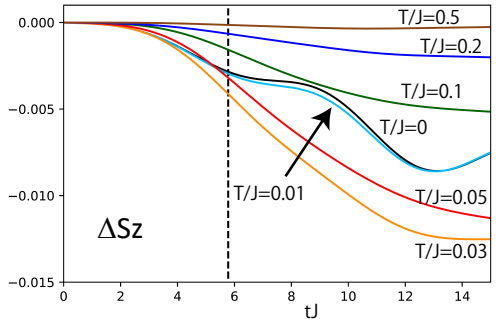

Figure 2: Real-time evolution of the change in the local magnetization in the right edge.

References

[1] T. Minakawa, Y. Murakami, A. Koga, and J. Nasu, Phys. Rev. Lett. **125**, 047204 (2020).

[2] H. Taguchi, Y. Murakami and A. Koga, Phys. Rev. B **105**, 125137 (2022).

Development of COMPutation ARchive of Exact Diagonalization (COMPARED)

Kota IDO

Institute for Solid State Physics,

The University of Tokyo, Kashiwa-no-ha, Kashiwa, Chiba 277-8581

Development of accurate numerical solvers for quantum many-body systems is one of the central issues in the field of computational materials sciences. To achieve this goal, the exact diagonalization method has been widely used for benchmarks on the systems smaller than 50 sites because this method enables us to obtain numerically exact results in the systems with arbitrary interactions. Although most numerical data obtained by the exact diagonalization method are available on articles, these representations such as definition of the Hamiltonians and the display digits of the results are dependent on the articles. Therefore, it is desirable for construction of database to easily check and obtain the exact diagonalization results without definition of notations.

In this project, we have constructed an open database for exact diagonalization results, which is called "COMPutation ARchive of Exact Diagonalization (COMPARED)" [1]. This database has been available on the ISSP data repository under the CC BY 4.0 license [2]. As a generator of the exact results, we use open-source software HPhi [3], which supports MPI/OpenMP hybrid parallelization to achieve highly efficient simulations on supercomputers. Although this parallelization is efficiently done for large system sizes such as 36 sites of quantum spin systems, it is not for single parameter set for small system sizes. To generate data for small system sizes, we develop a python tool which performs HPhi's simulations parallelly. This tool parallelizes input parameter sets and performs the simulations independently for each parameter set. Now we have released more than 20 million data focused on the energies of the ground state and the first excited state on quantum spin systems with small system sizes [2]. We will upload the results for large systems and electron systems.

This project has been done in collaboration with Kazuyoshi Yoshimi and Yuichi Motoyama.

References

[1] K. Yoshimi, K. Ido, Y. Motoyama, R. Tamura, T. Fukushima, Y. Nakanishi-Ohno: https://datarepo.mdcl.issp.u-tokyo.ac.jp/repo/3

[2] https://isspns-gitlab.issp.u-tokyo.ac.jp/compared/compared

[3] M. Kawamura, K. Yoshimi, T. Misawa, Y. Yamaji, S. Todo, and N. Kawashima: Comp. Phys. Commun. **217** (2017) 180.

Ground state and dynamical properties of the J_1-K-Heisenberg model on the square lattice

Matthias GOHLKE, Tokuro SHIMOKAWA
Theory of Quantum Matter Unit, Okinawa Institute of Science and Technology
1919-1 Tancha, Onna-son, Okinawa 904-0495

In the absence of conventional magnetic order of spin-dipolar moments, ordering with higher-order moments like spin-quadrupoles may occur. Such spin-quadrupolar—or spin-nematic (SN)—order was found theoretically in spin-1 model with biquadratic spin-exchange [1].

Magnets with spin-$\frac{1}{2}$ degrees of freedom, however, can only exhibit a SN states if two spin-$\frac{1}{2}$ are combined into an effective spin-1 [2]. In fact, such SN states on bonds has theoretically been observed in frustrated ferromagnets on the square lattice with dominant ferromagnetic Heisenberg exchange, J_1, antiferromagnetic next-nearest neighbor exchange, J_2, and cyclic permutation, K. It was found that the condensation of a two-magnon bound state, at strong magnetic fields along the z-axis, can stabilize a phase with bond-nematic order [3].

Experimentally, the nature of such a ground state is intrinsically difficult to verify, due to the lack of probes that couple directly to the spin-quadrupole moments. Instead, it is necessary to examine the dynamics of a SN: A continuous symmetry for the director of a spin-quadrupole remains, that give rise to a gapless Goldstone mode [4, 5].

We started by studying the square-lattice frustrated J_1-K model [2],

$$\begin{aligned}\mathcal{H} &= J_1 \sum_{\langle i,j\rangle} \boldsymbol{S}\cdot\boldsymbol{S} \\ &+ K \sum_{(i,j,k,l)} \left(P_{ijkl} + P_{ijkl}^{-1}\right) + h_z \sum_i S_i^z \ ,\end{aligned} \tag{1}$$

where J_1 represents dominant ferromagnetic Heisenberg exchange between nearest neighbor spins, K the cyclic ring exchange around squares, and h_z the Zeeman coupling to a magnetic field along the z-axis.

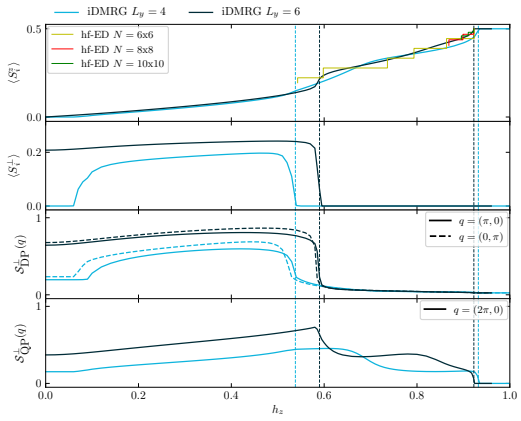

Figure 1: Ground-state of the square-lattice J_1-K-model in a magnetic field at fixed $K/|J_1|$. Different system sizes, geometries, and methods (iDMRG,high-field ED) are compared.

Using iDMRG and the matrix product states (MPS) framework as well as a recently developed exact diagonalization method near saturation [6], we confirm the existence of the bond-nematic phase in an extended range of $K/|J_1|$. In utilizing different methods combined with different geometries, we can assess possible finite-size effects, cf. Fig. 1. Overall we find a good agreement between high-field ED on symmetric clusters and iDMRG on cylindrical geometries with a circumference of $L_{\mathrm{circ}} = 6$ sites.

A significant amount of computational resources has been spent on mapping out the

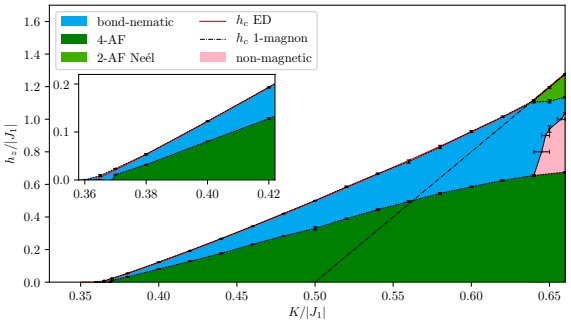

Figure 2: Phase diagram of the square-lattice J_1-K-model in a magnetic field obtained with iDMRG using $L_{circ} = 6$ sites circumference.

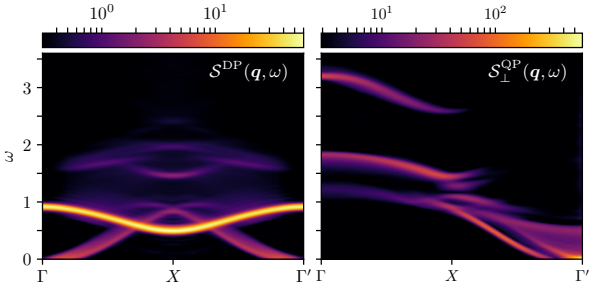

Figure 3: (a) Dynamical spin-structure factor and (b) dynamical quadrupole-structure factor.

entire phase diagram using a cylinder with $L_{\mathrm{circ}} = 6$, cf. Fig. 2. The bond-nematic phase is sandwiched between high-field polarized and 4-sublattice AF phase. Additional phases (Neél, non-dipolar) occur for large K.

Given the ground state wave function as an MPS, dynamical properties can then be studied by applying a time-evolution unitary $U(dt)$ represented as a matrix product operator. In doing so, we observe the condensation of two-magnon bound state at the corresponding wave vector of the SN state. Within the SN phase, we observe (1) the magnon-like excitation that remains fully gapped, and (2) a gapless mode with vanishing spectral weight in the dipolar structure factor and in the $\boldsymbol{q} \to 0$ & $\omega \to 0$ limit as predicted by prior mean-field studies, cf. Fig. 3. We do, however, observe relevant qualitative differences most prominent in the dynamical quadrupole-structure factor. Its origin is currently under investigation.

References

[1] K. Harada and N. Kawashima, Phys. Rev. B **65** (2002) 052403.

[2] A. Andreev and I. Grishchuk, Sov. Phys. JETP **60** (1984) 267.

[3] N. Shannon, T. Momoi, and P. Sindzingre, Phys. Rev. Lett. **96** (2006) 027213.

[4] R. Shindou, S. Yunoki, and T. Momoi, Phys. Rev. B **87**, (2013) 054429.

[5] A. Smerald, H. T. Ueda, and N. Shannon, Phys. Rev. B **91** (2015) 174402.

[6] H. Ueda, S. Yunoki, and T. Shimokawa, Comp. Phys. Comm. **277** (2022) 108369.

Numerical Diagonalization Study on Quantum Phase Transitions of Frustrated Spin Systems

Tôru SAKAI[1,2], Hiroki NAKANO[1], Rito FURUCHI[1],
and Tokuro SHIMOKAWA[3]
[1]*Graduate School of Science, University of Hyogo,*
Kouto, Kamigori, Hyogo 678-1297, Japan
[2]*National Institute for Quantum Science and Technology,*
SPring-8, Kouto, Sayo, Hyogo 679-5148, Japan
[3]*Theory of Quantum Matter Unit,*
Okinawa Institute of Science and Technology Graduate University,
Onna-son, Okinawa 904-0495, Japan

1 Magnetization plateau of the distorted diamond spin chain with anisotropic ferromagnetic interaction

The $S = 1/2$ distorted diamond spin chain with the anisotropic ferromagnetic interaction is investigated using the numerical diagonalization and the level spectroscopy analysis. It is known that the system exhibits a plateau of the magnetization curve at the 1/3 of the saturation. The present study indicates that as the anisotropy is varied the quantum phase transition occurs between two different mechanisms of the 1/3 magnetization plateau. The phase diagram with respect to the anisotropy and the ferromagnetic coupling is also presented[1].

2 Magnetization process of the S=1/2 Heisenberg antiferromagnet on the floret pentagon lattice

We study the S = 1/2 Heisenberg antiferromagnet on the floret pentagonal lattice by numericaldiagonalization method. We found that magnetization plateaux appear at one-ninth height of the saturation magnetization, at one-third height, and at seven-ninth height. The magnetization plateaux at one-third and seven-ninth heights come from interactions linking the sixfold-coordinated spin sites. A magnetization jump appears from the plateau at one-ninth height to the plateau at one third height. Another magnetization jump is observed between the heights corresponding to the one third and seven-ninth plateaux; however the jump is away from the two plateaux, namely, the jump is not accompanied with any magnetization plateaux[2].

References

[1] T. Sakai, K. Okamoto, H. Nakano and R. Furuchi, AIP Advances 12 (2022) 035030.

[2] R. Furuchi, H. Nakano, N. Todoroki and T. Sakai, J. Phys. Commun. 5 (2021) 125008.

Numerical Diagonalization Study on Magnetization Process of Quantum Spin Chain with the Biquadratic Interaction

Tôru SAKAI[1,2], Hiroki NAKANO[1], Rito FURUCHI[1], and Tokuro SHIMOKAWA[3]
[1]*Graduate School of Science, University of Hyogo, Kouto, Kamigori, Hyogo 678-1297, Japan*
[2]*National Institute for Quantum Science and Technology, SPring-8, Kouto, Sayo, Hyogo 679-5148, Japan*
[3]*Theory of Quantum Matter Unit, Okinawa Institute of Science and Technology Graduate University, Onna-son, Okinawa 904-0495, Japan*

1 Quantum spin nematic liquid in the S=1 antiferromagnetic chain with the biquadratic interaction

The magnetization process of the $S = 1$ antiferromagnetic chain with the biquadratic interaction is invesitgated using the numerical diagonalization. As a result, it is found that the quantum spin nematic liquid phase appears below the saturation magnetization for sufficiently large negative biquadratic interaction. The ground state phase diagram is also presented. [1].

2 Field-Induced Quantum Spin Nematic Liquid Phase in the S=1 Antiferromagnetic Heisenberg Chain with Additional Interactions

The $S = 1/2$ distorted diamond spin chain with the anisotropic ferromagnetic interaction is investigated using the numerical diagonalization and the level spectroscopy analysis. It is known that the system exhibits a plateau of the magnetization curve at the 1/3 of the saturation. The present study indicates that as the anisotropy is varied the quantum phase transition occurs between two different mechanisms of the 1/3 magnetization plateau. The phase diagram with respect to the anisotropy and the ferromagnetic coupling is also presented[2]

References

[1] T. Sakai, AIP Advances 11 (2021) 015306.

[2] T. Sakai, H. Nakano, R. Furuchi and K. Okamoto, J. Phys.: Conf. Ser. 2164 (2022) 012030.

A proximate Tomonaga-Luttinger state in the *S*=1/2 Kitaev-Γ model on a Honeycomb Lattice

Takafumi SUZUKI

Graduate School of Engineering,

University of Hyogo, Shosha, Himeji, Hyogo 670-2280

We have investigated the ground-state phase diagram and the dynamical properties of the S=1/2 Kitaev-Γ model [1] on a honeycomb lattice by the numerical exact diagonalization (ED) method and the density-matrix-renormalization-group (DMRG) method. The *S*=1/2 Kitaev- Γ model on a honeycomb lattice was proposed as the effective model of the honeycomb-lattice magnet, α-$RuCl_3$. The ground-state phase diagram of this model with the isotropic coupling strength has been much studied because of the simplicity of the model. However, the anisotropy of the coupling strength exists in α-$RuCl_3$, which originates from the reduction of the lattice symmetry, and the effect of the anisotropy has not been fully understood yet.

In the previous study, we reported the partial ground phase diagram of the *S*=1/2 Kitaev-Γ model on a honeycomb lattice shown in Fig. 1 and indicated that the dimerized phase, which appears in the isolated dimer limit ($d=\infty$), can survives up to the isotropically interacting model (*d=1*), when the Kitaev interaction and the Γ interaction are negative and positive respectively [2]. In this study, we investigated the ground-state phase diagram in $0 \leq d \leq 1$ [3]. We find that a proximate Tomonaga-Luttinger liquid (pTTL) is expected in the ground state with the negative Kitaev interaction and the positive Γ interaction (Γ). This pTTL becomes the Tomonaga-Luttinger liquid (TLL) in the spin chain limit (*d*=0), which was pointed out in ref. [4]. When the condition, Γ/|K|=1 (K<0), is satisfied at *d*=0, the model is mapped on the antiferromagnetic Heisenberg chains and recovers the hidden SU(2) symmetry [4]. Thus, a gapless linear excitation derived from spinon excitations appears in the low-energy excitation. These characteristics is also observed in the low-energy excitation of the pTTL phase. From the ED calculations for the N=24 site cluster with the C_3 symmetry of the lattice, we find that the pTTL phase can survive up to *d=1*. Next, we calculated the temperature dependence of the specific heat to investigate the emergence of the Majorana fermions in the vicinity of *d=1* and Γ=0. At *d=1* in $0 \leq \Gamma/|K|$, the presence of the double-peak structure was indicated in ref. [5]. We find that the higher-temperature peak at *d=1* corresponds to the prominent single peak in the spin chain limit and the lower-temperature peak rapidly develops in the vicinity of *d=1*. This means that the spinon-like excitation is continuously converted into the Majorana excitation.

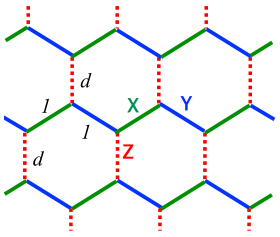

Fig. 1: Anisotropically interacting Kitaev-Γ model. The coupling strength on the X/Y bond is unity and *d* is the ratio of the coupling strength on the Z bond against that on the X/Y bond.

References

[1] J. G. Rau, E. Lee, and H. -Y. Kee, Phys. Rev. Lett. 112, 077204 (2014).
[2] T. Yamada, T. Suzuki, and S. Suga, Phys. Rev. B **102**, 024415 (2020).
[3] M. Gohlke, J. C. Pelayo, and T. Suzuki, in preparation.
[4] W. Yang, et al., Phys. Rev. Lett. 124, 147205 (2020) and W. Yang, A. Nocera, and I. Affleck, Phys. Rev. Research 2, 033268 (2020).
[5] A. Catuneanu, et al., npj Quant. Mater. 3, 23 (2018).

Hybrid Simulations on Fluid-Viscoelastic Membrane System Using Multi-Scale Simulation Platform for Complex Fluids

Yohei MORII and Toshihiro KAWAKATSU

Department of Physics, Tohoku University,

Aza-Aoba, Aramaki, Aoba-ku, Sendai 980-8578

We develop general multiscale simulation methods for inhomogeneous complex flows in viscoelastic fluids and elastoplastic solid. For such multiscale simulations, a general-purpose platform named Multis-Scale Simulation Platform for complex flows (MSSP) was developed by the present authors [1]. In our MSSP, the macroscopic flow is simulated by smoothed particle hydrodynamics (SPH) method, to which the microscopic information is introduced through a microscopic molecular dynamics (MD) simulator embedded in each of the SPH particles.

We simulate a viscoelastic flow of a dilute polymer solution passing through an obstacle and clarify the role of added polymers. To accurately simulate large scale dynamic flow patterns behind the obstacle, such as Karman vortex street, it is essential to use a large-scale system, where the flow velocity and velocity gradient are highly inhomogeneous. To avoid a large computational cost as well as a large unbalance in the computational load on the computer nodes, we proposed a hybrid method where we switch the MD simulators with simpler constitutive equations for the SPH particles with smaller velocity gradient. A preliminary result using linear viscoelastic constitutive equation was developed during the previous project in 2020 [1]. In the present project, we extended this hybrid method to nonlinear viscoelastic constitutive model. Figure 1 shows the flow pattern around the separation point on a cylindrical obstacle, where the red SPH particles contains particle MD simulators while blue SPH particles contain nonlinear constitutive equations. We can confirm that the switching is successfully implemented and 97% of 1,600,000 SPH particles are simulated with constitutive model.

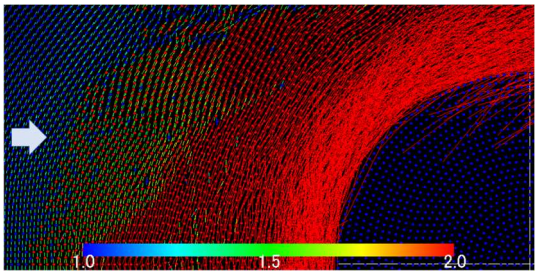

Fig.1 MSSP simulation of a polymer flow around a cylindrical obstacle. Bars attached to the particles show the average elongation and its direction of the polymer chains.

References

[1] Y. Morii and T. Kawakatsu: Phys. Fluids **33** (2021) 093106.

Thermal effects on quantum frustrated magnetisms

Tokuro Shimokawa

Theory of Quantum Matter Unit, Okinawa Institute of Science and Technology Graduate University, Onna-son Okinawa 904-0412

Quantum frustrated magnets are well-known sources of exotic states of matter, but investigating their true nature, particularly at finite temperatures, is still a demanding and challenging problem. This fiscal year, we have focused on the following topics with the ISSP supercomputer.

1) S=1/2 breathing bilayer kagome (BBK) magnet for $Ca_{10}Cr_7O_{28}$

$Ca_{10}Cr_7O_{28}$ is a newly quantum spin liquid (QSL) material, and the effective Hamiltonian was proposed as an S=1/2 BBK Heisenberg model. A recent semi-classical study [1] supported the scenario of a QSL ground state in this material and suggested possible realizations of exotic low-temperature multiple-*q* states in fields. But the true nature of the multiple-*q* states wasn't uncovered yet because of the difficulty of treating large systems.

We alternatively treated a classical J_1-J_2 Heisenberg model on the honeycomb lattice model, which could also be considered an effective model for $Ca_{10}Cr_7O_{28}$ to investigate the thermodynamic properties of the multiple-*q* states. Our large-scale Monte Carlo simulations succeeded in identifying them; we found that one of them is an intriguing six sub-lattice (anti) skyrmion-lattice state with topological nature.

2) High-field exact diagonalization code development and the low-*T* physics in the S=1/2 J_1-K square-lattice model

We developed an exact diagonalization code, quantum spin solver near saturation (QS^3), as an open-source software [2]. Using this high-field ED code, we investigated the low-T phase diagram of the S=1/2 square-lattice Heisenberg model with a ring exchange interaction (J_1-K model).

Our ED calculations revealed the existence of several ordered/disordered states in fields. Especially in the high-field regime around $K/J_1 \sim 0.5$, we clarified the realization of a bond-nematic state without any approximation to our Hamiltonian. We also computed the dynamical spin/quadrupole structure factors for future neutron scattering measurements on candidate materials.

References

[1] R. Pohle, et al, PRB **104**, 024426 (2021).

[2] H. Ueda, S. Yunoki, T. S., Comp. Phys. Commun. **277**, 108369 (2022).

Steady states realized by a global thermodynamic balance in nonequilibrium

Naoko NAKAGAWA
Department of Physics, Ibaraki University
2-1-1 Bunkyo, Mito, Ibaraki 310-8512

First-order phase transition and the separation of the phases have attracted scientific interests from various points of view, not only from physics but also from the biological mechanism. The phase coexistence induces sometimes complicated and singular properties to the system even though the bulks of respective phases may behave rather ordinary.

In this project, we work on particle systems interacting via a Lennard-Jones potential

$$V(r) = 4\epsilon \left[\left(\frac{\sigma}{r}\right)^{12} - \left(\frac{\sigma}{r}\right)^{6} \right] + \epsilon,$$

with a diameter σ of each particle and a coupling strength ϵ, which have been a standard model for numerical experiments. By choosing the total energy and the number density of the system appropriately, the system shows a liquid-gas transition. See Fig. 1 for the case of $N = 5 \times 10^4$. We also used Weeks-Chandler-Andersen (WCA) potential when we want to avoid the liquid-gas transition.

Our most interest is the liquid-gas coexistence in heat conduction. Due to the steady heat current, the coexistence pattern of the liquid and gas becomes much more stable compared with equilibrium systems. The local states around the liquid-gas interface become observable due to the induced stability. We here notice that the rich behaviors related to the first-order transition are often observed in complex systems such as mixtures and dense solutions. Their response to a nonequilibrium driving will be of great interest. To initiate them, we start with the construction of a method to know their thermodynamic properties in equilibrium. The details of the results follow.

We derived a formula for determining the mixing free energy for two-component fluids. The formula is numerically verified with a good accuracy by the molecular dynamics simulation using the LAMMPS package installed in the supercomputers at ISSP. We have compared two kinds of protocols creating a mixture of two pure substances. One is traditional protocol and the other is a protocol with "alchemical change" of molecules, which may be valid only in numerical experiments. We calculated the free energy changes of the two protocols by adopting the Jarzynski equality and information thermodynamics. The comparison of the two results in a formula for the mixing Gibbs free energy $\Delta_{\rm mix}G$ as

$$\Delta_{\rm mix}G = -k_{\rm B}T \ln \left[\frac{N!}{n!(N-n)!\rho_X(n)} \frac{\langle e^{-\beta \hat{W}_{(\#)}} \rangle}{\langle e^{-\beta \hat{W}_{(\rm ii)}} \rangle} \right],$$

where n and $N-n$ are the numbers of particles for the two components and $\rho_X(n)$ is the number density of the first component in the region $x < X$. $\hat{W}_{(\#)}$ is the work in each trajectory according to the alchemical process to create a mixture from the first pure substance, whereas $\hat{W}_{(\rm ii)}$ is the work according to the alchemical process to create the second from the first pure substance.

By applying the above formula, we examined $\Delta_{\rm mix}G$ for the mixture of argon and krypton. By changing the mole fraction of the krypton,

the system shows liquid-gas transition for a fixed temperature and pressure. The properties of the transition are well characterized in the calculated $\Delta_{\mathrm{mix}}G$ as a double-well-shaped function. The violation of convexity is likely due to the finiteness of the system.

We have used the L4 CPU of System B with 4 nodes in 512 parallel computation using MPI for the calculation of 10^4 particles, the L16 CPU of System B with 16 nodes in 2048 parallel computation using MPI for the calculation of 5×10^5 particles, the L72 CPU of System B with 72 nodes in 9216 parallel computation using MPI for the calculation of 8×10^6 particles.

References

[1] A. Yoshida and N. Nakagawa: to appear in *Phys. Rev. Res.* (2022)

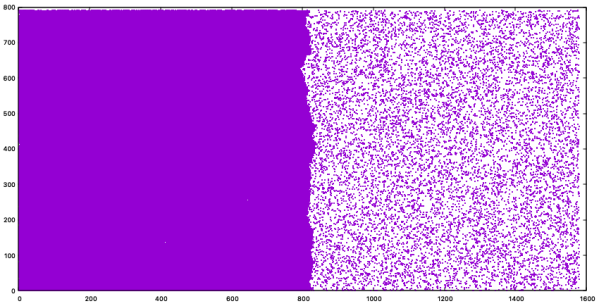

Figure 1: Snapshot of the particles interacting with Lennard-Jones potential in heat conduction. The system with $N = 5 \times 10^5$ exhibits a sharp liquid-gas interface.

Scrambling in quantum many-body systems

Masaki TEZUKA

Department of Physics,

Kyoto University, Kitashirakawa, Sakyo-ku, Kyoto 606-8502

Strongly correlated models realizable in condensed matter systems with possible holographic correspondence to gravitational systems including black holes have received much attention in the recent years. Of particular interest are scrambling and chaotic dynamics. The scrambling phenomena in quantum systems is delocalization of quantum information and has been discussed as the formation of quantum error correction (QEC) code. Thus, we have been trying to study scrambling and effect of dissipation in quantum many-body systems, toward experimental demonstration in condensed matter systems such as ultracold atoms.

The Sachdev-Ye-Kitaev (SYK) model is a model of Majorana fermions with all-to-all four-fermion interactions obeying the Gaussian distribution. It has an analytic solution in the limit of large number of fermions and is maximally chaotic at low temperatures. We have previously studied the effect of a random hopping term, two-fermion interactions, added to the model [1]. The maximally chaotic behavior is lost and the spectral statistics turns to an uncorrelated one. Furthermore, the localization transition is a Fock-space localization, a type of many-body localization, and quantities such as the location of the transition point, the moments of the eigenstate wavefunctions, and bipartite entanglement entropy have been obtained analytically with numerical confirmation [2].

A “sparse” version of the SYK model, in which the number of interaction terms is on the order of the number of fermions, instead of all the choices of four-fermion subsets, have been proposed a few years ago.

To quantify the scrambling properties of these models, we have studied the QEC capabilities of the unitary time evolution according to their Hamiltonians according to the Hayden-Preskill protocol [3]. In this protocol, the unknown quantum state thrown into a quantum many-body system is decoded by a person who, knowing the initial state of the remainder of the system and the time evolution, obtains the quantum state of some of the qubits comprising the system, and the error estimate for the time evolutions obeying the circular unitary ensemble (CUE) is known.

Using the ISSP Supercomputer, we analyzed the spectral statistics of a further simplification of the sparse SYK model [4]. Also, we numerically observed that while for the sparse SYK models, the QEC error estimate approaches the CUE value as soon as the spectral statistics becomes random-matrix like, for the case of two-fermion interactions, the departure from the CUE value is observed before the Fock space localization occurs [5].

References

[1] A. M. Garcia-Garcia, B. Loureiro, A. Romero-Bermudez, and M. Tezuka, Phys. Rev. Lett. **120** (2018), 241603.

[2] F. Monteiro, T. Micklitz, M. Tezuka, and A. Altland, Phys. Rev. Research **3** (2021), 013023; F. Monteiro, M. Tezuka, D. A. Huse, and T. Micklitz, Phys. Rev. Lett. **127** (2021), 030601.

[3] P. Hayden and J. Preskill, JHEP **0709** (2007), 120.

[4][5] M. Tezuka *et al.*, in preparation.

Investigation of the molecular origins of the mechanical and thermal properties of realistic biopolymers using all-atomistic molecular dynamics

Okazaki Susumu

Department of Advanced Materials Science,

The University of Tokyo, Kashiwa-no-ha, Kashiwa, Chiba 277-8581

Mechanical and thermal properties of biopolymers, PBI and its three copolymers PBO-*co*-PBI, PBI-*co*-PBO-*co*-*p*PA, and PBI-*co*-PBO-*co*-*m*PA, have been investigated based on all-atomistic molecular dynamics (MD) calculations to clarify molecular mechanism of fracture and glass transition of the polymers. We also investigated regular polymers, PC and PMMA [1], as a reference system. The calculations have been conducted on the supercomputers at ISSP using a MD software MODYLAS [2] developed by our group.

Modulus of elasticity, yielding stress, and fracture stress were studied in detail. The biopolymers showed the high modulus of elasticity at short strain followed by the high yielding stress and ductility showing strong strain hardening at large strains after the yielding point.

The biopolymers investigated here all exhibited very high glass transition temperatures at 800 K – 900 K. The temperatures are higher than their pyrolysis temperatures. These high glass transition temperatures are from hydrogen bonds among polymer chains forming network structures.

We also investigated the microscopic origins of the stress causing the elastic deformation, yield point, strain softening, and strain hardening observed in PC and OMMA, by decomposing the stress into contributions from various energetic energy terms. Our analysis showed that the stress of the fracture process is mainly determined by the bond, angle, and vdW terms, in addition to the system alignment in the pulling direction. In the elastic region, almost the entire system experiences affine deformation despite the existing local heterogeneous deformation in the later elastic region. As the deformation of the entanglement network begins, the stress on the bonds and angles rapidly increases.

References

[1] Z. Tang, K. Fujimoto, S. Okazaki, Polymer, **226**(2021)123809.

[2] Y. Andoh, S. Ichikawa, T. Sakashita, N. Yoshii, S. Okazaki, J. Comp, Chem., **42**(2021)1073.

Simulations of quantum-classical-hybrid algorithms for sensor materials with considering noise

Wataru Mizukami

Center for Quantum Information and Quantum Biology, Osaka University, Osaka 560-0043, Japan

The development of quantum computers has made significant progress in recent years: quantum computers with dozens or a hundred qubits have been built. We now expect to see quantum devices with hundreds or thousands of qubits near future. Such quantum computers are often called noisy-intermediate scale quantum devices (NISQs) since they do not have quantum error correction functionality. There have been intensive research efforts currently underway to exploit the computational potential of NISQs.

One promising algorithm for NISQs is the quantum-classical hybrid algorithm, which can operate even in the short coherence time of a NISQ. Among them, the variational quantum eigensolver (VQE) can be applied to first-principles calculations of materials or molecules. We are targeting applying the VQE to practical problems in material science. In particular, we aim to use the VQE for analyzing materials used in sensors. In this study, we use a quantum circuit simulator rather than real quantum computers to develop a new quantum-classical hybrid algorithm and validate it. The reasons we employ such an emulator are the following: the number of NISQs is limited at this moment; their use charges high fees; error rates of today's NISQs are still too high. Last year, we built a framework to efficiently emulate quantum circuits with (deplolarsing) noises using the supercomputer of the ISSP.

This year, we worked on improving the efficiency of the quantum circuit optimization part in the VQE. We parallelized the gradient evaluations of the VQE's cost function with respect to the quantum circuit parameters, using MPI. We tested our implementation by computing the H2O molecule with the 6-31G basis set. The benchmark calculation used a minimum of 128 cores and a maximum of 9216 cores. The observed parallelization efficiency was 75% with 4608 cores, relative to the execution time with 128 cores.

Moreover, we developed a method to consider solvation effects within the framework of the VQE. This was achieved by combining the VQE and 3D-RISM, an integral equation theory of molecular liquids. This method was used to investigate the impacts of solvents on the computational cost of quantum computing. Our calculations indicate that solvation effects virtually have no impact on it.

Molecular Dynamics Simulation of Stress Induced Crystallization in Robust-Toughening Hydrogel

Koichi Mayumi, Kosuke Aomura, Takeyoshi Masumoto, Haru Shinohara

Institute for Solid State Physics,

The University of Tokyo, Kashiwa-no-ha, Kashiwa, Chiba 277-8581

In this project, we studied crystallization of polymer chains in slide-ring gels under stretching by means of coarse-grained molecular dynamics simulation. In addition, we performed a full-atomistic molecular dynamics simulation of the melting process of stretched polymer crystals in water.

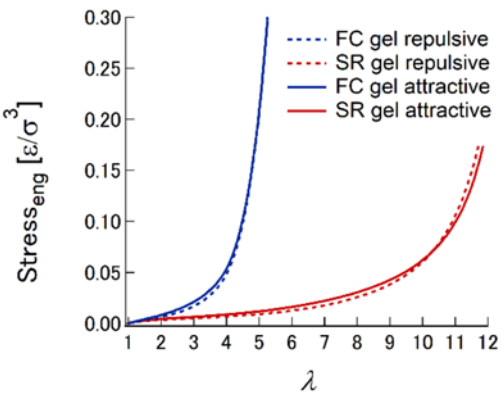

Fig. 1 Stress-extension ratio relation of fixed crosslink gel and slide-ring gel.

Coarse-Grained Molecular Dynamics Simulation of Strain-Induced Crystallization of Slide-Ring Gel

In this study, uniaxial elongation simulations of slide-ring gels were performed using coarse-grained molecular dynamics simulation [1]. In order to investigate the strain-induced crystallization of slide-ring gel which is observed in experiments [2], we introduced attractive interaction between polymer chains. Fig. 1 shows stress-extension ratio curve of a fixed crosslink (FC) gel and slide-ring (SR) gel with the same cross-linking density. SR shows smaller stress than FC gel because of the slidability of the cross-links.

Further analysis was performed to clarify aggregated structure under stretching. We calculated scattering function of SR gel before and after stretching. At the extension ratio λ=12, scattering function shows a circular peak on $q_z = 0\ \sigma^{-1}$ plane at $\sqrt{q_x^2 + q_y^2} = 6\ \sigma^{-1}$. The peak suggests the formation of aggregate structures in which polymer chains are aligned in the direction perpendicular to the elongation.

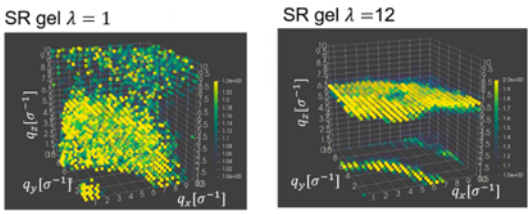

Fig. 2 Snapshots of a scattering function of SR gel at (a) λ=1 (b) λ=12

A region of neatly aligned polymer chains was extracted from the network, and the scattering function was calculated for the region. As a result, we observed spot peaks corresponding to a body-centered orthorhombic lattice crystal structure, as shown in Fig. 3. This indicates that the slidability of the cross-linking points equalizes the chain deformation and enhances the strain-induced crystallization.

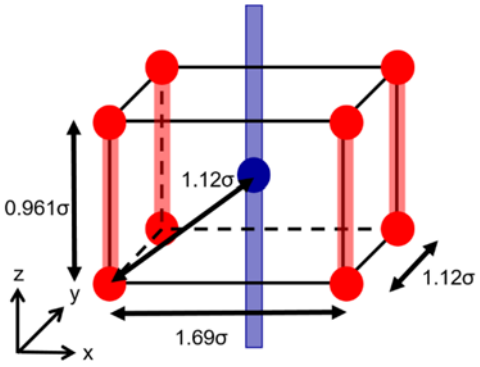

Fig. 3 Body-centered orthorhombic lattice crystal structure observed in SR gel at λ=12.

Analysis of Dissolution Process of Extended Polyethylene Glycol Crystal in Water

The reversibility of the strain-induced crystallization of PEG chains in water allows the tough hydrogel to rapidly recover from mechanical stress. To understand the dissolution process of extended PEG chain crystal in water, all-atom MD simulation was carried out. GROMACS 2016.5 [3] was used as simulation software. We investigated the dissolution process of helical PEG chain crystal and zigzag PEG chain crystal under stretching in water. For helical chain crystal, the crystal partly remain after 200 ns even at no elongation force. On the other hand, zigzag chain crystal dissolves faster than the helix chain crystal.

References

[1] Kremer, K.; Grest, G. S.: *J. Chem. Phys.* **92** (8), 5057–5086. (1990)

[2] C. Liu, N. Morimoto, L. Jiang, S. Kawahara, T. Noritomi, H. Yokoyama, K. Mayumi, K. Ito: *Science* **372** 1078-1081. (2021)

[3] Berendsen, H. J. C.; van der Spoel, D.; van Drunen, R. *Comp. Phys. Comm.* **91**, 43–56. (1995)

Molecular dynamics study of shear-induced long-range correlations in simple fluids

Hiroyoshi Nakano
Department of Applied Physics and Physico-Informatics, Keio University
Yokohama, Kanagawa 223-8522, Japan

We studied a nonequilibrium long-range correlation (LRC) in simple fluids using a molecular dynamics (MD) simulation. The nonequilibrium LRC means that same-time spatial correlations of locally conserved quantities exhibit power-law decays due to a lack of detailed balance condition [1]. It is known to be one of the general features of nonequilibrium systems with conserved quantities and anisotropy. Because in equilibrium the LRCs are specific to the critical phenomena, the nonequilibrium LRCs observed far from the critical points have been extensively studied as the novel phenomena induced by nonequilibrium conditions. However, the almost all of research have been performed using phenomenological models such as fluctuating hydrodynamics and stochastic lattice gases. Indeed, there are few attempts to directly observe the nonequilibrium LRCs and examine their nature from underlying molecular systems.

In the present study, with the aim of direct observation of the nonequilibrium LRCs, we focused on the simple fluids under uniform shear flow and performed the MD simulation [2]. All the MD simulations were performed by LAMMPS (Large-scale Atomic/Molecular Massively Parallel Simulator) [3, 4]. The schematic illustration of our system is given in Fig. 1. The particles interact via the Weeks–Chandler–Andersen (WCA) potential. The shear flow is imposed by using the Lees–Edwards boundary condition along the z-axis. Along the x and y-axes, the standard periodic boundary conditions are imposed. To maintain a constant temperature T under shear flow, the dissipative particle dynamics (DPD) thermostat is used. Thus, in the steady state, the following averaged velocity profile $\langle \boldsymbol{v}(\boldsymbol{r}) \rangle_{\rm ss} = (\dot{\gamma} z, 0, 0)$ is realized, where $\langle \cdot \rangle_{\rm ss}$ denotes time average in the steady state and the ensemble average over different noise realizations, and $\dot{\gamma}$ is shear rate.

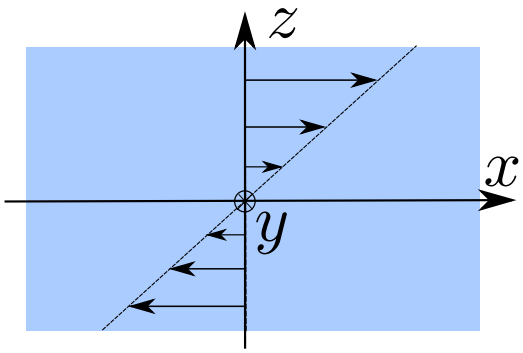

Figure 1: Schematic illustration of shear flow.

We observe the same-time correlations of momentum fluctuations in the steady state. The momentum fluctuations are given by

$$\delta \boldsymbol{g}(\boldsymbol{r}, t) = \sum_{i=1}^{N} \boldsymbol{p}_i(t) \delta(\boldsymbol{r} - \boldsymbol{r}_i(t)) - \langle \boldsymbol{v}(\boldsymbol{r}) \rangle_{\rm ss}, \quad (1)$$

where $\boldsymbol{r}_i(t)$ and $\boldsymbol{p}_i(t)$ are, respectively, the position and momentum of ith particle at time t. Then, the same-time correlations of momentum fluctuations are given by $C_{\alpha\beta}(\boldsymbol{r}, \boldsymbol{r}') = \langle \delta g^{\alpha}(\boldsymbol{r}, t) \delta g^{\beta}(\boldsymbol{r}', t) \rangle_{\rm ss}$, where $\alpha, \beta = x, y, z$.

We plot the Fourier transform of $C_{zz}(\boldsymbol{r}, \boldsymbol{r}')$ in Fig. 2. Because our system has the spe-

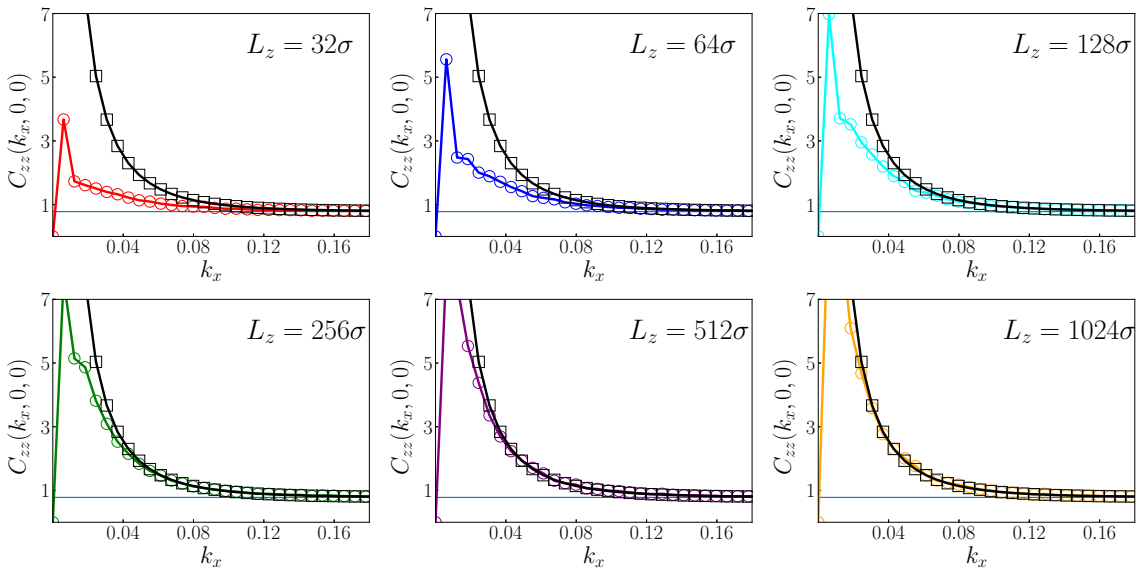

Figure 2: $C_{zz}(k_x, k_y = k_z = 0)$ for several system sizes $L_z = 32\sigma$, 64σ, 128σ, 256σ, 512σ, 1024σ. The color circle points represent the MD simulation results, and the black square points the results calculated from the fluctuating hydrodynamics.

cial Galelian invariance, the Fourier transform of $C_{zz}(\boldsymbol{r}, \boldsymbol{r}')$ is given as $C_{zz}(\boldsymbol{k}) = \int d^3\boldsymbol{r} C_{zz}(\boldsymbol{r}, \boldsymbol{0}) e^{-i\boldsymbol{k}\cdot\boldsymbol{r}}$. In Fig. 2, $C_{zz}(k_x, k_y = k_z = 0)$ for different L_z is presented. The other parameters are set to $L_x = 1024\sigma$, $L_y = 32\sigma$, and $\dot{\gamma} = 0.02\tau_{\text{unit}}^{-1}$, where σ and τ_{unit} are, respectively, the unit of length and time. The black square points represent $C_{zz}(k_x, k_y = k_z = 0)$ calculated from the phenomenological theory called the fluctuating hydrodynamics [5]. The result obtained from the fluctuating hydrodynamics is independent of L_z.

From Fig. 2, we find that the strong finite-size effects exist for $C_{zz}(k_x, k_y = k_z = 0)$. For sufficiently large L_z, the result calculated from the fluctuating hydrodynamics is in quantitative agreement with the MD simulation results. In contrast, for smaller L_z (e.g. 32σ or 64σ), there is the clear deviation between their results. In other words, the quite large system size is required to observe the shear-induced long-range correlations.

In summary, we performed the MD simulations of the WCA fluids under uniform shear flow. We successfully observed the nonequilibrium long-range correlations for the sufficiently large system that contains over 10 million particles.

References

[1] J. Dorfman, T. Kirkpatrick, and J. Sengers, Annual Review of Physical Chemistry **45**, 213 (1994).

[2] H. Nakano, and Y. Minami, Physical Review Research (in press).

[3] S. Plimpton, Journal of Computational Physics **117**, 1 (1995).

[4] A. P. Thompson, H. M. Aktulga, R. Berger, D. S. Bolin-tineanu, W. M. Brown, P. S. Crozier, P. J. in ' t Veld,A. Kohlmeyer, S. G. Moore, T. D. Nguyen, R. Shan, M. J.Stevens, J. Tranchida, C. Trott, and S. J. Plimpton, Computer Physics Communications **271**, 108171 (2022).

[5] J. Lutsko and J. W. Dufty, Phys. Rev. A **32**, 3040 (1985).

Theoretical analysis of absorption and fluorescence spectra for firefly bioluminescence related molecules

Miyabi HIYAMA
Graduate School of Science and Technology, Gunma University, Tenjin-cho, Kiryu, Gunma 376-8515

Because firefly bioluminescence is widely used such as *in vivo* imaging and reporter assay, many analogs of firefly bioluminescence substrates (luciferin) are developed [1, 2]. AkaLumine is one of the analogs of luciferin and its bioluminescence with firefly luciferase produces the near-infrared emission, which can penetrate through biological tissues [3]. For studying the bioluminescence mechanism, basic knowledge about the chemical structures, electronic states, and absorption properties of AkaLumine solution at various pH values of solution has to be acquired.

In this study, the absorption spectra for Alakumine in aqueous solutions were studied theoretically [4]. The optimization structure of ground state for AkaLumine and its conjugate acids and bases, which are expected to be main component in the aqueous solutions, were obtained from the density functional theory (DFT). The time dependent DFT (TDDFT) calculations were carried out to estimate the theoretical absorption spectra for these structures. The Gibbs free energies for the chemical structures were obtained using the vibrational analysis. Form these free energies, pK_a values for protonation/deprotonation of AkaLumine in aqueous solutions were estimated and the relative concentrations of AkaLumine and its conjugate acids and bases were obtained. All calculations were performed using the GAUSSIAN09 program [5] on system B and C of Super Computer Center in ISSP.

It was found that the main absorption peaks for AkaLumine and its conjugate acids ad bases appear at 369, 465, 314, 353, 352, 440, 322, and 317 nm and that all of these peaks correspond to the excitation from S_0 to the first excited state (S_1) [4]. These S_1 states can be described dominantly by the one electron excitation configuration of which the coefficients are large ($\sim$0.5). From the theoretical results, the peaks at pH 7–10, pH 4, and pH 2 of AkaLumine experimental absorption spectra are assigned to a carboxylate anion, a carboxylate anion with an N-protonated thiazoline ring, and a carboxylate anion with an N-protonated thiazoline ring and N-protonated dimethylamino group, respectively.

References

[1] Li et al. , Eur. J. Med. Chem., **211** (2020) 113111.

[2] Iwano et al. , Tetrahedron, **69** (2013) 3847.

[3] Kuchimaru et al. , Nat. Comm., **7** (2016) 1.

[4] Ogawa et al. Photochem. Photobiol. (2021) 97, 1016.

[5] Gaussian 09, Revision D.01, M. J. Frisch et al.

Skyrmion crystal phase in the RKKY Heisenberg model in two- and three- dimensions

Kota Mitsumoto and Hikaru Kawamura

Molecular Photoscience Research Center, Kobe University, Kobe 657-8501, Japan

Skyrmion, a swirling noncoplanar spin texture whose constituent spin directions wrap a sphere in spin space, has attracted much recent interest and been studied quite extensively. In magnets, skyrmion is usually stabilized in the form of the periodic array, i.e., the skyrmion crystal (SkX). While the SkX was first realized in chiral ferromagnets with the anti-symmetric Dzyaloshinskii-Moriya (DM) interaction, a recent study has revealed that the SkX state can also be realized in centrosymmetric magnets without the DM interaction [1]. Such a "symmetric" SkX state is induced by frustration among exchange interactions, and keeps the chiral degeneracy with respect to the right-left (R-L) symmetry, in sharp contrast to the DM-induced SkX.

Such a frustration-induced symmetric SkX is possible both in insulating and metallic magnets. In metallic magnets, the primary interaction is the long-range RKKY interaction which oscillates in sign with the distance leading to the frustration, in contrast to the insulating magnets possessing the short-range interactions. In this year's project, we study the ordering properties of the isotropic RKKY Heisenberg model on the two-dimensional triangular and the three-dimensional stacked-triangular lattices by extensive Monte Carlo simulations in order to get insights into the chiral-degenerate skyrmion crystal of metallic magnets in the weak-coupling regime [2].

We find that the symmetric SkX is stabilized under finite magnetic fields both in two and three dimensions, as shown in the temperature vs. magnetic-field phase diagram of the Figure below, both the 2D (upper) and 3D (lower) ones.

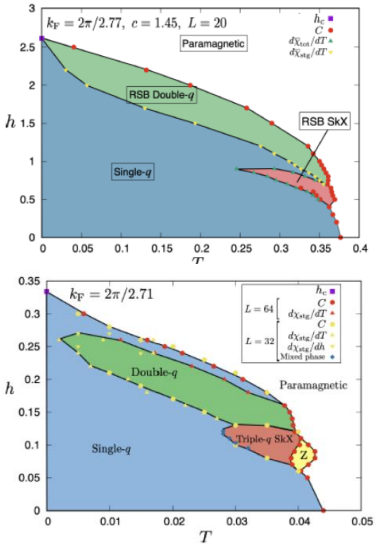

References

[1] T. Okubo, S. Chung and H. Kawamura, Phys. Rev. Letters, **108**, 017206-(1-5) (2012).

[2] K. Mitsumoto and H. Kawamura, Phys. Rev. B **104,** 184432-(1-17) (2021); Phys. Rev. B **105**, 094427(2022).

Topological phases and science of bulk-edge correspondence by numerical methods

Y. Hatsugai
Department of Physics, University of Tsukuba
1-1-1 Tennodai, Tsukuba 305-8571, Ibaraki, Japan

The bulk-edge correspondence[1] is widely used for the studies of topological phenomena in various systems that include not only microscopic quantum systems but also macroscopic classical ones such as photonic crystals and meta-materials. It is a scale-free concept. The abstract mathematical concept of topology is reflected by the physics of boundaries through generic edge states (zero to three-dimensional defects as well). We may further try to discuss various kinds of localized states as a consequence of non-trivial bulk. A typical example is an equatorial wave on earth where the equator is a boundary for the Coriolis force. Collecting such hidden reasons why the boundary states exist, we try to establish a universal view for the localized states in nature and more. This is the science of bulk-edge correspondence. In the current project, we try to apply the viewpoints for various systems using numerical techniques.

Topological pumps focusing on the role of edges are important systems where the bulk-edge correspondence governs the phenomena. We have numerically justified the bulk-edge correspondence of topological pumps for quantum spins and bosons with short-range interactions[2, 3] where a plateau transition analogous to the quantum Hall effects is realized in dimerized high-S quantum spins. Laughlin's argument of the quantum Hall effects can be assumed as a variant of the topological pump where bulk-edge correspondence plays a fundamental role. It is numerically considered for a series of anyons with various statistical parameters associated with the adiabatic heuristic argument[4]. Also, its spinful extension is discussed in details[5].

Fermion quantum Monte Carlo techniques are applied for three dimensional Hubbard model on a pyrochlore lattice where the bulk-corner correspondence has been justified[6]. We further develop bulk-edge correspondence to non-quantum systems. One is heat conduction in 1-dimension[7]. Surprising another example is a bulk-edge correspondence for the evolutional game theory[8] where non-zero Chern number characterizes a boundary flow in the two-dimensional game theory (Figure 1.).

References

[1] Y. Hatsugai, "Chern Number and Edge States in the Integer Quantum Hall effect", Phys. Rev. Lett. 71, 3697 (1993).

[2] Y. Kuno and Y. Hatsugai, "Plateau transitions of a spin pump and bulk-edge correspondence", Phys. Rev. B 104, 045113 (2021).

[3] Y. Kuno and Y. Hatsugai, "Topological pump and bulk-edge-correspondence in an extended Bose-Hubbard model", Phys. Rev. B 104, 125146 (2021).

[4] K. Kudo, Y. Kuno, and Y. Hatsugai, "Bulk-edge correspondence in the adiabatic heuristic principle", Phys. Rev. B **104**, L241113(2021)

[5] K. Kudo and Y. Hatsugai, "Adiabatic Continuity of the Spinful Quantum Hall States", arXiv:2201.07893

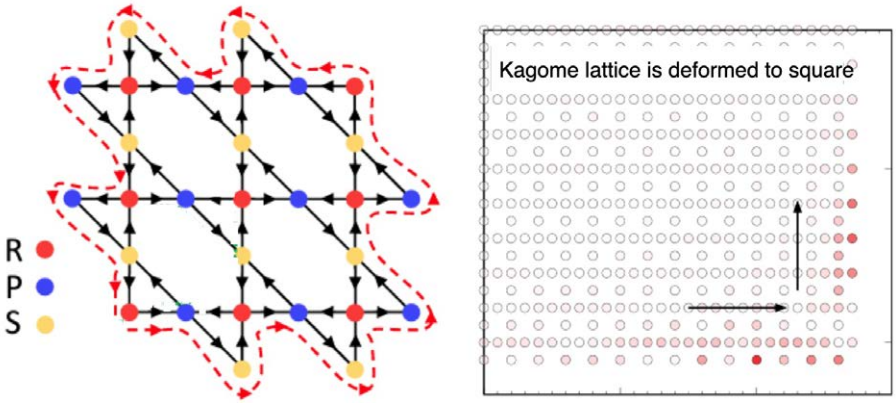

Figure 1: RPS-game on a Kagome lattice (left) and its bundary flow governed by non zero Chern number of the evolutionary game theory (right). (See ref.[8].)

[6] Y. Otsuka, T. Yoshida, K. Kudo, S. Yunoki and Y. Hatsugai , "Higher-order topological Mott insulator on the pyrochlore lattice", Scientific Reports 11, 20270 (2021)

[7] S. Makino, T. Fukui, T. Yoshida and Y. Hatsugai, "Edge states of a diffusion equation in one dimension: Rapid heat conduction to the heat bath", Phys. Rev. E 105, 024137 (2022).

[8] T. Yoshida, T. Mizoguchi, and Y. Hatsugai, "Chiral edge modes in evolutionary game theory: A kagome network of rock-paper-scissors cycles", Phys. Rev. E 104, 025003 (2021).

Molecular dynamics simulation of $BaTiO_3$ nano structure

T. Hashimoto
National Institute of Advanced Industrial Science and Technology (AIST), Tsukuba Central 2, 1-1-1 Umezono, Tsukuba, Ibaraki 305-8568, Japan

Dielectrics clusters have fascinating new properties. It is shown that large off-center displacements of atoms exists even for very small clusters as small as 5 nm, and vortex structures of local polarization vectors could be used as memory devices[1, 2]. However, despite the efforts of preceding studies, the surface termination dependence of the vortex structures and the toroidal moments are not well understood. In this project, we studied these issues by molecular dynamics (MD) simulations using a shell model.

The calculations were performed with the code developed by us. We used a shell model potential developed by Tinte et al.[3, 4]. The calculations were performed under constant (N, V, T) conditions. To simulate isolated clusters, the open circuit boundary condition was used; i.e., we calculated interactions for all the atom pairs in the cluster. The temperature was fixed to 10 K to monitor the structures near the ground state while preventing the system from converging to false structures. We controlled the temperature by the massive Nose-Hoover chain method[5]. For each cluster model, the system was equilibrated for more than 20000 time steps, and data collection runs for more than 100000 time steps followed. One time step was 0.1 fs.

We studied BaO-terminated, TiO_2-terminated, and stoichiometric models. The former model was rounded apex cubic models with eight Ba atoms missing, while the latter two were cubic models. The number of the unit cells on one edge, n, were varied from 3 to 12. The TiO_2 terminated surfaces were unstable, and the TiO_2 terminated clusters were unstable for $n \leq 5$. In all terminations, the toroidal moments become non-zero for clusters larger than $n = 6$. We also studied the toroidal moment direction dependent energy for the BaO-terminated clusters, because they were stable for all n. In these clusters, the structures with the toroidal moments parallel to [111] which are naturally formed in other studies were stable, and structures in which the toroidal moments were parallel to [110] or [001] were metastable. We also analyzed the domain structures inside these clusters. They were found to have domain walls that are known to be stable in the rhombohedral phase.

[1] H. Fu and L. Bellaiche: Phys. Rev. Lett. **91** (2003) 257601.

[2] I. I. Naumov, L. Bellaiche, and H. Fu: Nature **432** (2004) 737.

[3] S. Tinte, M. Stachiotti, S. Phillpot, M. Sepliarsky, D. Wolf, and R. Migoni: J. Phys.: Condens. Matter **16** (2004) 3495.

[4] M. Sepliarsky, A. Asthagiri, S. R. Phillpot, M. G. Stachiotti, and R. L. Migoni: Curr. Opin. Solid. St. M. **9** (2005) 107.

[5] G. Martyna, M. Tuckerman, D. Tobias, and M. Klein: Mol. Phys. **87** (1996) 1117.

DPD simulations of cross-linked networks to study topological effect using MP-SRP method

Katsumi HAGITA,[1] Takahiro MURASHIMA,[2] and Hayato SHIBA[3]

[1]*Department of Applied Physics, National Defense Academy, Yokosuka 239-8686*

[2]*Department of Physics, Tohoku University, Sendai 980-8578*

[3]*Information Technology Center, University of Tokyo, Kashiwa 277-0882*

Ring-linear blends have garnered increasing interest among researchers in recent years for both basic science and industrial applications. In ring–linear blends, a deeper understanding of penetration behaviors among rings and linear chains is important for controlling the mechanical properties of the blends and their applications. Hagita and Murashima [1–4] investigated the dependence between ring size and the penetration of linear chains into the ring through coarse-grained molecular dynamics (CGMD) simulations of the Kremer–Grest (KG) model [5]. They estimated the distribution of the number of chains penetrating a ring by estimating the Gauss linking number (GLN) for all pairs of linear chains and rings. The number n_P of linear chains penetrating a ring was presented as a function of the size of the ring (the number of KG particles in a ring, N_{ring}). These penetration behaviors are governed by the spread and concentration of the ring polymers.

In this study, we investigated the topological effect caused by chain crossing prohibition in ring-linear blends through dissipative particle dynamics (DPD) simulations [6]. Multipoint segmental repulsive potential (MP-SRP) [7] was used to ensure thermodynamic consistency while comparing between the systems that permitted and prohibited chain crossing in DPD polymer simulations. To extract the topological effect of ring polymers, we observed the distribution of penetration in ring–linear blends and the radius of gyration of rings.

Based on a prototype code as an in-house user package of MP-SRP [7] for LAMMPS [8], we remade a public open version of the user package of MP-SRP [7,9]. To reduce computational cost, we improved several implementations as shown in Figure 1. We also confirmed the high scalability in the MPI-based parallel computing.

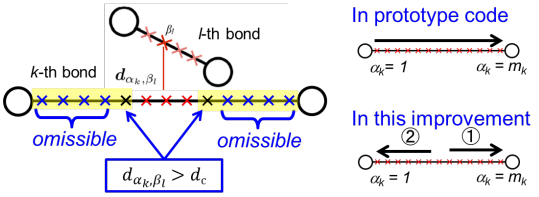

Fig. 1: Schematic of the applied improvement to reduce omissible computations by changing sweep of the SRP points along a bond.

In this study, DPD simulations (MP-SRP and sDPD) of ring–linear blends with a ring fraction of approximately 0.1. Here, sDPD means the standard DPD polymer simulation with the Groot–Warren model [6].

Figure 2 shows the results of (N_{ring}, N_{linear}) = (80, 80), where N_{ring} and N_{linear} denote the number of DPD particles in a ring and in a linear chain, respectively. Compared to the sDPD model, the number of penetrations in the MP-SRP model decreased owing to the prohibition of ring–ring crossing. It should be noted that the penetration state of the initial configuration generated by the push-off procedure was far from equilibrium in both models.

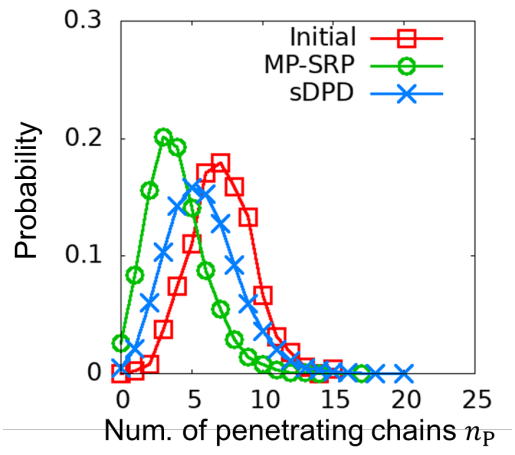

Fig. 2: Probability distributions of linear chains penetrating into a single ring with (N_{linear}, N_{ring}) = (80,80).

We also confirmed the decrease of the squared radius of gyration in comparison to the phantom chain of the sDPD model. The uncatenated rings repel each other because of the topological constraints.

We performed systematic investigations for other values of (N_{ring}, N_{linear}) as shown in the published paper [9]. We concluded that the topological effect prohibits ring–ring crossing, resulting in a small radius of gyration of the rings. In the DPD polymer system with MP-SRP, the minimum size of a ring with penetration was found to be 30, which is less than half of the value of 80 observed in previous work using the Kremer–Grest bead-spring model.

References

[1] K. Hagita and T. Murashima: Polymer **218** (2021) 123493.

[2] K. Hagita and T. Murashima: Polymer **223** (2021) 123705.

[3] K. Hagita and T. Murashima: Macromolecules **54** (2021) 8043-8051.

[4] T. Murashima, K. Hagita, and T. Kawakatsu: Macromolecules **54** (2021) 7210-7225.

[5] K. Kremer and G. S. Grest: J. Chem. Phys. **92** (1990) 5057.

[6] R. D. Groot and P. B. Warren: J. Chem. Phys. **107** (1997) 4423.

[7] N. Iwaoka, K. Hagita and H. Takano: J. Chem. Phys. **149** (2018)114901.

[8] S. Plimpton: J. Comp. Phys. **117** (1995) 117.

[9] K. Hagita, T. Murashima, H. Shiba, N. Iwaoka, and T. Kawakatsu: Comput. Mater. Sci., **203** (2022) 111104.

Kinetics of phase transition and polyamorphism

Kazuhiro Fuchizaki, Hiroki Naruta, and Katsumi Nakamura
Department of Physics, Ehime University, Matsuyama 790-8577

The problem of what drives a liquid-liquid transition motivated us to study entropy estimation for liquids. We first report the results attained in FY2021. The latter part of the report consists of the outcomes obtained from a study of memory hysteresis using machine learning (ML).

The two-phase model's justifiability for entropy estimation [1]

The two-phase model [2] extends the one-phase model for describing the thermodynamics of crystalline phases, regarding them as an aggregate of harmonic oscillators with $3N$ degrees of freedom (DF). Then, the logarithm of the partition function Z is given by $\ln Z = \sum_j \ln z_j$, where z_j is the partition function of the jth oscillator. If the microscopic states are densely distributed to allow a continuum description, we may rewrite this relation as $\ln Z = \int \mathrm{d}\epsilon D(\epsilon) \ln z(\epsilon)$, where $D(\epsilon)$ defines the density of states (DOS) in the energy range between ϵ and $\epsilon + \mathrm{d}\epsilon$. Berens *et al.* [3] prescribed obtaining the DOS from Fourier transforming the velocity autocorrelation function. Thus, the entropy for a solid state may be approximated as $S = k_\mathrm{B} \int_0^\infty \mathrm{d}\omega D(\omega) W_S^\mathrm{HO}(\omega)$, where k_B is Boltzmann's constant. The analytic expression for the entropy spectrum W_S^HO is easily obtainable.

The one-phase model is not applicable to estimating thermodynamic properties of liquid and amorphous states with non-negligible low-frequency modes of $D(\omega)$. Goddard *et al.* [2] have constructed the two-phase model based on their intuitive observation that the DOS of such non-crystalline systems looks like a superposition of DOSs of solid and gas states. They introduced the notion "fluidicity" f, in terms of which the DOS of non-crystalline systems could be divided into $3Nf$ DFs of gas component D^g and remaining crystalline component D^s. Thus, the two-phase model modifies the above expression for the entropy as

$$S/k_\mathrm{B} = \int_0^\infty \mathrm{d}\omega\, D^\mathrm{g}(\omega|f) W_S^\mathrm{g}(\omega) + \int_0^\infty \mathrm{d}\omega\, D^\mathrm{s}(\omega|1-f) W_S^\mathrm{HO}(\omega). \quad (1)$$

Goddard *et al.* [2] assumed a hard-sphere gas to evaluate D^g and W_S^g. For W_S^g, they employed the entropy per DF for a HS system W_S^HS obtainable from the Carnahan–Starling (CS) equation of state (EOS), whereas they invoked the Chapman–Enskog (CE) theory to settle the expression for D^g. The CE theory also allowed them to determine f. Thus, if the actual DOS $D(\omega)$ is available from experiments or simulations, Eq. (1) gives us an entropy estimate by putting $D^\mathrm{s} = D - D^\mathrm{g}$.

We employed a simple liquid whose thermodynamic properties are well studied to test the two-phase model's prediction. Thus, we chose the modified Lennard-Jones system [4] with 2048 particles, to which we conducted isothermal–isochore molecular dynamics simulation at slightly above the critical temperature. We adopted three densities; one was the critical density ρ_c, and the other two are below and above ρ_c. We used the λ- and thermodynamic integrations to estimate the entropies precisely. We calculated the entropy also from the modified Benedict–Webb–Rubin EOS [5].

The entropies resulting from the former three approaches coincided within the error margin. However, the two-phase model

gave systematically lower entropies than those three. The deviation increases with density. However, the most significant deviation was limited to 6% at the highest density examined. Because both the CS EOS and the CE theory would not be appropriate to capture such a high-density liquid (even though simple), many factors employed in the two-phase model would cancel to attain such an accuracy. Unfortunately, because the two-phase model was constructed in an ad-hoc way, we cannot give any suggestions to improve it at this moment.

Judging the (dis)continuity of phase transition using ML [7]

Based on the valuable discovery that the sum of weights $W_{\rm sum}$ in a convolutional neural network (CNN) behaves like an order parameter when it learns spin configurations of a 2-dimensional Ising system as a function of (inverse) temperature, we have proposed a method to detect the phase-transition point at an early stage of learning processes. The latter work prompted us to consider whether a CNN can judge the order of phase transition from the viewpoint of memory hysteresis.

When we see a series of continuously changing pictures from, say, A to B, we notice a salient change at C on its way. However, when we view the same series in reverse order from B to A, the noticeable point of change does not necessarily coincide with C. This hysteresis may be related to the mechanism of our short-term memory equipped with our brain. A CNN could already implement such a mechanism. Thus, it will exhibit a hysteretic behavior depending on an impetus applied through a learning process.

Here we only outline what we examined. We used the same CNN as employed in [6]. However, the crucial difference was the way of learning. In [6], learning data has been input randomly, as usually employed in ML. This time, the data was input in order of increasing (decreasing) magnitude of external parameters such as magnetic field and temperature. Under various magnetic fields, we prepared equilibrium spin configurations of the 2-dimensional 64×64 Ising system below and above the critical temperature. We also made equilibrium patterns of 256 q-state Potts model for $q = 3$ through 7 at various temperatures below and above the critical temperature. System B took care of generating these data sets.

In all of the cases examined, for a discontinuous phase transition, a sharp peak showed up precisely at the transition point when $W_{\rm sum}$ was plotted as a function of the external parameter, regardless of the direction of its change. In contrast, $W_{\rm sum}$ offered a rounded peak for a continuous transition with the peak position shifted as if the CNN missed the exact transition point, leaving a clear-cut hysteresis against a cyclic change of the external parameter. We thus conclude that our approach will be applicable to judge the order of a general phase transition if the learning data are available.

References

[1] H. Naruta and K. Fuchizaki: to be presented at The 18th International Conference on Liquid and Amorphous Metals.

[2] S-T. Lin, M. Blanco, and W. A. Goddard: J. Chem. Phys. **119** (2003) 11792.

[3] P. H. Berens, D. H. J. Mackay, G. M. White, and K. R. Wilson: J. Chem. **79** (1983) 2375.

[4] Y. Asano and K. Fuchizaki: J. Chem. Phys. **137** (2012) 174502.

[5] Y. Asano and K. Fuchizaki: J. Phys. Soc. Jpn. **86** (2014) 034601.

[6] K. Fuchizaki, K. Nakamura, and D. Hiroi: J. Phys. Soc. Jpn. **90** (2021) 055001.

[7] K. Nakamura and K. Fuchizaki: in preparation.

Three-Dimensional Finite Element Analysis of Friction between solids

Michio OTSUKI

Graduate School of Engineering Science, Osaka University,

Osaka University, Kashiwa-no-ha, Kashiwa, Chiba 277-8581

According to Amontons' law, the maximum static friction force of a solid object is proportional to the applied loading force and independent of the apparent contact area, which indicates that the static friction coefficient does not depend on the applied pressure and the shape of the solid. Previous studies have clarified that Amontons' law systematically breaks down for macroscopic objects due to precursor slip before the onset of bulk sliding [1], which is consistent with experiments [2]. However, the analysis in the previous works is restricted to 2D systems. Therefore, it is not clear whether the result is applicable to more realistic 3D systems.

This year, we numerically investigate the sliding motion of a 3D viscoelastic object with length L, width W, height H, and Young's modulus E on a solid substrate using the finite element method (FEM) with 500,000 nodes by MPI of 1000 processors, as shown in Fig. 1. A rigid rod slowly pushes the object with a constant velocity. A uniform pressure P_{ext} is applied to the top of the object. The friction force at the bottom locally satisfies Amontons' law with the local static and kinetic friction coefficients μ_{S} and μ_{K}, respectively.

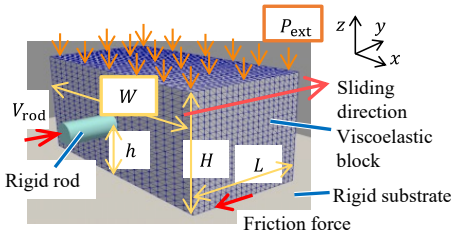

Fig. 1: Schematic of the 3D FEM calculation.

The object exhibits macroscopic stick-slip motions, which are characterized by the macroscopic static friction coefficient μ_{M}. μ_{M} decreases with the external pressure P_{ext} and the width W, as shown in Fig. 2, which contradicts Amontons' law. We also find that quasi-static precursor slip occurs in the 2D interface between the object and the substrate before bulk sliding, which is related to the decrease of μ_{M}.

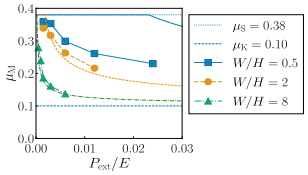

Fig. 2: Static friction coefficient μ_M against

References

[1] M. Otsuki and H. Matsukawa: Sci. Rep. **3** (2013) 1586.

[2] Y. Katano. et al.: Sci. Rep. **4** (2014) 6324

Constructing a Dataset of Dielectric and Thermal Properties of Polymeric Materials

Yuta YOSHIMOTO

Department of Mechanical Engineering,

The University of Tokyo, 7-3-1 Hongo, Bunkyo-ku, Tokyo 113-8656

We have constructed a dataset of dielectric and thermal properties of polymeric materials using quantum chemical (QC) calculations and molecular dynamics (MD) simulations. Seventy-seven polymer systems are constructed from the repeating units of previously synthesized polymers [1,2], where atomic charges are derived from QC calculations using the Gaussian 16 electronic structure package [3] and MD simulations are performed using the LAMMPS software package [4]. All calculations are automated using RadonPy [5] and performed on System B (ohtaka).

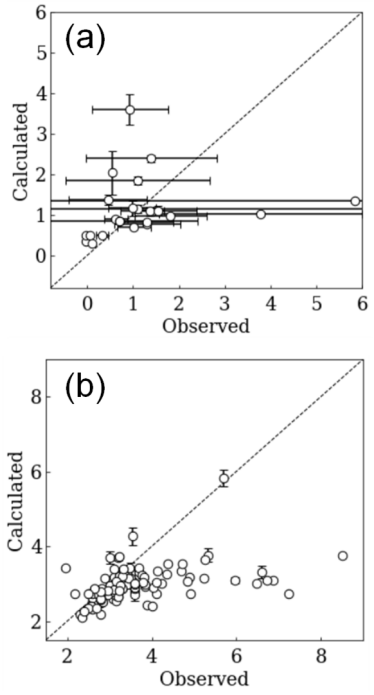

Fig. 1: Comparison of calculated and experimental values for coefficients of linear thermal expansion [10^{-4}/K] (a) and static dielectric constants (b).

Figure 1(a) compares calculated and experimental values of coefficients of linear thermal expansion, exhibiting a weakly linear relation between them, although the experimental values have large uncertainties. Calculated static dielectric constants also show reasonable agreements with the experimental values except for several polymers, as shown in Fig. 1(b). These results validate our simulation methodology, although more thorough investigation is required to further improve the predictive performance.

References

[1] L. Chen et al.: npj Comput. Mater. **6** (2020) 61.

[2] S. Otsuka et al.: Int. Conf. on Emerging Intelligent Data and Web Technologies (2011) 22.

[3] M. J. Frisch et al.: Gaussian 16, Revision C.01 (2019).

[4] A. P. Thompson et al.: Comput. Phys. Commun. **271** (2022) 108171.

[5] Y. Hayashi et al.: arXiv:2203.14090 (2022).

Nanoscale phonon transport across ceramics interfaces

Susumu FUJII
Division of Materials and Manufacturing Science, Osaka University
Yamadaoka, Suita, Osaka, 565-0871
Nanostructures Research Laboratory, Japan Fine Ceramics Center
Mutsuno, Atsuta, Nagoya 456-8587

Lattice thermal conductivity is a fundamental property of materials, which is important for a wide spectrum of applications, e.g., thermoelectrics, thermal barrier coatings, and electronic devices. Interfaces embedded in materials, such as grain boundaries and heterogeneous interfaces, are known to significantly suppress lattice thermal conduction because of their distinguished atomic/electronic structures from the corresponding crystal, which induce the scattering of group motion of atoms, i.e., phonons. Recently, miniaturization of electronic devices and development of nanostructuring techniques have led to an increase of number of cases in which the interfaces are the rate-limiting factor for the thermal conduction in materials. For more precise control of thermal conductivity, it is necessary to reveal the mechanisms of thermal transport across interfaces from the microscopic point of view. However, there are few studies that quantitatively reveal the correlations between interfacial atomic structures and thermal conduction, and that investigate the scattering mechanisms of phonons at interfaces. The main obstacles are follows: (1) the lack of method to quantitatively connect the structure and thermal conduction; and (2) the lack of method to evaluate thermal conductivity of local structure at atomic-scale.

In this project, we have attempted to elucidate the microscopic mechanisms of interfacial thermal transport by using two kinds of molecular dynamics simulations. One is the perturbed molecular dynamics simulations, in which atomic contributions to overall lattice thermal conduction (atomic thermal conductivity) can be estimated. The other is the phonon wave packet simulations, in which transmission coefficient of individual phonons can be estimated. Combinations of these two methods can provide the insights of interfacial phonon scattering from the phenomenological and theoretical perspectives. The necessary codes were developed by the author and implemented to the Large-scale Atomic/Molecular Massively Parallel Simulator (LAMMPS) [1]. We chose grain boundaries of crystalline silicons and interfaces between (1) crystalline silicon and amorphous silica (SiO_2) and (2) crystalline and amorphous silicons as model systems, because it has many technologically important applications.

For silicon grain boundaries, we used a machine learning potential for Si distributed in MACHINE LEARNING POTENTIAL REPOSITORY [2], which accurately reproduce the results of *ab initio* calculations but are less computationally demanding. Thermal conductivity calculations using perturbed molecular dynamics require a large computational cells with at least a few thousands of atoms, with the time steps of more than one million. Such large-scale calculations were per-

formed with five different magnitudes of perturbations for each grain boundary, to obtain the thermal conductivity with high statistical accuracy. The results indicates that thermal conductivity of Si grain boundaries highly depends on their microscopic atomic structures as well as their crystal misorientations, as shown in Fig. 1 [3]. On the other hand, phonon wave packet simulations shows that acoustic phonons mainly conduct heat across interfaces and the transmission coefficients are not significantly different between the grain boundaries with different crystal orientation and/or atomic structures. This indicates that anharmonic nature of atomic vibrations at grain boundaries, which is naturally included in the perturbed molecular dynamics but is intentionally excluded in the phonon wave packet simulations, determines the interfacial thermal conduction. Additional calculations for 18 silicon grain boundaries suggest that bond strains induced by the open-core structures of silicon grain boundaries highly correlate with the reduction of atomic thermal conductivities, which should be related with the magnitude of anhamonicity.

For heterogenious interfaces between crystalline and amorphous silica, we have performed a large number of perturbed molecular dynamics and phonon wave packet simulations, by using an empirical Tersoff potential, which is less computationally demanding than the machine learning potential. The computational cells typically contains about a million of atoms for phonon wave packet simulations. It was found that the transmission coefficients of acoustic phonons dramatically decrease as a function of the thickness of amorphous SiO_2 layer, resulting in very low thermal conductivity. The significant amount of reflected phonons at the interface make the spatial depdendence of thermal conductivity even in the crystalline silicon. Comparisons with the interfaces between crystalline and amorphous silicons indicates that compositional differences between two materials enhance the scattering and reflection of phonons at the interfaces, because of the mismatch of phonon frequencies between the two adjoined materials.

All the molecular dynamics calculations were performed in a single node rather than multiple nodes. This is because it is necessary to perform many calculations with different structures and different conditions, and performing calculations on a single node is more efficient than parallel.

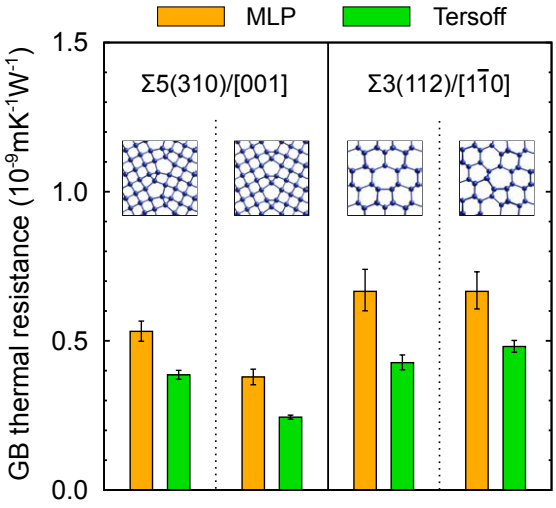

Figure 1: Interfacial thermal resistances of Σ5(310) and Σ3(112) grain boundaries estimated by perturbed molecular dynamics simulations, with the machine learning potentinal (MLP) and an empirical atomic potential (Tersoff) [3]. The results of two different atomic sturctures are shown for each grain orientation.

References

[1] S. Plimpton, J. Comput. Phys. **117** (1995) 1.

[2] A. Seko, arXiv:2007.14206.

[3] S. Fujii, A. Seko, Comput. Mater. Sci. **204** (2022) 111137.

Numerical Study of Spin Systems on the Honeycomb Lattice

Chitoshi YASUDA
Department of Physics and Earth Sciences, Faculty of Science, University of the Ryukyus, Okinawa 903-0213, Japan

The quasi-two-dimensional (quasi-2D) antiferromagnetic Heisenberg (AFH) model on a cubic lattice consisting of the nearest-neighbor intra-layer ($J = 1$) and inter-layer (J') interactions has a finite-temperature phase transition at which the critical behavior belongs to the universality class same as the three-dimensional classical Heisenberg system. In the previous work [1] on the quasi-2D square-lattice AFH model using the quantum Monte Carlo method, it was numerically found that the Néel temperature $T_{\rm N}$ obeys an universal relation between J' and the staggered susceptibility $\chi_{\rm s}(T_{\rm N})$ of the 2D system on the square lattice, i.e., besides an effective coordination number defined by $\zeta(J') \equiv 1/(J'\chi_{\rm s}(T_{\rm N}(J')))$ does not depend on J' for $J' \leq 0.02$, the value becomes $\zeta(J') \approx 0.65z$ ($z = 2$) all for $S = 1/2$, 1 and ∞. The universal relation has also been predicted by an analysis of the quantum nonlinear sigma model [2].

In this project, we research the renormalized coordination number in the quasi-2D honeycomb lattice AFH model with spin $S = 1/2$ using the quantum Monte Carlo method with the continuous imaginary-time loop algorithm, and compare the results with those of the square lattice to investigate the universality. The Néel temperatures were evaluated by finite-size scaling analysis using data up to the system size $80 \times 40 \times 40$, and it was confirmed that there is a relation $T_N \propto 1/(b - \ln(J'))$. Here, b is a constant. We have also estimated the renormalized coordination numbers by evaluating the staggered susceptibility on the honeycomb lattice at the Néel temperature. Our results suggest that $\zeta/z \approx 0.65$ in the small J' region. The consistent value of ζ/z in the square and honeycomb lattices indicates that ζ is a universal quantity independent of the lattice. However, the accuracy of the result for the smallest J', $J' = 0.001$, is not yet sufficient, and further calculations for larger sizes might be needed in the future. Hastings *et al.* have proposed that there exists a universal function even in the region of J' larger than J' where ζ is constant [2]. Our results suggest that there is one lattice-independent function $\zeta(J')$ at $J' = 0.05$ and 0.1.

In this project, we also research zinc phthalocyanine ($ZnC_{32}N_8H_{16}$(ZnPc)) and the fluorinated ZnPc ($ZnC_{32}N_8F_{16}$ (F_{16}ZnPc)) consisting of hexagon as with the honeycomb lattice as testing calculations for the density functional method using the program package VASP. The compound ZnPc is an aromatic compound composed of four isoindoline units (C_8H_4N) consisting of a six-membered ring of benzene bonded to hydrogen and a five-membered ring containing nitrogen. We confirmed that the energy levels of F_{16}ZnPc are deeper than those of ZnPc. The numerical result corresponds to the electron-accepting property of F_{16}ZnPc and the electron-releasing property of ZnPc.

References

[1] C. Yasuda *et al*, Phys. Rev. Lett. **94** (2005) 217201.

[2] M. B. Hastings and C. Mudry, Phys. Rev. Lett. **96** (2006) 027215.

Data analysis method using a tensor network representation

KENJI HARADA
Graduate School of Informatics, Kyoto University, Kyoto 606-8501, Japan

We study data analysis methods based on tensor network representations in this study project.

The first topic is quantum machine learning. Using tensor network schemes, we numerically study the relationship between the performance of a quantum circuit and the entanglement properties. In particular, the quantum circuits on a tree tensor network structure can be efficiently estimated about the entanglement capability[1]. We found that a quantum circuit with a high entanglement capability shows good performance in a classification problem until some hundred qubit cases. Therefore, the entanglement capability is an important property for estimating performance[2]. In this study, we use the system B for calculation of a tensor contraction to estimate the entanglement capability through tensor network representations.

The second topic is tensorized neural networks[3]. A tensor network as MPO represents the weight matrix in a neural network. We numerically evaluate the profile of an entanglement property in MPO in the learning process. It much depends on the initial tensors in MPO[4]. We derive a stable initialization method for MPO in the tensorized neural network. The deeper tensorized neural network can also be stably converged by the initialization. In this study, we use the system B for the systematic calculation of the profile of entanglement in MPO in the learning process.

[1] S. Sim, Peter D. Johnson, and Alán Aspuru-Guzik, Expressibility and entangling capability of parameterized quantum circuits for hybrid quantum-classical algorithms. Advanced Quantum Technologies 2, 1900070 (2019).

[2] H. Manabe and K. Harada, Quantum circuit learning with tensor network structure, 23pA1-1, JPS Autumn meeting (2021).

[3] A. Novikov, D. Podoprikhin, A. Osokin, D. Vetrov, Tensorizing Neural Networks, NIPS 2015.

[4] Y. Asoshina and K. Harada, Entanglement Analysis of Neural Networks, 22pL4-9, JPS Autumn meeting (2021).

Numerical Analysis for Stability and Dynamics of Magnetic Structures such as Skyrmions

Kenji KONDO

Research Institute for Electronic Science, Hokkaido University, Sapporo, Hokkaido, 001-0020.

Magnetic skyrmions are expected to be promising candidates for representing and transferring one bit of information. This is because they are topologically protected from external perturbations, which ensures the stability of information. Moreover, they are very small in size and they are able to be driven using the current. In this study, we utilize the spin dynamics code *"Spirit"* [1] which can incorporate the demagnetization fields or can calculate three-dimensional magnetic structures in order to perform the numerical calculations of the dynamics of topological magnetic structures such as skyrmions. In our previous work, we investigated the dynamics of skyrmions driven by the spin polarized current [2,3] using a handmade finite-element-method (FEM) program. At that time, we did not take the demagnetization fields into consideration since we considered the influence to be negligible. Also, there was an aspect that we avoided considering the demagnetization fields since it takes much time to calculate them. Thus, in this study, we investigate the influence on the velocities of the skyrmions with the demagnetization fields or without them using *Spirit*. Figure 1 shows the current density dependences of the average velocities of the skyrmions in the ferromagnets (FMs) driven by the spin-transfer torque (STT) with the demagnetization fields or without them. In this calculation, we assume Co thin film as the FM and use the material parameters of the FM from the references [4–6]. The blue and the red lines represent the average velocities of the skyrmions in the FMs with and without the demagnetization fields, respectively. It is found that the existence or the non-existence of the demagnetization fields have only 3.729% influences on the velocities of the skyrmions, which is almost negligible. Our previous estimation of the influences on the velocities of the skyrmions is found to be right. On the other hand, we investigate the dynamics of three-dimensional topological magnetic structures, so-called skyrmion strings, using *Spirit*. The skyrmions can form string structures by spreading in the out-of-plane direction. Especially, we investigate the differences of the skyrmion string structures under the positive and negative Dzyaloshinskii-Moriya interaction (DMI) constants. The signs of DMI constants are defined in Fig. 2. When the DMI vectors point outwards, we define the DMI constant as positive. When the DMI vectors point inwards, we define the DMI constant as negative. Figures 2(a) and 2(b) show the skyrmion string structures in the FMs in the cases of the positive and negative DMI constants, respectively. It is found that the directions of the magnetization vectors of the skyrmion strings are counterclockwise and clockwise when seeing from the top view in the cases of the positive and negative DMI constants, respectively. Figures 3(a)-3(c) show the contour plots of the x, y, and z components of the effective magnetic fields H_{eff} in the case of the positive DMI constant, respectively. Moreover, figures 3(d)-3(f) show the contour plots of the x, y, and z components of H_{eff} in the case of the negative DMI constant, respectively. Comparing these results, it is found that the effective magnetic fields H_{eff} point to the opposite directions in the xy-plane.

Therefore, the positive and negative DMI constants cause the magnetization vectors of the skyrmion strings to point to the opposite directions in the xy-plane. As a result, there manifest themselves the counterclockwise skyrmion strings and the clockwise skyrmion strings depending on the signs of DMI constants. It took approximately one month to perform all of these calculations as the computer run time using the ISSP supercomputer system B (Ohtaka). Also, we have calculated the dynamics of the logic gates consisting of the skyrmions in the antiferromagnets, which we will not state here in detail. We are preparing the paper concerning the logic gates consisting of the skyrmions in the antiferromagnets.

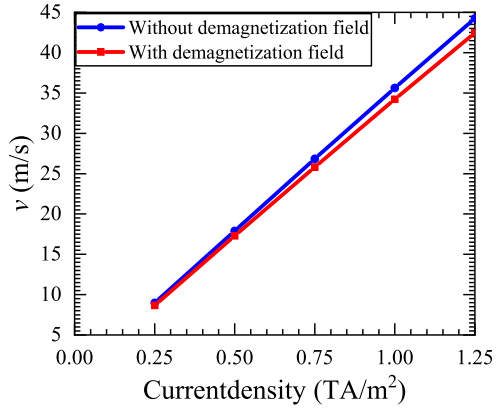

Fig. 1: The current density dependences of the average velocities of the skyrmions in the FMs with the demagnetization fields or without them.

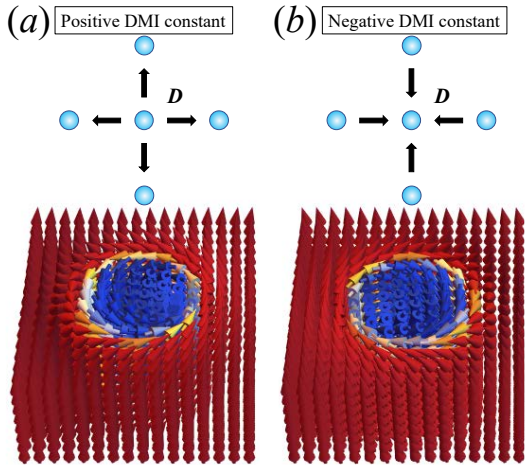

Fig. 2: The 3D vector plots of the skyrmion string structures in the FMs in the cases of (a) the positive and (b) the negative DMI constants.

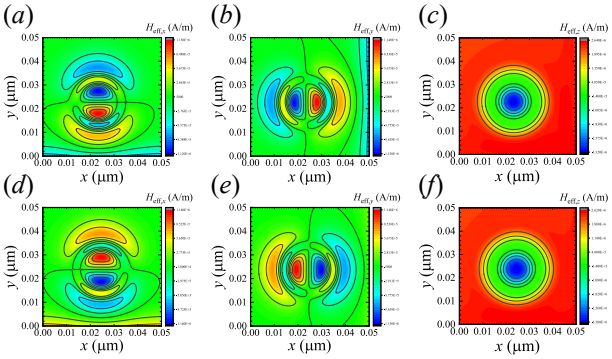

Fig. 3: The contour plots of the x, y, and z components of $H_{\rm eff}$ of skyrmion strings are shown in figures (a)-(c) in the case of the positive DMI constant, respectively. The contour plots of the x, y, and z components of $H_{\rm eff}$ of skyrmion strings are shown in figures (d)-(f) in the case of the negative DMI constant, respectively.

References

[1] G. P. Müller, M. Hoffmann, C. Dißelkamp, D. Schürhoff, S. Mavros, M. Sallermann, N. S. Kiselev. H. Jónsson, and S. Blügel, Phys. Rev. B. **99**, 224414 (2019).

[2] Y. Ishida and K. Kondo, J. Magn. Magn. Mater. **493**, 165687 (2020).

[3] Y. Ishida and K. Kondo, Jpn. J. Appl. Phys. **59**, SGGI04 (2020).

[4] J. Sampaio, V. Cros, S. Rohart, A. Thiaville, and A. Fert, Nat. Nanotechnology. **8**, 839-844 (2013).

[5] L. S. E. Alvarez, K.-Y. Wang, S. Lepadatu, S. Landi, S. J. Bending, and C. H. Marrows, Phys. Rev. Lett. **104**, 137205 (2010).

[6] D. J. Monsma and S. S. P. Parkin, Appl. Phys. Lett. **77**, 883 (2000).

Numerical study on low-energy states of quantum spin systems

Hiroki NAKANO
Graduate School of Science, University of Hyogo
Kouto, Kamigori, Hyogo 678-1297, Japan

Many-body problems have to been tackled in the field of the condensed matter physics; therefore, it is difficult to estimate physical quantities precisely in many cases. Quantum spin systems are such a typical one. To investigate these systems, numerical approaches have widely and effectively been used. A lot of computational studies have been carried out; useful information of the target systems has been provided.

Generally speaking, three methods are effectively used within the Field of quantum spin systems. The first and traditional one is the numerical diagonalization method; the second is the quantum Monte Carlo (QMC) method. The third method is the density matrix renormalization group (DMRG) method. Each of them has some advantages; on the other hand, it has disadvantages, too. The QMC simulations can treat significantly large systems irrespective of the spatial dimensions of the systems; however, the negative sign problem in this approach prevent us with a difficulty in precise evaluation of physical quantities in frustrated systems. The DMRG method is a very useful method for a one-dimensional system irrespective of whether the target system includes frustration or not. However, this method is still under development for the cases when the spatial dimension is larger than one. The numerical diagonalization method can be applicable irrespective of the presence of frustrations and the spatial dimension. This method, on the other hand, has a severe weak point that it can treat only very small system sizes. To overcome this disadvantage of the numerical diagonalization, we developed a hybrid-type parallelized code of Lanczos diagonalization[1]. This code enables us to treat various large systems that have not been previously treated yet within this method and to evaluate physical quantities precisely. Therefore, we examine various quantum spin systems by this method as a primary approach in this project.

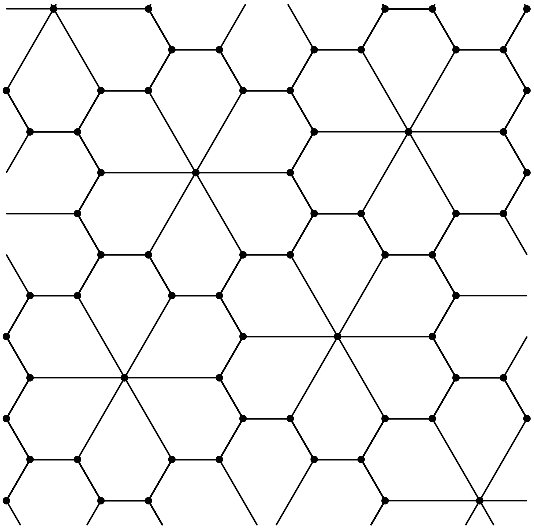

Figure 1: Floret-pentagonal lattice.

In the project in 2021, we tackled the $S = 1/2$ Heisenberg antiferromagnet on the floret-pentagonal lattice[5]. Among pentagonal lattices, studies concerning the Cairo-pentagonal-lattice antiferromagnet has been known[2, 3, 4]. However, the floret-pentagonal-lattice an-

tiferromagnet has not been investigated to the best of our knowledge; this system is the second example as pentagonal lattices that include equivalent two directions in the system. (See Fig.1.) We have observed the magnetization process of this system and find magnetization plateaux at one-ninth height of the saturation magnetization, at one-third height, and at seven-ninth height. We have also discovered a magnetization jump between the one-third-height and seven-ninth-height plateaux. The jump is a peculiar phenomenon because this jump is away from the two plateaux. Our study contributes much to our deeper understandings of the frustrated quantum antiferromagnets. Further investigations would clarify nontrivial quantum effects due to frustration.

References

[1] H. Nakano and A. Terai: J. Phys. Soc. Jpn. **78**, 014003 (2009).

[2] I. Rousochatzakis, A. M. Läuchli and R. Moessner: Phys. Rev. B **85**, 104415 (2012).

[3] H. Nakano, M. Isoda, and T. Sakai: J. Phys. Soc. Jpn. **83**, 053702 (2014).

[4] M. Isoda, H. Nakano, and T. Sakai: J. Phys. Soc. Jpn. **83**, 084710 (2014).

[5] R. Furuchi, H. Nakano, N. Todoroki, and T. Sakai: J. Phys. Commun. **5**, 125008 (2021).

Development of the Low-Temperature Oxidation Model for Alternative Fuels Using Machine Learning

Minhyeok LEE, Tomotaka MIZUNO, and Yuji SUZUKI

Department of Mechanical Engineering, School of Engineering,

The University of Tokyo, 7-3-1 Hongo, Bunkyo-ku, Tokyo 113-8656

To improve thermal efficiencies and reduce pollutant emissions of Internal Combustion engines simultaneously, it is crucial to understand the detailed reaction mechanism of fuels. Recently, various reaction kinetic models have been proposed to precisely explain the reaction process of the target fuel. However, as shown in Fig. 1, as increasing the size of the fuel molecule, the number of reactions involved is increased exponentially. It makes hard to solve the entire model numerically without reducing the reaction size due to high computational costs. Note that such model reduction causes a decrease in accuracy of the numerical estimation, particularly in the low-temperature region [1]. Therefore, we conducted numerical simulations with full mechanisms by means of the supercomputer system at ISSP to evaluate the ignition process of cool flames.

One-dimensional axisymmetric stagnation flows formed by impinging a mixture of fuel and air on a heated wall were assumed. The nozzle-to-wall distance was 15 mm. The outlet velocity, temperature, and equivalence ratio of the fuel/air mixture were 50 cm/s, 300 K, and 1, respectively. The wall temperature was ramped up from 600 K to 850 K under the quasi-steady state. Normal-heptane (n-C_7H_{16}) and -decane (n-$C_{10}H_{22}$) were used as the fuel. Two reaction models including both fuels were used, which respectively proposed by the CRECK modeling group [2]

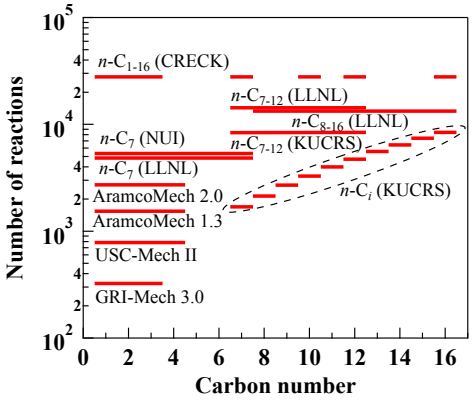

Fig. 1: Reaction size of various kinetic models for normal-alkane fuels.

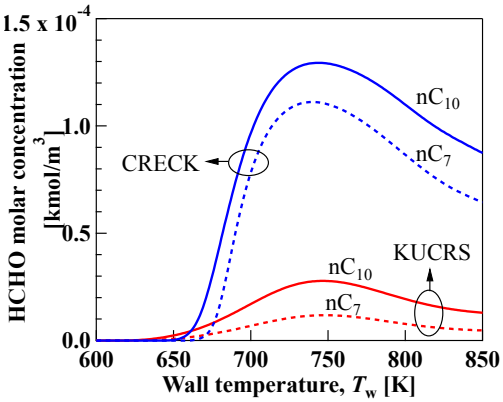

Fig. 2: Cool flame ignition of n-C_7 and n-C_{10}.

and generated by using the KUCRS (Knowledge-basing utilities for complex reaction systems) [3]. The Cantera code [4] was employed to conduct numerical simulation under the above condition.

As increasing the wall temperature, cool flames are ignited on the wall due to initiation of the low-temperature oxidation. Figure 2 shows increases of the calculated HCHO molar concentration on the wall as a function of the wall temperature. While the HCHO concentration estimated by the CRECK model is higher, the onset temperature calculated by the KUCRS model is slightly lower for both fuels. Furthermore, a difference in the onset temperature between two fuel is negligible for the KUCRS model, but *n*-decane's onset temperature is approximately 12 K lower than that of *n*-heptane in the CRECK model. It means that two models show the discrepancy in estimating not only the low- and intermediate-temperature reactivity of each fuel, but also hierarchical difference with respect to the molecule (chain) size.

Further improvements in the reaction model should be made through the experimental validation.

References

[1] C.B. Reuter, M. Lee, S.H. Won, Y. Ju: Combust. Flame **179** (2017) 23.

[2] A. Miyoshi: KUCRS software library, http://akrmys.com/KUCRS/

[3] The CRECK Modeling Group: http://creckmodeling.chem.polimi.it

[4] D.G. Goodwin, R.L. Speth, H.K. Moffat, B.W. Weber: Cantera: An object-oriented software toolkit for chemical kinetics, thermodynamics, and transport processes, https://www.cantera.org

Formation of Lipid Rafts Studied by Molecular Dynamics Simulation

Satoru G. ITOH

Institute for Molecular Science, Okazaki, Aichi 444-8787

Exploratory Research Center on Life and Living Systems, Okazaki, Aichi 444-8787

The Graduate University for Advanced Studies, Okazaki, Aichi 444-8787

In cell membranes, lipid rafts are formed by aggregation of sphingolipids and cholesterol molecules [1]. It has been clarified that lipid rafts play important roles in functions such as signal transduction and protein transport in vivo [2,3]. Lipid rafts are also related to virus infection and protein aggregation [4,5]. It is essential to elucidate their structures and formation processes to understand their functions. Therefore, we aim to elucidate these by using molecular dynamics (MD) simulation. In particular, we are interested in lipid rafts containing GM1 gangliosides, which are abundant in nerve cell membranes. To investigate the structure of GM1 ganglioside clusters, we employed the Coulomb replica-permutation molecular dynamics simulation [6]. The Coulomb replica-permutation method is one of the Hamiltonian replica-permutation methods, and it is possible to efficiently investigate the complex structure of biomolecules by using this method.

In the last year, we have made significant improvements to our own program to be able to perform MD simulations with various force fields for the all-atom model. We have also made it possible to perform MD simulations on molecules other than proteins. In addition, the program has been modified to allow the Coulomb replica-permutation method to scale only the intermolecular electrostatic interactions between GM1 ganglioside molecules.

References

[1] K. Simons and E. Ikonen: Nature **387** (1997) 569.

[2] K. Simons and D. Toomre: Nat. Rev. Mol. Cell Biol. **1**, (2000) 31.

[3] D. Lingwood and K. Simons: Sience **327** (2010) 46.

[4] N. Chazal and D. Gerlier: Microbiol. Mol. Biol. Rev. **67** (2003) 226.

[5] J. M. Cordy, N. M. Hooper and A. J. Turner: Mol. Membr. Biol. 23 (2006) 111.

[6] S. G. Itoh and H. Okumura: J. Comput. Chem. **34** (2013) 2493.

Numerical calculation of spin Hall magnetoresistance by the quantum Monte Carlo method

Takeo KATO
Institute for Solid State Physics, University of Tokyo
Kashiwa-no-ha, Kashiwa, Chiba 277-8581

Spin Hall magnetoresistance (SMR), that is a magnetoresistance caused by the absorption of spin current generated by the spin Hall effect in a bilayer system composed of a metal and a magnetic insulator [1], is being actively studied for potential applications in spintronics devices such as memory applications. Although SMR is well described quantitatively by a phenomenological theory [2], its temperature dependence for a metal/antiferromagnetic-insulator bilayer system [3] are difficult to be described by it.

In this numerical study, we evaluate the spin conductance at the interface by expanding the theory of Ref. [4]. The spin current is expressed in terms of the spin susceptibility of the antiferromagnetic insulator and is calculated by the quantum Monte Carlo method. In order to obtain dynamic properites, we need to perform the numerical analytic continuation. However, this is usually an ill-defined probpem and is difficult to be applied for obtaining the spin conductance. We improved the method to stably obtain the spin conductance using only the component of Matsubara frequency of Green's function and succeeded in its accurate calculation.

As a result of examining the temperature dependence and the thickness dependence of the SMR, the sign was reversed as the rising temperature rose in the negative sign from the low temperature region, and the result agreed with the experimental result with the peak of the positive sign. In addition, it was confirmed that the behavior of SMR differed depending on the size of the spin of the antiferromagnetic insulator, and that SMR at $S = 1$ was larger than $S = 1/2$. We also showed that SMR vanishes above the magnetic transition temperature unlike the experiment. We are now preparing for a paper on these results [5].

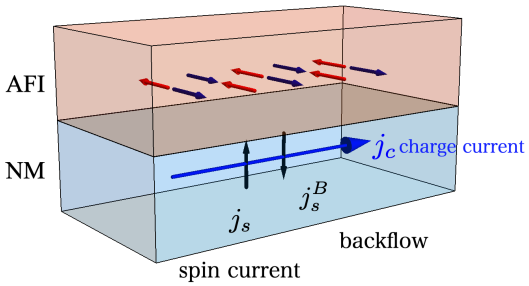

Figure 1: SMR Measurement Setup.

References

[1] H. Nakayama, et al., Phys. Rev. Lett. **110**, 206601 (2013).

[2] Y. T. Chen, et al., Phys. Rev. B **87**, 144411(2013).

[3] D. Hou, et al., Phys. Rev. Lett. **118**, 147202 (2017).

[4] T. Kato, Y. Ohnuma, and M. Matsuo, Phys. Rev. B **102**, 094437(2020).

[5] T. Ishikawa, M. Matsuo, and T. Kato in preparation.

Dynamical property of a resistively shunted Josephson junction

Tsuyoshi Yamamoto
Institute for Solid State Physics, University of Tokyo
Kashiwa-no-ha, Kashiwa, Chiba 277-8581

Physical properties of quantum systems are drastically changed by interaction with an environment, because thousand of modes in the environment are complexly entangled with quantum states of systems. A typical example is the Kondo problem, in which a spin of a magnetic impurity is screened by surrounding conduction electrons in a normal metal [1]. Such kind of a dissipative system has been a central topic of condensed matter physics for a long time.

One of the most notable problems in dissipative systems is a dissipation-driven quantum phase transition. In 1983, Schmid predicted that a single Josephson junction connected to a resistance, which is called the resistively shunted Josephson junction (RSJJ), undergoes a superconductor-insulator transition at zero temperature [2]. When the resistance is larger than a resistance quantum ($R > R_Q = h/4e^2$), the Josephson junction becomes insulating, while when $R < R_Q$, it becomes superconducting (see Fig. 1). However, there is no clear experimental evidence to have observed the transition, and it is still controversial [3]. The recent development of superconducting circuits allows us to access the dynamical property of the RSJJ using microwave spectroscopy while it has been discussed in the dc limit. This development motivates us to approach the RSJJ from the dynamical response, and it provides a new perspective to solve the controversial problem, the Schmid transition.

To this end, we calculated frequency dependence of an impedance of the RSJJ circuit and examined dynamic properties in the microwave reflection via the RSJJ circuit. We first calculated the phase-phase correlation function defined on the imaginary-time axis using the path-integral Monte Carlo simulation [4] and then performed the analytical continuation to the phase-phase correlation function numerically to obtain the dynamic impedance of the RSJJ. We checked that our numerical results agree well with analytical results at some solvable points such as the Toulouse point and the free-fermion point. This work is expected to provide a deep understanding of the Josephson junction on environments, which pushes further development for the superconducting circuit using Josephson junctions.

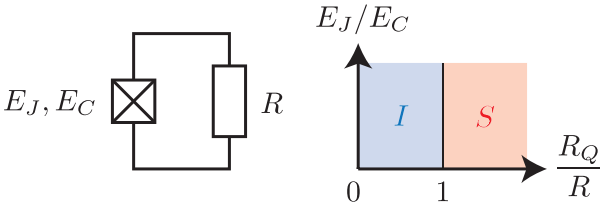

Figure 1: (left) A Josephson junction with the Josephson energy E_J and the charging energy E_C connected to a resistance R. (right) Schmid transition diagram. In the phase I (S), the Josephson junction becomes an insulator (a superconductor) at zero temperature.

References

[1] J. Kondo, Prog. Theor. Phys. **32**, 37 (1964).

[2] A. Schmid, Phys. Rev. Lett. **51**, 1506 (1983).

[3] A. Murani *et al.*, Phys. Rev. X **10**, 021003 (2020).

[4] P. Werner and M. Troyer, Phys. Rev. Lett. **95**, 060201 (2005).

Elucidation of Pathways for the Crystallization of Ionic Liquids by Large-Scale Metadynamics Simulation

Hiroki NADA

Environmental Management Research Institute,

National Institute of Advanced Industrial Science and Technology (AIST), Onogawa 16-1, Tsukuba 305-8569

A classical molecular dynamics (MD) simulation combined with the metadynamics (MTD) method (hereafter, MTD simulation) was performed for an ionic liquid, 1-alkyl-3-methylimidazolium hexafluorophosphates ($[C_n\text{min}]PF_6$, n=1 [1]), at 298 K in the NVT ensemble. A force field proposed by Canongia Lopes et al. was used for estimation of the interionic interaction [2]. The simulation system was a rectangular-parallelepiped consisting of 108 ion pairs. The MTD simulation was carried out using DL_POLY 2.20 [3], in which PLUMED 1.3 [4] was implemented to permit combination with the MTD method.

A free energy surface (FES) obtained using discrete C-C and P-F radial distribution functions quantified by Gaussian window functions as collective variables indicated a few shallow local minima. The structure of the system at each shallow local minimum represented an ordered arrangement of ions. The pathway for the formation of this ordered structure from the bulk ionic liquid, which was predicted with the FES, did not show any energetic barrier.

In addition, a crystal-like structure, which was different from the ordered structures for the shallow local minima, also appeared at a high free energy region on the FES. The arrangement of ions in this crystal-like structure was different from those for the crystalline forms, which were reported in literature [1]. This crystal-like structure might correspond to a high-pressure phase, which has not yet been found experimentally.

References

[1] T. Endo, H. Masu, K. Fujii, T. Morita, H. seki, S. Sen and K. Nishikawa: Cryst. Growth & Des. **13** (2013) 5383.

[2] J. N. Canongia Lopez, J. Deschamps and A. A. H. Pádua: J. Phys. Chem. B **108** (2004) 2038.

[3] W. Smith and T. R. Forester: J. Mol. Graph. **14** (1996) 136.

[4] M. Bonomi et al.: Comput. Phys. Commun. **180** (2009) 1961.

Creation of a Method for Design of Scale Formation Control Molecules by a Metadynamics Method

Hiroki NADA

Environmental Management Research Institute,

National Institute of Advanced Industrial Science and Technology (AIST), Onogawa 16-1, Tsukuba 305-8569

Classical molecular dynamics (MD) simulations combined with the metadynamics (MTD) method [1] (hereafter, MTD simulation) were conducted to elucidate the stable binding conformations of a deprotonated polymaleic acid (PMA) additive and two deprotonated polyacrylic acid (PAA) additives with different polymerization degrees in the presence of various countercations at a hydrated $CaCO_3$ calcite (104) surface. The MTD simulations were performed using DL_POLY 2.20 [2] in which PLUMED 1.3 [3] was implemented.

The simulated free-energy surfaces (FES) suggested the existence of several slightly different stable binding conformations for each additive. The appearance of these distinct binding conformations is speculated to originate from different balances of the interactions between the additive, calcite surface, and countercations. The binding conformations and binding stabilities at the calcite surface were affected by the countercations, with Ca^{2+} ions displaying a more pronounced effect than Na^{+} ions. Furthermore, the simulation results suggested that the binding stability at the calcite surface was higher for the PMA additive than for the PAA additives, and the PAA additive with a polymerization degree of 10 displayed a binding stability that was similar to or lower than that of the PAA additive with a polymerization degree of 5.

The present simulation method provides a new strategy for analyzing the binding conformations of complex additives at material surfaces, developing additives that stably bind to these surfaces, and designing additives to control crystal growth.

References

[1] A. Laio and M. Parrinello: Proc. Natl. Acad. Sci. USA **99** (2002) 12562.

[2] W. Smith and T. R. Forester: J. Mol. Graph. **14** (1996) 136.

[3] M. Bonomi et al.: Comput. Phys. Commun. **180** (2009) 1961.

Stability of the hedgehog-lattice topological spin texture in breathing-pyrochlore antiferromagnets

Kazushi AOYAMA
Department of Earth and Space Science, Graduate School of Science, Osaka University
Machikaneyama-cho, Toyonaka-shi, Osaka 560-0043

The quest for topological spin textures in solids is one of the central issues in condensed matter physics because of their possible applications to spin-electronic devices. A magnetic skyrmion in two dimensions and a magnetic hedgehog in three dimensions are typical examples of such topological objects. In magnetic materials, they often appear in the form of crystal orders, so-called skyrmion crystal (SkX) and hedgehog lattice (HL), where the Dzaloshinskii-Moriya (DM) interaction is known to be essential for their stabilities. Concerning the SkX, it has been shown that magnetic frustration serves as another stabilization mechanism [1], but as for the HL, a counter ordering mechanism has not been reported so far. In view of such a situation, we have searched for a new mechanism other than the DM interaction for the HL. Previously, we theoretically demonstrated that the HL is realized in breathing-pyrochlore antiferromagnets in the absence of the DM interaction, where the nearest-neighbor (NN) exchange interactions for small and large tetrahedra, J_1 and J_1', are assumed to be antiferromagnetic [2]. In this work, we extend our previous theoretical work, examining the stability of the HL in a wider parameter space.

We consider the J_1-J_3 classical Heisenberg model on the breathing pyrochlore lattice which is given by

$$\mathcal{H} = J_1 \sum_{\langle i,j\rangle_S} \mathbf{S}_i \cdot \mathbf{S}_j + J_1' \sum_{\langle i,j\rangle_L} \mathbf{S}_i \cdot \mathbf{S}_j + J_3 \sum_{\langle\langle i,j\rangle\rangle} \mathbf{S}_i \cdot \mathbf{S}_j \quad (1)$$

where J_1 and J_1' take different positive or negative values due to the breathing bond-alternation and J_3 is the third NN antiferromagnetic interaction along the bond direction. In the model, the breathing bond-alternation of the lattice is characterized by J_1'/J_1, and J_3 is essential for the occurrence of the HL which in the present case, is a quadruple-**Q** state characterized by the ordering vectors of $(\pm\frac{1}{2}, \pm\frac{1}{2}, \pm\frac{1}{2})$. By performing Monte Carlo simulations, we investigate the ordering properties of the Hamiltonian (1). In our simulations, 2×10^5 MC sweeps are carried out under the periodic boundary condition and the first half is discarded for thermalization. Our 1 MC sweep consists of 1 heatbath sweep and successive 10 overrelaxation sweeps, and observations are done at every MC sweep. The statistical average is taken over 4 independent runs starting from different random initial configurations.

It is found that the quadruple-**Q** $(\frac{1}{2}, \frac{1}{2}, \frac{1}{2})$ HL is stable irrespective of the signs of J_1 and J_1' and that in an applied magnetic field, there appear six quadruple-**Q** states depending on the values of J_1 and J_1', among which three phases including the in-field hedgehog-lattice state exhibit nonzero total chirality [3]. We have also checked that the HL is robust against relatively weak single-ion magnetic anisotropies.

In addition to the three-dimensional system, we investigate an associated two-dimensional

system. We have demonstrated that the J_1-J_3 Heisenberg model on the breathing kagome lattice exhibits a chiral transition and that the low-temperature chiral state can be viewed as a miniature SkX [4]. In contrast to conventional SkX appearing in an applied magnetic field, the miniature SkX is realized at zero field, suggesting that a zero-field topological Hall effect is possible in a metallic system.

References

[1] T. Okubo, S. Chung, and H. Kawamura, Phys. Rev. Lett. **108**, (2012) 017206.

[2] K. Aoyama and H. Kawamura, Phys. Rev. B **103** (2021) 014406.

[3] K. Aoyama and H. kawamura, in preparation.

[4] K. Aoyama and H. Kawamura, Phys. Rev. B **105**, (2022) L100407.

Dimensional reduction effect in the two-dimensional maple-leaf lattice Heisenberg antiferromagnet

Chisa HOTTA
Department of Basic Science, University of Tokyo
3-8-1 Komaba, Meguro, Tokyo 153-8902, Japan

We aim to clarify the features of uniform magnetic susceptibilities of a series of frustrated magnets in two dimensions. This year, we focused on the maple-leaf lattice spin-1/2 Heisenberg model, whose lattice structure is regarded as a 1/7-site-depleted triangular lattice. There is recently experimental evidence that the material called bluebellite $Cu_6I_6O_3(OH)_{10}Cl$ shows a particular magnetic susceptibility that almost perfectly matches the Bonner-Fisher curve, namely the susceptibility curve of the one-dimensional (1D) spin-1/2 antiferromagnetic Heisenberg model[1]. Motivated by this experiment, we analyzed the ground state and the finite temperature properties of the maple leaf lattice Heisenberg model. By combining the analysis of the several energy eigen states of the model on a finite cluster using the exact diagonalization (ED), we found that the constituent of the low energy eigenstates have the UUD/DDU configurations, i.e. the spins on all the triangular units of the lattice are two-up-one-down or two-down-one-up. This situation is similar to the antiferromagnetic triangular lattice Ising model, where the UUD/DDU state contributes macroscopically to the residual entropy. However, in our model, not all the interactions are antiferromagnetic, but the interactions on bonds forming a hexagon around the depleted sites are staggard in their sign. Even in such a case, there is a substantial frustration effect, and UUD/DDU are favored. Due to the quantum fluctuation effect, these UUD/DDU manifold mixes, and a stripe-type ground state appears. The temperature dependence of the susceptibility turned out not to match the Bonner-Fisher curve even though we vary the sign and amplitudes of five different Heisenberg interaction parameters. Instead, we found that the susceptibility shows an almost perfect coincidence with that of the 1D XXZ model having a finite spin gap. The reason for this dimensional reduction behavior is that the magnetic excitation from the ordered ground state resembles the spinon excitation of the 1D XXZ model above the spin gap. Indeed, flipping one of the spins of the stripge ground state, the two plaquettes(two+two triangles) with UUUD spins are formed, each carrying spin-1/2. The Heisenberg exchange interactions separate these two plaquettes into opposite directions, while such spinon propagation takes place only in a particular spatial direction. A series of calculations on the susceptibility of both the maple leaf lattice and the 1D XXZ model was done using a TPQ method combined with SSD[2] The variation of parameters we needed to search for was large and the 2D susceptibility is maximally given for $N = 24, 30$ sites[3].

References

[1] Y. Haraguchi, *et.al.*: Phys. Rev. B **104**, 174439 (2021).

[2] C Hotta and K Asano: Phys. Rev. B **98**, 140405 (2018).

[3] R. Makuta and C. Hotta: Phys. Rev. B **104**, 224415 (2021).

The effect of a quantum phase transition on quantum approximate optimization algorithm

Tatsuhiko Shirai
Department of Computer Science and Communications Engineering, Waseda University
Ookubo, Shinjuku-ku, Tokyo 169-8555

We have studied the effect of a quantum phase transition on the performance of quantum approximate optimization algorithm (QAOA) in the transverse-field Ising model. QAOA is a hybrid quantum-classical algorithm designed to approximate the ground state of a Hamiltonian H with N spins [1]. It has a wide application in chemistry, physics, and computer science.

QAOA consists of calculations in a quantum computer and classical computer. The quantum computer calculates the expectation value of H over a variational state, which is given by

$$|\vec{\beta},\vec{\gamma}\rangle := e^{-i\beta_p H}e^{-i\gamma_p X}\cdots e^{-i\beta_1 H}e^{-i\gamma_1 X}|+\rangle\,, \tag{1}$$

where $\vec{\beta}=(\beta_1,\ldots,\beta_p)$ and $\vec{\gamma}=(\gamma_1,\ldots,\gamma_p)$. p denotes a circuit depth. X is called a mixer and adopted as $X=\sum_{i=1}^{N}\sigma_i^x$ where $\vec{\sigma}_i=(\sigma_i^x,\sigma_i^y,\sigma_i^z)$ is the Pauli operator acting on site i. $|+\rangle$ is defined as $\sigma_i^x|+\rangle=|+\rangle$ for all i. The classical computer optimizes $(\vec{\beta},\vec{\gamma})$ to minimize the value of $\langle\vec{\beta},\vec{\gamma}|\,H\,|\vec{\beta},\vec{\gamma}\rangle$. Here, we adopt the transverse field Ising model given by

$$H=-g\sum_{i=1}^{N}\sigma_i^z\sigma_{i+1}^z-\sum_{i=1}^{N}\sigma_i^x, \tag{2}$$

where the periodic boundary condition is imposed (i.e., $\vec{\sigma}_{i+N}=\vec{\sigma}_i$). This model shows a quantum phase transition at $g=g_c=1$. The ground state is ferromagnetic for $g>g_c$, while it is paramagnetic for $0\le g<g_c$.

We numerically study p-dependences of the residual energies ΔE (i.e., the energy difference between the variational state at the optimum values of $(\vec{\beta},\vec{\gamma})$ and the ground state) in the ferromagnetic phase, critical point, and paramagnetic phase in the thermodynamic limit. The numerics is based on the Jordan–Wigner transformation and time-dependent Bogoliubov transformation. Figure 1 shows that the asymptotic behavior discontinuously changes at the critical point. It indicates the intimate relation between the quantum phase transition and the performance of QAOA.

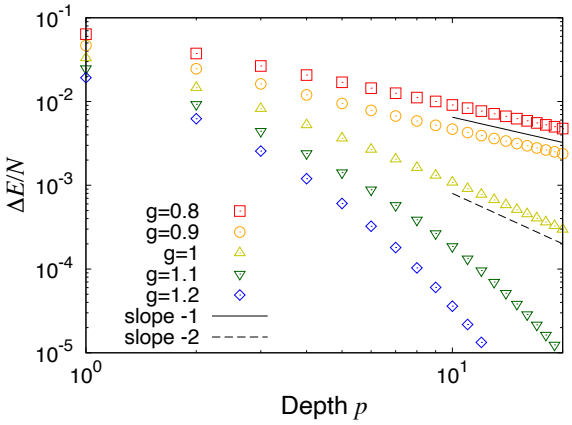

Figure 1: p-dependences of the residual energies ΔE

References

[1] E. Fahri, et al., arXiv:1411.4028 (2014).

Calculation of ordered structures, dynamics and optical properties of soft materials

Jun-ichi FUKUDA

Department of Physics, Kyushu University, Motooka 744, Nishi-ku, Fukuoka 819-0395

Motivated by a recent experimental study [1] demonstrating the structural transformation of a cholesteric blue phase liquid crystal (BPLC) by an electric field, we carried out a simulation study on the behavior of BPLC under an electric field. Ref. [1] showed that a structure with tetragonal ($I4_122$) symmetry, which had been known to be stable under an electric field, can be stable even after the cessation of the electric field when the temporal variation of the applied electric field is appropriately controlled. Possibility of stable (or metastable) tetragonal structures of BPLC under no electric field has never been discussed theoretically.

Previous numerical studies on BPLCs under an electric field focused on the bulk behavior (to be precise, in an infinite system with periodic boundaries). We are interested in how the planar boundaries confining the BPLC will affect its structural stability. Elucidation of the dynamical behavior under a temporally varying electric field turns out to be a daunting task even with the aid of the ISSP supercomputer, and therefore we restrict ourselves to static behavior.

Our numerical study is based on the Landau-de Gennes continuum theory describing the orientational order by a second-rank tensor. We use the program developed in Ref. [2] where we were particularly interested in the surface behavior, and dealt with relatively thin systems. In the present study, to simulate a system whose thickness is close to a realistic experimental value ($\simeq$12μm in Ref. [1]), 1,351 grid points are taken in the thickness direction. Our numerical system is on a regular grid and allows a use of OpenMP for efficient calculations.

Our calculations demonstrate that the presence of confining boundaries discretize the number of periodic structures along the thickness direction, and that the tetragonal structure is indeed metastable under no electric field. We are carrying out systematic studies on the free energy versus the number of periodic structures, and on the optical properties of the BPLC structures we find numerically.

References

[1] D.-Y. Guo et al., Nature Mater. **19** (2020) 94.

[2] J. Fukuda and S. Žumer, Phys. Rev. Research 2 (2020) 033407.

Non-equilibrium response and phase transition in the dense hard sphere systems

Masaharu ISOBE
Nagoya Institute of Technology
Gokiso-cho, Showa-ku, Nagoya, 466-8555

As the simplest models, the hard disk/sphere systems have been investigated via molecular simulation in both equilibrium and non-equilibrium phenomena [1]. In this project, we focus on the equilibration and the non-equilibrium response interfered with the phase transition in the hard disk/sphere model system with modern algorithms, *i.e.*, Event-Chain Monte Carlo (ECMC) [2, 3], Newtonian ECMC (NEC) [4] and Event-Driven Molecular Dynamics(EDMD) [5].

Equilibration and relaxation times in dense molecular systems

The equilibration and relaxation times of the physical properties have historically been fundamental issues in molecular simulation. As practical tasks in the molecular simulation, 'equilibration' (relaxation toward equilibrium states) from initial non-equilibrium states is just preprocessing step before a production run. Such a step needs to obtain the physical properties in the equilibrium state in the specific system. However, the computational cost often becomes high, especially for high-density and larger scale particle systems, and may sometimes exceed the human lifetime. In general, the equilibration of particle positions in dense systems is much more difficult due to the excluded volume effect being dominant, which is why the crystallization and glass/jamming transition problems remain one of the critical issues and have been actively studied recently. The two standard molecular simulation methods for many-body systems are often used; one is molecular dynamics (MD) using Newton's equations of motion, and the other is Markov chain Monte Carlo (MC) using a pseudo-random number generator. Various novel algorithms focusing on equilibration based on MD and MC have been implemented in the history of molecular simulation, which enables to reduce the relaxing time. An efficient algorithm for the acceleration of equilibration, termed the 'event-chain Monte Carlo (ECMC)' [2] was the breakthrough on this topic. The ECMC has become one of the milestones, and its variants have been investigated actively over the past decade [3]. To obtain the 'true' equilibrium states, it is a reasonable choice to use ECMC for positional relaxation at first, which is the idea of a hybrid scheme [1]. Recently, an ECMC variant termed the Newtonian ECMC (NEC) was proposed [4]. In NEC, the velocity collision rule was added to dictate the direction of particle movement. This is often used in EDMD of hard-sphere systems. The NEC clearly improves the efficiencies of the diffusion coefficient, nucleation rate, and melting process. Recently, this efficient algorithm has been extended to anisotropic hard polygons without any approximations [6].

In these ECMC and its variants (including NEC), the systems are driven by the sequential collisions composed of a dozen of particles that seem to behave like a chain. The efficiency depends on chain length, physical properties, and system size. However, the microscopic mechanism of equilibration for each parameter re-

mains elusive. To identify key factors affecting equilibration in the hard disk system, we focus on the event-based algorithms [2, 4, 5] described above and investigate the comparison between them in cases of (i) the diffusional characteristics per event (collision) and (ii) the relaxing process toward the liquid states as a non-equilibrium response after disturbance of the homogeneous expansion.

(i) Diffusional characteristics of the event-based algorithms in hard disk systems

To survey the key factors explaining why the efficiency of equilibration differed between the event-based algorithms, we focus on the diffusional characteristics per event (collision) between event-based algorithms in the liquid states of the hard disk systems. We defined the self- and pair-diffusion coefficient based on the displacement number of disks and compared the dependence in terms of the chain length and the system size systematically. In ECMC and NEC, as the chain length increases, the diffusion coefficient grows and reaches the highest values at a specific chain length. We visualized the spatial distribution of the accumulated number of displacements per particle and calculated its probability density distribution. We found that NEC has an advantage over ECMC in the diffusion coefficient in this system since NEC samples homogeneously in the system due to the Maxwell Boltzmann distribution of disk velocities for each displacement during the event chain, which can sample disks uniformly in the liquid state [7].

(ii) *Non-equilibrium response and equilibration in hard disk melting*

We then focus on the non-equilibrium response during the equilibration process induced by a disturbance of the homogeneous expansion. In the case of EDMD, we observed the anomalous slow equilibration in the hard disk systems around the co-existence phases toward the liquid states in large-scale simulation via a couple of physical properties. As the physical mechanism of this anomalous slow equilibration, we assumed that the spatial inhomogeneity of the initial equilibrated phases would contribute to the relaxation time significantly. The assumption was confirmed by the probability distribution of local density and orientational order parameter [8]. We also observed anomalous slow equilibration both in ECMC and NEC; however, the distinct differences between methods in the efficiency and functional forms of relaxation of physical properties are detected. We found that NEC and NEC are more efficient than EDMD.

As a typical non-equilibrium response, we also investigated the thermodynamic cycles by modeling the Stirling engine (SE) at the nanoscale molecular level [9]. We established a numerical model of a β-type SE with a displacer piston and figured out the minimal necessary conditions for stable rotation, as well as the lower limits of both the difference in temperature and the particle number.

References

[1] M. Isobe: Mol. Sim. **42** (2016) 1317.

[2] E. P. Bernard, W. Krauth, and D. B. Wilson: Phys. Rev. E **80** (2009) 056704.

[3] W. Krauth: Front. Phys. **9** (2021) 229.

[4] M. Klement and M. Engel, J. Chem. Phys. **150** (2019) 174108.

[5] M. Isobe: Int. J. Mod. Phys. C **10** (1999) 1281.

[6] M. Klement, S. Lee, J. A. Anderson and M. Engel, J. Chem. Theor. and Comp. **17** (2021) 4686.

[7] H. Banno, D. Mugita, and M. Isobe: J. of Phys.: Conf. Ser. **2207** 012011 (2022).

[8] D. Mugita and M. Isobe: EPJ Web Conferences, **249** 14004 (2021).

[9] K. Kitaya and M. Isobe: J. of Phys.: Conf. Ser. **2207** 012006 (2022).

Structural Formation of Patchy Particles

Takamichi TERAO

Department of Electrical, Electronic and Computer Engineering,

Gifu University, Yanagido 1-1, Gifu, 501-1132

Patchy particles are spheres in which the effective interaction between particles is anisotropic. Among the patched particles, there is interest in those that have anisotropy in interparticle interactions due to inhomogeneous surface charges [1]. Charged patchy particles are expected to have a new structure, different from previous patchy particle systems, because the interaction between particles can be both attractive and repulsive.

In this study, we focused on the structural formation of charged patchy particles, in which the particle surface is charged and the sign of the surface charge is reversed between the bipolar part and the other parts. Cluster formation in these systems was studied by molecular dynamics simulations. Modeling of charged Patchy particles is shown in Figure 1. Figure 2 shows an example of the structure formation of the system when the motion of the charged patchy particles was constrained between a pair of two-dimensional planes. In thermal equilibrium, the charged patchy particles exhibit a variety of configurations, including triangular, square, pentagonal, and hexagonal lattices.

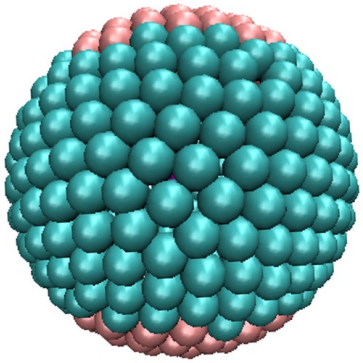

Fig. 1: Modeling of a charged patchy particle

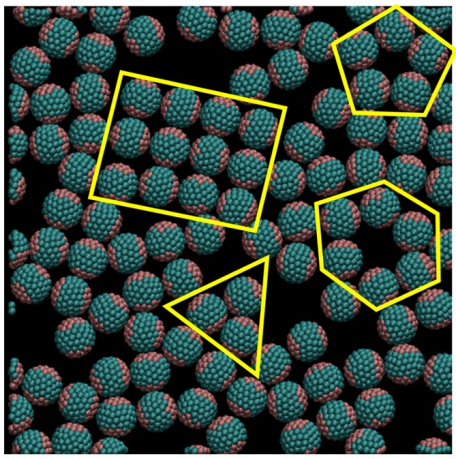

Fig. 2: Snapshot of charged patchy particles

References

[1] P. D. J. van Oostrum, M. Hejazifar, C. Niedermayer, and E. Reimhult: J. Phys.: Condens. Matter **27** (2015) 234105.

Tensor-network study of real-time dynamics in two-dimensional quantum many-body systems

Ryui KANEKO
Department of Physics, Kindai University
Higashi-Osaka, Osaka 577-8502, Japan

The nonequilibrium physics of quantum many-body systems have attracted much interest in recent years. Among others, real-time dynamics of isolated quantum systems has been investigated intensively in experiments very recently. Such examples include analog quantum simulators using ultracold atoms in optical lattices [1–3] and those using Rydberg atom arrays [4, 5]. The former is suitable for studying the Bose-Hubbard models in 1D, 2D, and 3D, and the latter is often used for studying the quantum Ising systems. The number of controllable Rydberg atoms has now exceeded 200 [6–8], which would be more qubits than classical computers can handle. These recent developments of analog quantum simulators demand cross-validating the accuracy of experiments and numerical simulations. Although numerical methods based on matrix product states are powerful in 1D [1, 3, 9], no decisive methods exist for simulating dynamics in 2D systems.

In the present study, we examine the applicability of the 2D tensor-network method based on the infinite projected entangled pair state (iPEPS) [10, 11] for simulating the real-time dynamics. We first focus on the 2D Bose-Hubbard model, whose time-dependent single-particle correlation functions have been measured in the recent experiment [3], and investigate sudden and short-time quench dynamics starting from the Mott insulator [12]. We calculate the real-time evolved states by the simple update algorithm. The tensor-network library TeNeS [13] is adopted.

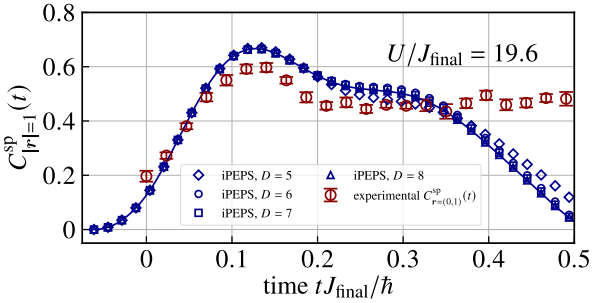

Figure 1: Comparison of the time-dependent single-particle correlation functions between the experiment (red squares) and the iPEPS simulations (blue line with symbols). We consider a finite-time quench and optimize the wave functions up to the bond dimensions $D = 8$.

We show the calculated single-particle correlation functions for the short-time quench to the Mott insulating region in Fig. 1. They are in good agreement with the recent experiment. We also predict how group and phase velocities behave for the sudden quench to the weaker interaction region, which has not been explored in experiments. Our findings would serve as a quantitative benchmark for future experiments.

After checking the applicability of the iPEPS method to the 2D Bose-Hubbard model, we apply the method to the 2D transverse-field Ising model. We focus on a sudden quench starting from the fully disordered state ($\Gamma/J \to \infty$) to the disordered region ($\Gamma > \Gamma_{\mathrm{c}}$). Calculated longitudinal spin-

spin correlation functions agree very well with the results obtained by the small-size exact diagonalization method and by the spin-wave approximation. We extract the group velocity from the correlation functions in the stronger field region. The group velocity is known to be bounded above by the Lieb-Robinson bound [14, 15]. The estimated group velocity in the present iPEPS study is much slower than the recently updated bound [16], suggesting that there is room for improving the analytical bound.

References

[1] M. Cheneau *et al.*, Nature **481**, 484 (2012).

[2] P. Jurcevic *et al.*, Nature **511**, 202 (2014).

[3] Y. Takasu *et al.*, Sci. Adv. **6**, eaba9255 (2020).

[4] E. Guardado-Sanche *et al.*, Phys. Rev. X **8**, 021069 (2018).

[5] V. Lienhard *et al.*, Phys. Rev. X **8**, 021070 (2018).

[6] S. Ebadi *et al.*, Nature **595**, 227 (2021).

[7] P. Scholl *et al.*, Nature **595**, 233 (2021).

[8] D. Bluvstein *et al.*, Science **371**, 1355 (2021).

[9] P. Barmettler *et al.*, Phys. Rev. A **85**, 053625 (2012).

[10] T. Nishino *et al.*, Prog. Theor. Phys. **105**, 409 (2001).

[11] F. Verstraete and J. I. Cirac, arXiv:cond-mat/0407066.

[12] R. Kaneko and I. Danshita, Commun. Phys. **5**, 65 (2022).

[13] Y. Motoyama *et al.*, arXiv:2112.13184.

[14] E. H. Lieb and D. W. Robinson, Commun. Math. Phys. **28**, 251 (1972)

[15] M. B. Hastings, arXiv:1008.5137.

[16] Z. Wang and K. R. Hazzard, PRX Quantum **1**, 010303 (2020).

Tensor-network study of the SU(4) Heisenberg model on a tetramerized square lattice

Ryui KANEKO
Department of Physics, Kindai University
Higashi-Osaka, Osaka 577-8502, Japan

The SU(N) Hubbard and Heisenberg models have attracted much attention recently [1–4]. They can be realized in the ultracold atoms in optical lattices and in specific antiferromagnets. Since these models possess many internal degrees of freedom and would realize novel quantum states that are absent in the well-known SU(2) model, it is desirable to explore ground states of the models on various lattices.

In the present study, we focus on how multimerization affects the ground states of the SU(N) Heisenberg model. To this end, we consider the SU(4) antiferromagnetic Heisenberg model [5]

$$H_0 = J \sum_{\langle ij\rangle_{\rm intra}} P_{ij} + J' \sum_{\langle ij\rangle_{\rm inter}} P_{ij} \qquad (1)$$

on a tetramerized square lattice [6] (see Fig. 1), where P_{ij} is a transposition operator which exchanges flavors at site i and j, namely, $P_{ij}|\alpha_i\beta_j\rangle = |\beta_i\alpha_j\rangle$ ($\alpha_i, \beta_i \in \{0,1,2,3\}$). It can be written by using the flavor-changing operator $S^\beta_\alpha(i) = |\alpha_i\rangle\langle\beta_j|$ as

$$H_0 = J \sum_{\langle ij\rangle_{\rm intra}} \sum_{\alpha\beta} S^\beta_\alpha(i) S^\alpha_\beta(j) + J' \sum_{\langle ij\rangle_{\rm inter}} \sum_{\alpha\beta} S^\beta_\alpha(i) S^\alpha_\beta(j). \qquad (2)$$

We specifically investigate the ground state of the model in the presence of the population imbalance (effective field), which favors the flavors 0 and 1:

$$H = H_0 + H_{\rm imb} \qquad (3)$$

$$H_{\rm imb} = D_z \sum_i [-S^0_0(i) - S^1_1(i) + S^2_2(i) + S^3_3(i)]. \qquad (4)$$

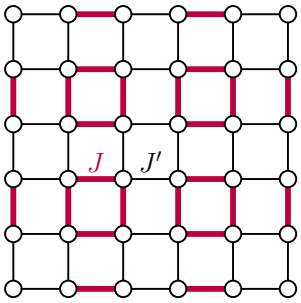

Figure 1: Tetramerized square lattice. When $J \gg J'$ or $J \ll J'$, the system decouples into isolated four-site chains. When $J = J'$, the system becomes the conventional square lattice, whose ground state is believed to exhibit simultaneous dimerization and SU(4) symmetry breaking [5].

In the limit of $J'/J = 0$ or $J/J' = 0$, the system decouples into four-site chains. The ground state is an SU(4) singlet for lower fields, while it is a resonating-valence-bond (RVB) state consisting of the 0 and 1 flavors for higher fields. In the presence of weak couplings among four-site chains ($0 < J'/J \ll 1$), a previous cluster-mean-field study with a small 2×1 sublattice structure [6] suggests the emergence of the crystal, which is a mixture of the singlet and RVB states, in the intermediate field region.

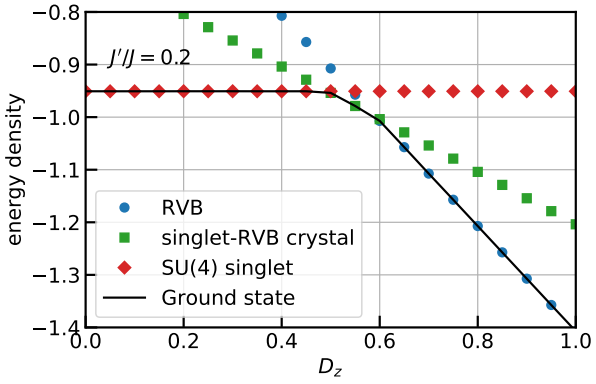

Figure 2: Energy comparison of selected ground-state candidate states at $J'/J = 0.2$. The states are obtained for the bond dimensions $D = 7$. In the intermediate field region ($0.5 \lesssim D_z/J \lesssim 0.6$), we have confirmed that the ground state is the singlet-RVB crystal.

To investigate the stability of such a crystal state beyond the mean-field study, we apply the 2D tensor-network method based on the infinite projected entangled pair state (iPEPS) [7,8]. The ground-state candidate singlet and RVB states can be represented by the iPEPS with the bond dimensions $D = 7$ and $D = 3$, respectively. The singlet-RVB crystal can also be represented by the iPEPS with $D = 7$. We consider a variety of crystal states that can be realized within a 2×2 sublattice. We take these states as initial states and optimize these wave functions. We adopt the TeNeS library [9] and calculate the ground-state candidates at $D = 7$ using the simple update algorithm [10].

Figure 2 shows the energy comparison of selected ground-state candidate states in the presence of weak couplings $J'/J = 0.2$. The iPEPS energy is slightly lower than the result obtained by the previous cluster-mean-field study [6]. On the other hand, the phase boundaries are found to be nearly consistent with the previous study; the singlet-RVB crystal ($0.5 \lesssim D_z/J \lesssim 0.6$) emerges between the lower-field SU(4) singlet and the higher-field RVB states. The ground-state singlet-RVB crystal is found to be a mixture of the SU(4) singlet and RVB states in equal proportions, and mixing in different ratios result in higher energy. As for the ground-state candidate states we have studied, the intermediate singlet-RVB crystal is stable in the presence of weak couplings among four-site chains.

References

[1] C. Wu *et al.*, Phys. Rev. Lett. **91**, 186402 (2003).

[2] C. Honerkamp and W. Hofstetter, Phys. Rev. Lett. **92**, 170403 (2004).

[3] M. A. Cazalilla *et al.*, New J. Phys. **11**, 103033 (2009).

[4] A. V. Gorshkov, Nat. Phys. **6**, 289 (2010).

[5] P. Corboz *et al.*, Phys. Rev. Lett. **107**, 215301 (2011).

[6] Y. Miyazaki *et al.*, AIP Advances **11**, 025202 (2021).

[7] T. Nishino *et al.*, Prog. Theor. Phys. **105**, 409 (2001).

[8] F. Verstraete and J. I. Cirac, arXiv:cond-mat/0407066.

[9] Y. Motoyama *et al.*, arXiv:2112.13184.

[10] H. C. Jiang *et al.*, Phys. Rev. Lett. **101**, 090603 (2008).

Simulated scanning tunneling microscopy images of graphene nanoribbons with armchair edges

Junhuan LI, Kenta ARIMA

Graduate School of Engineering, Osaka University, Yamada-oka, Suita, Osaka 565-0871

We are aiming at elucidating local electronic structures of finite-size graphene sheets and their impacts on scanning tunneling microscopy (STM) images [1]. For this purpose, we simulated STM images of armchair-edged graphene nanoribbons (AGNRs), using a simulation package named STATE (Simulation Tool for Atom TEchnology).

We simulated STM images at a V_s of -0.05 V for AGNRs with the width ranging from $W = 22$ to $W = 30$ (in terms of ribbon width, W is defined as the number of dimer lines across the ribbon width). STM images change periodically as the ribbon width increases. Figures 1(a)−1(c) summarize the results for AGNRs with $W = 3a - 2$, $3a - 1$, $3a$, respectively. For Figure 1(a) and 1(b), the electron density is slightly high at the armchair edges. The dot patterns form a $(\sqrt{3} \times \sqrt{3})R30°$ superstructure in the interior of the ribbons. In contrast, for the case of $W = 3a$ in Figure 1(c), electrons are not localized at edges and bright dots in the images appear to form a rectangular lattice, which resembles superstructures observed experimentally. This periodic change of simulated images was also confirmed to continue until reaching a width of at least 8 nm, in which the value of W was 65.

Simulated STM images at higher sample biases, or larger absolute values than that in Figure 1, were also calculated in the same ribbons. Besides, the bandgaps of ribbons were investigated based on their band structures. It helps to check the validity of our simulations and discuss more details in simulated images.

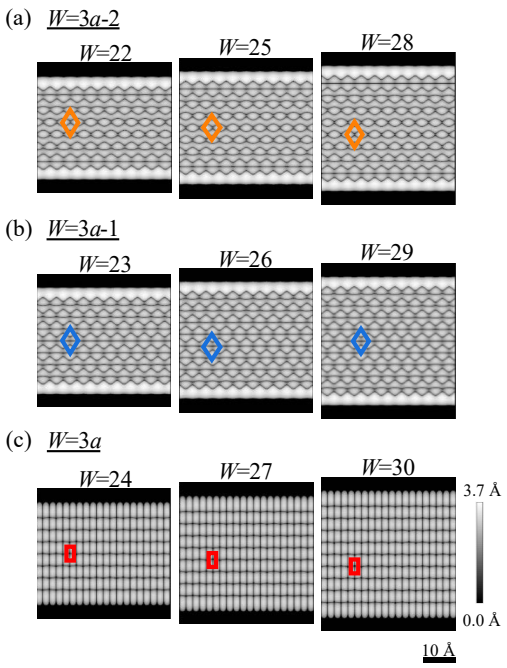

Fig. 1: Simulated STM images. A unit structure is superimposed in each image.

References

[1] J. Li, S. Li, T. Higashi, K. Kawai, K. Inagaki, K. Yamamura, and K. Arima: Phys. Rev. B **103** (2021) 245433.

Towards a unified understanding of thermodynamic properties in S=1/2 spherical kagome systems $\{W_{72}V_{30}\}$ and $\{Mo_{72}V_{30}\}$

Yoshiyuki Fukumoto
Department of Physics, Faculty of Science and Technology, Tokyo University of Science
2641 Yamazaki, Noda, Chiba 278-8510

The spherical kagome systems, or quantum-spin icosidodecahedrons, are frustrated magnetic clusters with 30 spins. It has been argued that $\{W_{72}V_{30}\}$ can be described as a regular, non-distorted, icosidodecahedron, and $\{Mo_{72}V_{30}\}$ contains structural distortion [1]. The experimental magnetization curves for those increase linearly with magnetic field [2], although a cluster Heisenberg antiferromagnet should show stepwise behavior. In a theoretical study on $\{W_{72}V_{30}\}$, Schnack *et al.* has reported that the discrepancies are attributed to the distribution of nearest-neighbor exchange couplings, which is called bond-randomness, where the width of the variance in exchange interactions was estimated to be 30% of the average value $J = 115$K [2]. On the other hand, our group has reported that the incorporation of about 10% of Dzyaloshinskii-Moriya (DM) interactions also leads to the collapse of the staircase structure [3].

Subsequently, Kihara *et al.* experimentally measured specific heats of both materials at temperatures $T < 11$K under magnetic fields up to 15T [4], and revealed that magnitudes of the specific heats are comparable to calculated results of the non-distorted and distorted Heisenberg models [1]. For $\{Mo_{72}V_{30}\}$, temperature dependence of the specific heats has a shoulder around $2 \sim 3$K and depends on magnetic field, which is consistent with calculated results with the distorted Heisenberg model [1]. However, for $\{W_{72}V_{30}\}$, the calculated specific heats with the non-distorted Heisenberg model shows a peak around 2K and significant magnetic field dependence, but the experimental result has no peak and does not show magnetic field dependence. As for the disappearance of the 2K peak, a possible origin is blurring of the density of states due to the bond randomness. Because the 2K peak comes from low-energy singlet excitations, we expect that the 2K peak is readily dispersed by about 10% bond randomness, which is much smaller than Schnack's value [2]. We actually calculate the density of state and specific heat to confirm this expectation [5]. However, quantitative reproduction of experiment is not achieved.

It is interesting to study whether larger bond randomness leads to quantitative reproduction of experimental specific heat or not. We also calculate the case of 30% bond randomness and find that the magnetic field dependence becomes smaller and the shape of the curve approaches to the experiment, which suggests an adequate choice of bond randomness, which would be 40-50%, gives quantitative reproduction. On the other hand, because the specific heat of $\{Mo_{72}V_{30}\}$ has magnetic field dependence and a shoulder in it's temperature dependence, we naively expect $\{Mo_{72}V_{30}\}$ has no bond randomness. The investigation of the origin of presence or absence of the bond randomness will be an issue in the future.

[1] N. Kunisada *et al.*, PTEP 2014, 41I01 (2014).
[2] J. Schnack *et al.*, arXiv:1304.2603v1.
[3] Y. Fukumoto *et al.*, JPSJ 87, 124710, 2018.
[4] T. Kihara *et al.*, PRB 99, 064430 (2019).
[5] M. Motohashi *et al.*, arXiv:2112.07923v1.

Numerical studies on excitation spectra of Heisenberg antiferromagnets on the triangular and kagome lattices

Yoshiyuki Fukumoto
Department of Physics, Faculty of Science and Technology, Tokyo University of Science
2641 Yamazaki, Noda, Chiba 278-8510

This project consists of two research topics, (i) virational study of the triangular-lattice system with the fermionic representation and (ii) series expansion study of the kagome-lattice system in $Cs_2Cu_3SnF_{12}$.

As for (i), a neutron scattering experiment on $Ba_3CoSb_2O_9$ revealed the existence of spinon continuum in the dynamical structure factor, in addition to magnon excitations [1]. Zhang *et al.* used the fermionic spinon operators to study the spinon continuum within random-phase approximation (RPA) [2]. This RPA treatment, however, does not exclude unphysical states exactly. This year, we have developed a program code using Monte-Carlo method to obtain the energy of the variational wave function proposed by Zhang *et al.* [1], completely considering the constraints. We also developed a program code to calculate the variational energy for a 36-site system exactly, without using Monte-Carlo sampling. The variational parameter is the strength of the staggered magnetic field conjugate to the 120 degree structure. We use wavenumbers that satisfy periodic or anti-periodic conditions in two directions of the triangular lattice. There are four combinations of wave numbers, and we make four states from each. The optimal combination of the four states is found by solving the generalized eigenvalue problem. In the next fiscal year, we will start developing a program code for the particle-hole excitations to obtain the dynamic structure factor.

As for (ii), $Cs_2Cu_3SnF_{12}$ has the q=0 order, and a theoretical analysis, based on the linear spin wave theory, of the observed magnon dispersion resulted in the exchange parameter which is 40% less than the result by an analysis of susceptibility. This fact indicates difficulty in the linear spin wave theory for frustrated systems.

In this study, we calculate the dispersion relation by series expansion from the Ising limit. We include Dzyaloshinskii-Moriya (DM) interactions into our model, where we set the DM vector to be perpendicular to the plane on which ordered moment lies. The direction of the DM vector is chosen to stabilize the q=0 state. The linked cluster expansion algorithm is used to make expansion coefficients. We developed a calculation program using the previous research that applied the cluster expansion method to the triangular-lattice system as a benchmark test [3], and extended it to the kagome-lattice system. As a result, it is clarified that the bandwidth of the magnon spectrum in the series expansion is about 1/4 of the linear spin wave theory, and its shape is also changed significantly. We also find that the correction for the linear spin wave theory is larger in the kagome lattice than in the case of the triangular lattice. Also, the shape of the magnon spectrum obtained by series expansion is comparable to the experimental results of $Cs_2Cu_3SnF_{12}$. It is speculated that the agreement can be improved by making the DM interaction more realistic in the future.

[1] S. Ito *et al.*, Nat. commn. 8, 235, 2017.
[2] C. Zhang *et al.*, PRB 102, 075108, 2020.
[3] W. Zheng *et al.*, PRB 74, 224420, 2006.

Gapless symmetry-protected topological phase of quantum spin system

Yuichiro HIDAKA[1], Shunsuke C. FURUYA[2,3], Atsushi UEDA[1], and Yasuhiro TADA[4]
[1]*Institute for Solid State Physics, University of Tokyo*
Kashiwa-no-ha, Kashiwa, Chiba 277-8581
[2]*Department of Physics, Ibaraki University*
Mito, Ibaraki 310-8512
[3]*Department of Basic Science, University of Tokyo*
Meguro, Tokyo 153-8902
[4]*Quantum Matter Program, Graduate School of Advanced Science and Engineering, Hiroshima University, Higashihiroshima, Hiroshima 739-8530*

Classifying phases of matter is one of the paramount issues in condensed matter physics. One of the important classes of the quantum phase of matter is symmetry-protected topological (SPT) phases. A SPT phase is a gapped phase which preserves some given symmetries but not adiabatically connected to a trivial phase without breaking the symmetries [1]. Recently many researchers attempt to extend the concept of SPT phase into gapless system [2, 3].

In the present study, we proposed a quantum spin model that has the properties of gaplessness and nontrivial SPT phase simultaneously. The model we proposed is the anisotropic triangular strip (ATS) XXZ model, shown in Fig.1, which consists of three-leg antiferromagnetic ladder with frustrated interchain couplings. We used the density matrix renormalization group (DMRG) method to calculate the ground state of the ATS XXZ model at the specific parameters, $J = 1.0$, $\Delta = 0.8$, and $J_\times = 0.5$. We used the ITensor and TeNPy libraries [4, 5].

We found that the entanglement entropy of the ATS XXZ model fits with Calabrese-Cardy formula of open boundary condition. According to the conformal field theory, it is expected that the central charge of the ATS XXZ model is one. The calculation result of central charge is shown in Fig.2, and the central charge become close to one, which is derived from the extrapolation of the entanglement entropy about the system size. In addition, Fig.3 shows the calculation result of entanglement spectrum and we can see double degeneracy, which is an important feature of Haldane state in quantum spin system. From these two results, the ground state of ATS XXZ model is Tomonaga-Luttinger liquid which has the property of nontrivial SPT phase. Therefore we can conclude that the ground state of ATS XXZ model with $J = 1.0$, $\Delta = 0.8$, and $J_\times = 0.5$, is in gapless SPT phase. We presented these results at the 2022 Annual (77th) Meeting of the Physical Society of Japan [6].

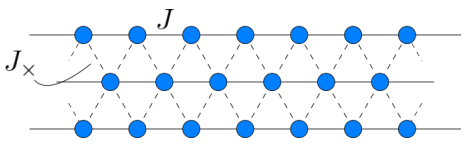

Figure 1: ATS XXZ model

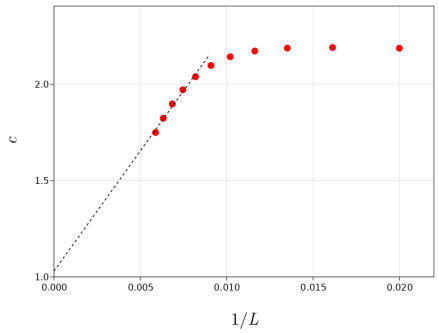

Figure 2: Entanglement entropy of the ATS XXZ model. The purple line is the fitting line of entanglement entropy by the Calabrese-Cardy formula.

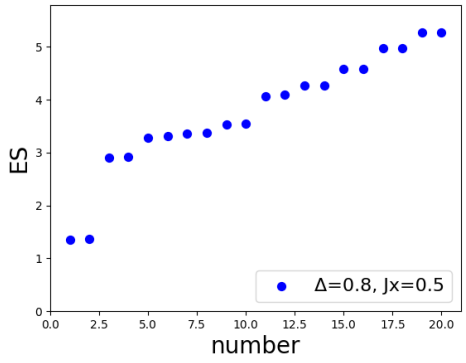

Figure 3: Entanglement spectrum of ATS XXZ model.

References

[1] X. Chen, Z.-C. Gu, and X.-G. Wen, Phys. Rev. B 83, 035107 (2011).

[2] T. Scaffidi, D. E. Parker, and R. Vasseur, Phys. Rev. X 7, 041048 (2017).

[3] S. C. Furuya and M. Oshikawa, Phys. Rev. Lett. 118, 021601(2017).

[4] M. Fishman, S. R. White, and E. M. Stoudenmire, arXiv:2007.14 (2020).

[5] J. Hauschild and F. Pollmann, SciPost Phys. Lect. Notes , 5 (2018).

[6] Y. Hidaka, S. C. Furuya, A. Ueda, and Y. Tada: in preparation.

Development of multiscale simulation technique for liquids and solids

Takahiro MURASHIMA

Department of Physics, Tohoku University,

6-3, Aramaki-Aza-Aoba, Aoba-Ward, Sendai, Miyagi 980-8578

Predicting the flow and deformation of soft matter and composite materials is still a very difficult problem. Aside from the problem of solving macroscale continuum equations, there are difficulties in determining constitutive laws that characterize materials. An approach to determine the constitutive law (rheology) of a material using molecular simulations has been popular in recent years. Multiscale simulations that connect these molecular simulations to continuum simulations as constitutive laws do not explicitly require constitutive laws, thus avoiding the difficulty of deriving constitutive laws [1]. However, there is a problem of boundary conditions for treating general flow fields in molecular dynamics simulations. Therefore, in this research project, we attempted to extend the boundary conditions to solve this problem.

Recently, we have developed the UEFEX method [2], which enables large-elongation flow simulations. Here, the elongation axis and the unit cell are not parallel to each other to avoid collapsing the unit cell under elongational deformation.（Figure 1 shows the steady state of polymer chains under uniaxial elongational flow.)

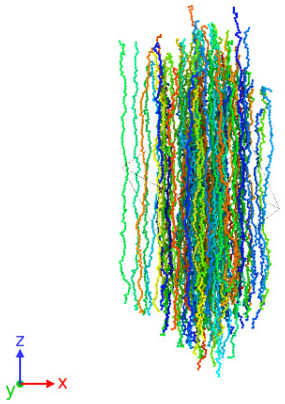

Fig.1: Polymers under uniaxial elongation $\kappa = \begin{pmatrix} \dot{\epsilon} & 0 & 0 \\ 0 & \dot{\epsilon}/2 & 0 \\ 0 & 0 & \dot{\epsilon}/2 \end{pmatrix}$.

For general deformations in the molecular dynamics simulation, we proposed a method that uses QR decomposition to exclude the rotational component of the deformation tensor and impose only pure deformations on the molecular simulation system [3]. Here, we considered problems in which large deformations and rotations do not occur. This time, we extended this method to include vortex flow in fluids. (Figure 2 shows a polymer chain in a rotating flow.) Before

conducting multiscale simulations using this method, we are currently conducting an analysis assuming a corner vortex phenomenon that appears in polymer melts. We intend to summarize the results in a future paper.

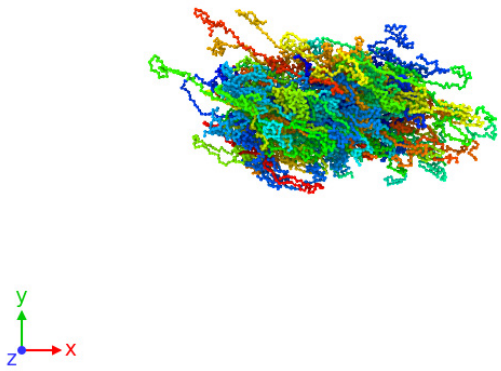

Fig. 2: Polymers under rotational flow $\kappa = \begin{pmatrix} 0 & \dot{a} & 0 \\ -\dot{b} & 0 & 0 \\ 0 & 0 & 0 \end{pmatrix}$, where $\dot{a} > \dot{b}$.

References

[1] T. Murashima, T. Taniguchi, EPL **96** (2011) 18002.

[2] T. Murashima, K. Hagita, T. Kawakatsu, Nihon Reoroji Gakkaishi **46** (2018) 207.

[3] T. Murashima, S. Urata, S. Li, Euro. Phys. J. B **92** (2019) 211.

Ashkin-Teller-like phase transition in the two-dimensional classical dimer-monomer model

Satoshi MORITA
Institute for Solid State Physics, University of Tokyo
Kashiwa-no-ha, Kashiwa, Chiba 277-8581

An attractive interaction between dimers aligning on a square induces finite-temperature phase transitions [1, 2]. The phase transition between the liquid and columnar phases is known as the Kosterlitz-Thouless transition. When monomers are introduced, the critical exponents smoothly change and its universality class is the same as the Ashkin-Teller (AT) model. On the other hand, another ordered phase appears between the two phases when the nearest-neighbor attractive interaction along the dimer direction is sufficiently large [3]. This phase called the nematic phase breaks only the lattice rotational symmetry. Although preceding studies reported these interesting features, an intermediate parameter region, where two attractive interactions are comparable, were not investigated. It is not known yet how the phase transition between the columnar and disordered phases splits into two transitions involving the nematic phase.

To address this problem, we investigate a classical dimer-monomer model on the square lattice by using the Monte Carlo (MC) method and the tensor network (TN) method. For the MC method, we generalize the worm algorithm to the grand-canonical ensemble of this dimer model. The TN method for infinite systems is complementary to the MC method. From the TN representation of the partition function, the row-to-row transfer matrix is constructed as the matrix product operator (MPO). Its eigenvector with the maximum eigenvalue is approximated by the uniform matrix product state (uMPS). We determine the phase structure and find the existence of the multi-critical point. The universality classes of the phase transitions are discussed by estimating the scaling dimension and the central charge. We find that the columnar and nematic orders correspond to the magnetization and polarization in the Ashkin-Teller model, respectively. The estimated scaling dimensions clearly indicate the Ashkin-Teller universality class. We also confirm the 4-state Potts universality at the multi-critical point.

Figure 1: A typical configuration of the nematic and disordered phases generated by the MC simulations.

References

[1] F. Alet, et al., Phys. Rev. Lett. **94**, 235702 (2005).

[2] F. Alet, et al., Phys. Rev. E **74**, 041124 (2006).

[3] S. Papanikolaou, D. Charrier, and E. Fradkin, Phys. Rev. B **89**, 035128 (2014).

[4] S. Morita, H. Lee, K. Damle, N. Kawashima, in preparation

Nematic Tomonaga-Luttinger Liquid Phase in an $S=1/2$ Ferromagnetic-Antiferromagnetic Bond-Alternating Chain

Takashi Tonegawa

Kobe University, University of Hyogo, and Osaka Metropolitan University

Recently, using mainly numerical methods, we [1] have investigated the ground-state phase diagram of an anisotropic $S=1/2$ two-leg ladder with different leg interactions. The xy and z components of the leg interactions between nearest-neighbor spins in the a (b) leg are denoted, respectively, by $J_{\mathrm{l},a}$ and $\Delta_{\mathrm{l}}J_{\mathrm{l},a}$ ($J_{\mathrm{l},b}$ and $\Delta_{\mathrm{l}}J_{\mathrm{l},b}$). On the other hand, the xy and z components of the uniform rung interactions are, respectively, denoted by $\Gamma_{\mathrm{r}}J_{\mathrm{r}}$ and J_{r}. In the above, Δ_{l} and Γ_{r} are the XXZ-type anisotropy parameters for the leg and rung interactions, respectively. This system has a frustration when $J_{\mathrm{l},a}J_{\mathrm{l},b}<0$ irrespective of the sign of J_{r}.

We [1] have numerically determined the phase diagram on the Δ_{l} ($0.0\le|\Delta_{\mathrm{l}}|\le1.0$) versus $J_{\mathrm{l},b}$ ($-2.0\le J_{\mathrm{l},b}\le3.0$) plane in the case where $J_{\mathrm{l},a}=0.2$, $J_{\mathrm{r}}=-1.0$, and $\Gamma_{\mathrm{r}}=0.5$. It is noted that the rung interaction is ferromagnetic and its anosotropy is of the Ising-type. Furthermore, the a leg interaction is antiferromagnetic, while the b leg interaction are either ferromagntic or antiferromagnetic, the anisotropies of both leg interations being of the XY-type. We have employed the physical consideration, and the level spectroscopy and phenomenological renormalization-group analyses of the numerical date obtained by the exact diagonalization method. Interestingly enough, we have found that two kinds of nematic Tomonaga-Luttinger Liquid (nTLL) phases appear; one of which appears in the unfrustrated and the other in the frustrated one. The nTLL state is characterized not only by the formation of two-magnon bound pairs but also by the dominant nematic four-spin correlation function. It shuold be emphasized that the asymptotic form of this correlation function in the unfrustrated region and that in the frustrated region show the power-law decay with the uniform chracter and the power-law decay with the staggered character, respectively. Thus, both nTLL phases are different phases, and the latter nTLL phase may be called the staggered nTLL phase.

According to the above result, it is reasonably expected that the nTLL state appears as the zero-field ground state in general $S=1/2$ unfrustrated one-dimensional systems in which pairs of $S=1/2$ spins coupled strongly with the Ising-type ferromagnetic interaction are connected by the weak XY-type antiferromagnetic interactions. Some examples of such systems are (A) the $S=1/2$ ferromagnetic-antiferromagnetic bond-alternating chain, (B) the $S=1/2$ two-leg ladder with ferromagnetic rung and antiferromagnetic leg interactions, (C) the $S=1/2$ Kondo necklace chain with ferromagnetic rung and antiferromagnetic leg interactions, and so on.

The purpose of this report is to discuss the system (A), which is governed by the Hamiltonian

$$\mathcal{H}=-J_{\mathrm{F}}\sum_{j=1}^{N/2}[\vec{S}_{2j-1},\vec{S}_{2j}]+J_{\mathrm{AF}}\sum_{j=1}^{N/2}[\vec{S}_{2j},\vec{S}_{2j+1}]\,,$$

with

$$[\vec{S}_{2j-1},\vec{S}_{2j}]=\Gamma_{\mathrm{F}}\left(S^x_{2j-1}S^x_{2j}+S^y_{2j-1}S^y_{2j}\right)+S^z_{2j-1}S^z_{2j}\,,$$

$$[\vec{S}_{2j},\vec{S}_{2j+1}]=S^x_{2j}S^x_{2j+1}+S^y_{2j}S^y_{2j+1}+\Delta_{\mathrm{AF}}S^z_{2j}S^z_{2j+1}\,,$$

where $J_{\mathrm{F}}>J_{\mathrm{AF}}>0.0$ and $1.0\ge\Gamma_{\mathrm{F}}$, $|\Delta_{\mathrm{AF}}|\ge0.0$, and also N, being assumed to be a multiple of four, is the number of spins in the ststem. It is noted that the ferromagnetic interactions are stronger than the antiferromagnetic ones, and the anisotropies of the former and latter interactions are of the Ising-type and the XY-type, respectively.

We have determined three ground-state phase diagrams; these are for $J_{\mathrm{F}}=1.0$, $J_{\mathrm{AF}}=0.1$, for $J_{\mathrm{F}}=1.0$, $\Gamma_{\mathrm{F}}=0.8$, and for $J_{\mathrm{F}}=1.0$, $\Delta_{\mathrm{AF}}=-0.12$. The results are shown in Fig. 1, Fig. 2, and Fig. 3, respectively. These diagrams contain the ferromagnetic (F), $XY1$, singlet-dimer (SD), and up-up-down-down (uudd) phases as well as the nematic Tomonaga-Luttinger liquid (nTLL) phase which appears in wide regions, where $J_{\mathrm{F}}\gg J_{\mathrm{AF}}>0.0$, of the interaction parameters.

Finally, we discuss how to obtain the phase boundary lines in these phase diagrams. We denote, respectively, by $E_0^{\mathrm{P}}(N,M)$ and $E_1^{\mathrm{P}}(N,M)$, the lowest and second-lowest energy eigenvalues of the Hamiltonian $\mathcal{H}$ under the periodic boundary condition within the subspace of N and M, where $M(=0,\pm1,\cdots,\pm N/2)$ is the total magnetization. Furthermore, we denote by $E_0^{\mathrm{T}}(N,M,P)$ the lowest eigenvalue of $\mathcal{H}$ under the twisted boundary

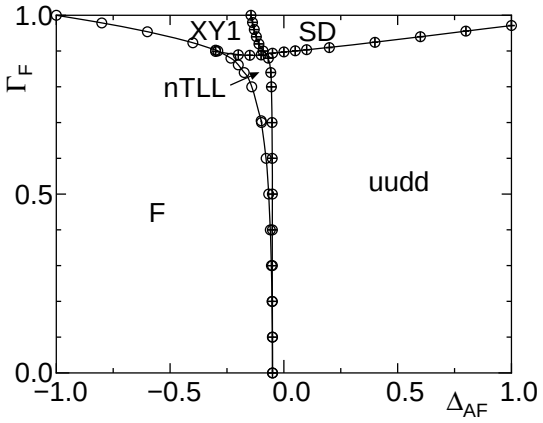

Figure 1: Ground-state phase diagram for $J_{\rm F}=1.0$ and $J_{\rm AF}=0.1$.

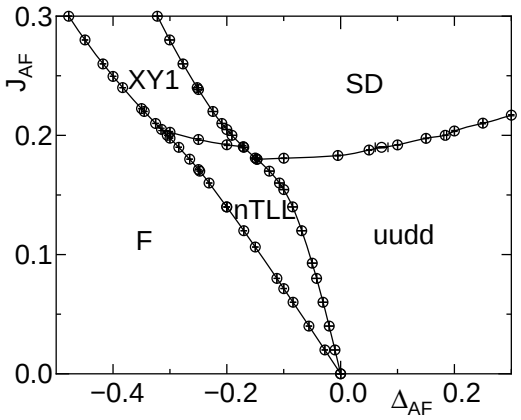

Figure 2: Ground-state phase diagram for $J_{\rm F}=1.0$ and $\Gamma_{\rm F}=0.8$.

condition within the subspace of N, M, and P, where $P(=\pm 1)$ is the eigenvalue of the space inversion operator with respect to the twisted bond. We have numerically calculated these energies for finite-size systems with up to $N=28$ spins by means of the exact-diagonalization method. The ground-state energy of the finite-N system is given by $E_0^{\rm P}(N,N/2)$ in the F region and by $E_0^{\rm P}(N,0)$ in the other regions. In the following way, we have estimated the finite-size critical values of the interaction parameters for each phase transition. Then, the phase boundary line for the transition has been obtained by connecting the results for the $N\to\infty$ extrapolation of the finite-size critical values.

First, the phase transitions between the $XY1$ and SD phases and between the nTLL and uudd phases are the Berezinskii-Kosterlitz-Thouless transition [2]. In these transitoions, the level spectroscopy method develped by Nomura and Kitazawa [3] is very powerful for calculating the finite-size critical values, which are esimated from $E_0^{\rm P}(N,0)=E_0^{\rm T}(N,M,-1)$. Secondly, the

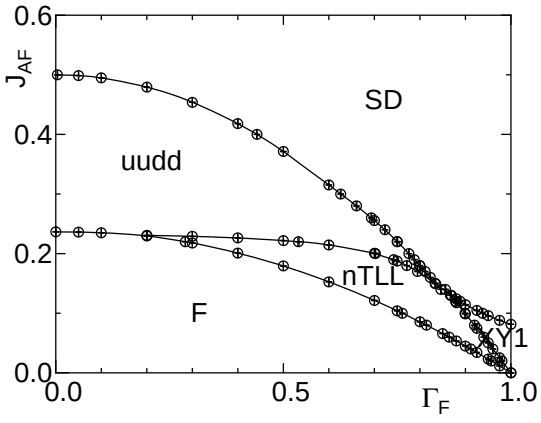

Figure 3: Ground-state phase diagram for $J_{\rm F}=1.0$ and $\Delta_{\rm AF}=-0.12$.

phase transition between the SD and uudd phases is the 2D Ising-type transition. It is well known that the phase transition line is determined by the phenomenological renormalization-group (PRG) method [4]. Then, to estimate the finite-size critical values, we solve the PRG equation, $N\,\Delta_{00}(N)=(N+4)\,\Delta_{00}(N+4)$, where $\Delta_{00}(N)=E_1^{\rm P}(N,0)-E_0^{\rm P}(N,0)$. Thirdly, the nTLL state accompanies two-magnon bound-states, while the $XY1$ state does not. Then, in the ground-state magnetization curve for the finite-size system, the magnetization increases from $M=0$ to $M=2$ in the former state and from $M=0$ to $M=1$ in the latter state. Thus, the finite-size critical values are estimated from $\Delta_{10}(N)=\Delta_{20}(N)/2$, where $\Delta_{M0}(N)=E_0^{\rm P}(N,M)-E_0^{\rm P}(N,0)$. Lastly, it is apparent that the finite-size critical values for the phase transitions between the F phase and one of the nTLL, $XY1$, and uudd phases are estimated from $E_0^{\rm P}(N,N/2)=E_0^{\rm P}(N,0)$.

In conclusion, we have found the appearance of the nTLL phase in the ground-state phase diagram of an unfrustrated $S=1/2$ chain under no external magnetic field.

The present work has been done in collaboration with Kiyomi Okamoto, Kiyohide Nomura, and Tôru Sakai.

[1] T. Tonegawa, T. Hikihara, K. Okamoto, S. C. Furuya, and T. Sakai, J. Phys. Soc. Jpn. **87**, 104002 (2018).
[2] Z. L. Berezinskii, Sov. Phys. JETP **34**, 610 (1971); J. M. Kosterlitz and D. J. Thouless, J. Phys. C **6**, 1181 (1973).
[3] K. Nomura and A. Kitazawa, J. Phys. A **31**, 7341 (1998).
[4] M. P. Nightingale, Physica A **83**, 561 (1976).

First Principle Calculation and Charge Order Structure in Organic Charge Order Materials

Masatoshi SAKAI, Ryoma ISHII

Department of Electrical and Electronic Engineering,

Chiba University, 1-33 Yayoi-cho Inage, Chiba 263-8522

We tried to calculate the electronic structure of β-(BEDT-TTF)$_2$PF$_6$ from the first principle calculation using Quantum Espresso, RESPACK, and mVMC. Starting from the loading cif file into Quantum Espresso, we obtained the results of the scf calculation. After that, Wannier calculation was carried out by RESPACK to calculate Wannier orbitals so that the band dispersion curve around HOMO orbitals in scf calculation is reproduced by using the Wannier function. Fig. 1 (a) shows one of the selected Wannier functions used in this calculation, and Fig. 1(b) shows the band dispersion curves of the Wannier function superimposed into the result of the scf calculation. Wannier function represents the molecular orbital of the BEDT-TTF, and band dispersion curves are also well reproduced. Therefore, we obtained reasonable results in RESPACK calculation in the 3x3x3 K-mesh condition. Then we carried out the cRPA calculation to obtain dielectric function, Coulomb integrals, and exchange integrals. We spent a long time converging these calculations; however, we obtained the interaction parameters in β-(BEDT-TTF)$_2$PF$_6$. Now we are trying to execute mVMC calculation both in β-(BEDT-TTF)$_2$PF$_6$ and α-(BEDT-TTF)$_2$I$_3$ organic charge order system to elucidate our experiment.

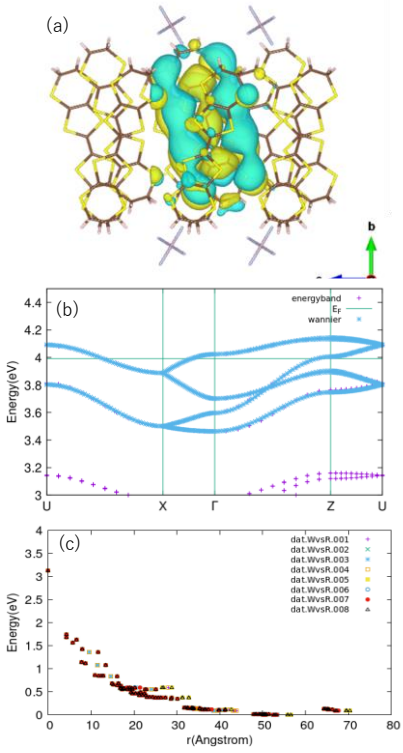

Fig. 1 (a) One of the calculated Wannier orbital around the Fermi level of β-(BEDT-TTF)$_2$PF$_6$. (b) Band dispersion curves of Wannier function superimposed in the scf calculation. (c) Coulomb interaction as a function of inter center distance.

Structural analysis of surface superstructures and atomic layer materials using by 2DMAT on supercomputer system at ISSP

Akari TAKAYAMA

Department of Physics,

Waseda University, Ohkubo, Shinjuku-ku, Tokyo 169-8555

In our research, we use supercomputers for structural analysis in terms of determining the structure of materials. Since structure and physical properties are closely related, it is essential to know the exact structure in order to correctly understand the physical properties. Generally, surface and interface structures are complicated than bulk crystal due to structural relaxation and structural reconstruction at surface and interface. For instance, structure of epitaxial graphene growth on SiC is still controversial due to the underlying-buffer layer with a long-period ($6\sqrt{3}\times6\sqrt{3}$-R30°). Also the $\sqrt{3}\times\sqrt{3}$-Pb/Si(111) surface superstructure, which is known to undergo a structural phase transition at T = 86 K, forms a "mosaic" structure, thus its detailed structure is fully understood. In this study, we investigated the structure of graphene on SiC including a buffer layer and Pb/Si(111) surface superstructure by using total reflection high-energy positron diffraction (TRHEPD) method. For structure analysis, we used "2DMAT" [1], an open source framework for 2D material structure analysis, which is included as standard software in ISSP's supercomputer. Using massive parallel computer simulations on supercomputer is very useful for structure analysis of large periodic structure and surface superstructure with lattice reconstruction because they require many variables for analysis.

Figure 1 shows the rocking curve under the one-beam condition obtained from the experiment (circles) and from calculation (solid line) for 0-BL graphene (buffer layer) of SiC(0001). From the fitting calculation for this rocking curve, we determined the buckling structure of buffer layer and found that our determined structure corresponds well with the structural model proposed by Lima *et al*. [2]. Moreover, the ratio of bounding and free-standing regions with/from substrate were determined to be 22 % and 78 %, respectively, in this sample. The ratio is consistent with previous studies [3, 4].

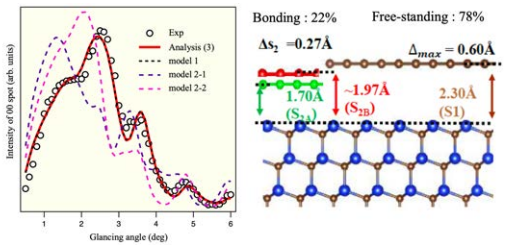

Fig. 1: Structure analysis results of buffer layer on SiC.

Figure 2 shows the rocking curve under the one-beam condition obtained from the experiment (circles) and from calculation (solid line) for mosaic phase of √3×√3-Pb/Si(111). We have succeeded in determining the structure of the mosaic phase by analyzing the Pb occupancy as a variable. In addition, no noticeable changes in the rocking curves were observed at low (T = 13 K) and room temperatures. This suggests that the phase transition in this structure is caused by soft phonons [5].

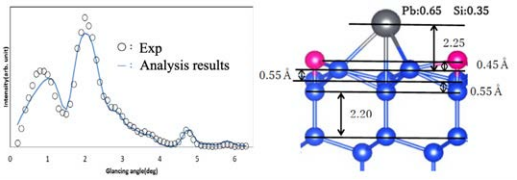

Fig. 2: Structure analysis results of mosaic phase of Pb/Si(111).

References

[1] Y. Motoyama, *et al*., arXiv:2204.04484

[2] L. H. de Lima, *et al*, Chem. Commun., **50** (2014) 13571.

[3] M. Conrad, *et al*., Phys. Rev. B **96** (2017) 195304.

[4] J. D. Emery, *et al*., Phys. Rev. Lett. **111** (2013) 215501.

[5] I. Brihuega *et al*., Phys. Rev. Lett. **94** (2005) 046101.

Minority Driving Transition in Collective Movement

Katsuyoshi Matsushita
Department of Biological Science, Osaka University
Machikaneyama, Toyonaka 560-0043

In biological organisms, cells aggregate and form tissues to function. Cell aggregation exhibits various dynamics, including rotation and translational movements. The transition from the rotation to the translational movements is well known in the developmental process in *Dictyostelium Discoideum* (dicty) [1]. The physical mechanism of this transition has been theoretically investigated on the basis of the behavior of cells [2, 3]. In particular, the works consider the response of cells to chemical gradients, which is observed in a earlier stage of development. These works successfully explained the transition and apperently unified the cell movements throughout the developmental process of dicty combined with the works for later stages [4].

These works assume homogeneous cell systems. However, as well known, the transition is tightly associated with cell differentiation. Cell differentiation means the change in the material properties of the cells. Therefore, the response property to the chemical gradient may not be conserved in the transition. Recent advances in the investigations of this transition showed the lack of the response of dicty cells [5]. Furthermore, both the rotational and translational movements do not depend on the response [6, 7]. These results imply the existence of another physical mechanism associated with cell differentiation.

A possible mechanism is the material parameter change in the cells. In particular, the rate of differentiation in population gradually changes during the transition process with several hours [1]. Therefore, we can expect the following situation: The collective movement is rotational when the differentiated cells are a minority in the cell population. Otherwise, the collective movement is a transnational movement. Namely, the minority change in cell population in the differentiation process drives the transition in collective movements.

To examine this scenario of the transition, we theoretically considered the process of cell population change [8]. We use the cellular Potts model [9, 10]. The cell population is assumed to consist of leader and follower cells [11]. The leader cells correspond to the differentiated cells and can lead the following cells using the cell-cell adhesion [12]. We also consider cell polarities by memorizing the cell trajectories [13, 14]. These polarities correlate with the adhesion [15] and stabilize the ordering of the cell movements [16, 17].

From the simulation results based on the above model, we examine the population dependence of the collective cell movements. We showed that the minority change in cell population in the differentiation process drives the transition of collective movements. A motility-inducing phase separation (MIPS) inner the cell aggregation appears for intermediate populations. The MIPS divides the cell aggregation into two aggregations: a homogeneous un-differentiated population and a highly differentiated population. Therefore, this minority change cannot explain the transition from rotation to translational movements for stable cell aggregations. The improvement of the scenario based on the minority change remains in the future.

The clarification of the origin of this aggregation division is expected to give us hints to improve the scenario. In our recent work, we investigate a homogeneous cell system to identify the parameters of collective movements [18]. We find that the occurrence of the collective movement, including the rotation and transnational movements, depends on the interface tension of the cell aggregations. This result implies the transition due to minority change originates from a change in the interface tension of the aggregation. The minority change is speculated to reduce the interface tension, and aggregation division is associated with the transition. This speculation implies the fine-tuning of the interface tension in the differentiation. However, it is not realizable in a realistic system and the necessity for another idea.

References

[1] J. T. Bonner, The Social Amoebae: The Biology of Cellular Slime Molds (Princeton University Press, Princeton, 2009).

[2] T. Umeda and K. Inouye, J. theor. Biol. **219**, 301 (2002).

[3] B. Vasiev C. J. Weijer. J. Theor. Biol. **223**, 347 (2003)

[4] A. Maree et al. J Their. Biol. **199**, 297 (1997); Proc. Natl. Acad. Sci. USA **98**, 3879 (2001) (2000).

[5] H. Hashimura, Y. V. Morimoto, M. Yasui, and M. Ueda, Communications Biology **2**, 34 (2019).

[6] W.-J. Rappel, A. Nicol, A. Sarkissian, H. Levine, and W. F. Loomis, Phys. Rev. Lett. **83**, 1247 (1999)

[7] Y. Kida, K. Pan, and H. Kuwayama, Differentiation **105**, 71 (2019).

[8] K. Matsushita, S. Yabunaka, H. Hashimura, H. Kuwayama, and K. Fujimoto, Proc. Sympo. Traffic Flow Self-Driven Particles **26** 39-42 (2020).

[9] F. Graner and J. A. Glazier, Phys. Rev. Lett. **69**, 2013 (1992).

[10] F. Graner, J. Theor. Biol. **164**, 455 (1993).

[11] A. J. Kabla, J. R. Soc. Interface **9**, 3268 (2012).

[12] K. Matsushita, Phys. Rev. E **97**, 042413 (2018).

[13] P. Szabó, M. Nagy, and T. Vicsek, Phys. Rev. E **79**,021908 (2007).

[14] K. Matsushita, Phys. Rev. E **97**, 042413 (2018).

[15] J. C. Coates and A. J. Wood. J. Cell Sci. **114**, 4349 (2001)

[16] K. Matsushita, K. Horibe, N. Kamamoto, and K. Fujimoto, J. Phys. Soc. Jpn. **88**, 103801 (2019).

[17] K. Matsushita, S. Yabunaka, and K. Fujimoto, J. Phys. Soc. Jpn. **90**, 054801 (2021).

[18] K. Matsushita, N. Kamamoto, M. Sudo, and K. Fujimoto, Proc. Sympo. Traffic Flow and Self-Driven Part. **27**, 23 (2021).

Non-uniform thermal transport properties in proteins

Takahisa YAMATO

Graduate School of Science,

Nagoya University, Furo-cho, Chikusa-ku, Nagoya 464-8602

Protein molecules are thermally fluctuating and tightly packed amino acid residues strongly interact with each other. Such interactions are characterized in terms of heat current at the atomic level. We calculated the thermal conductivity of a small globular protein, villin headpiece subdomain, based on the linear response theory using equilibrium molecular dynamics simulation. The value of its thermal conductivity was 0.3 ± 0.01 [W m^{-1} K^{-1}], which is in good agreement with experimental and computational studies on the other proteins in the literature (Figure 1). Heat current along the main chain was dominated by local vibrations in the polypeptide bonds, with amide I, II, III, and A bands on the Fourier transform of the heat current autocorrelation function [1] (Figure 2).

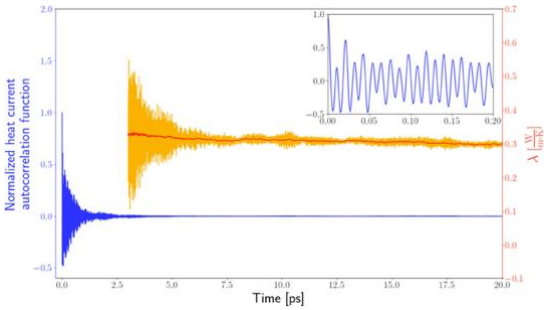

Figure 1: Thermal conductivity. The time evolution of the average heat current autocorrelation function is shown in blue. Its short time behavior is shown in the inset. The value of λ is shown in orange as a function of integration time, τ, for τ > 3.0 ps. The red line indicates the running mean of λ with a window size of 100 fs.

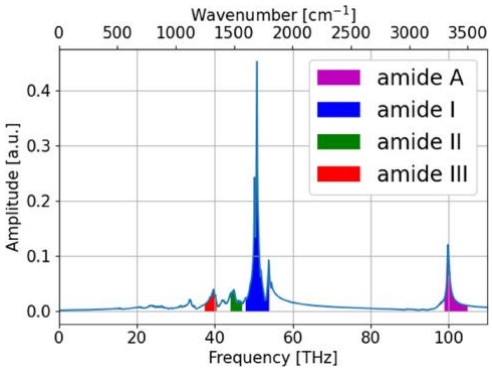

Figure 2: Fourier transform of the backbone heat current autocorrelation function. The Fourier transform of the average heat current autocorrelation function is shown for the backbone heat current.

References

[1] T. Yamato, T. Wang, W. Sugiura, O. Laprévote, T. Katagiri: J. Phys. Chem. B (2022) https://doi.org/10.1021/acs.jpcb.2c00958

Majorana Kramers Qubits and Yang-Lee Anyons in Topological Superconductors

Takeshi MIZUSHIMA
Department of Materials Engineering Science, Osaka University
Toyonaka, Osaka 560-8531

We have investigated non-Abelian statistics of Majorana Kramers pairs (MKPs) in time-reversal invariant topological superconductors (TRITSCs) [1]. We have also demonstrated that a Yang-Lee anyon system is constructed from Majorana bound states in topological superconductors [2].

In Ref. [1], we numerically simulated braiding dynamics of MKPs in a network of one-dimensional TRITSCs, and examined the tolerance against various perturbations which may cause decoherence of MKPs. We first considered effects of a magnetic field which breaks time-reversal symmetry. In contrast to a naive expectation, we find the non-Abelian braiding of MKPs is robust against applied magnetic fields provided that the initial and final states of a braiding process are invariant under the combination of a time reversal and a mirror reflection, even when intermediate states break the combined symmetry. In addition, we investigated the tolerance of non-Abelian braidings against gate-induced inhomogeneous potentials at junctions between superconducting nanowires. The potential generally generates a non-Majorana nearly zero-energy Andreeev bound state at the junctions. We demonstrated that the non-Majorana states interfere with MKPs, resulting in the failure of non-Abelian braidings.

Yang-Lee anyons, described by the non-unitary conformal field theory with the central charge $c = -22/5$, are non-unitary counterparts of Fibonacci anyons, obeying the same fusion rule. Therefore, the Yang-Lee anyon system is expected to be a platform for realizing universal topological quantum computation. In Ref. [2], we considered a topological superconductor junction system coupled with dissipative electron baths (see Fig. 1), which realizes a non-Hermitian interacting Majorana system. Numerically estimating the central charge, we examined the condition that the non-Hermitian Majorana system can simulate the Ising spin model of the Yang-Lee edge singularity, and confirmed that, by controlling model parameters in a feasible way, the Yang-Lee edge criticality is realized. We also discuss the scheme for the measurement and the braiding of Yang-Lee anyons, aiming at the application to the universal quantum computation.

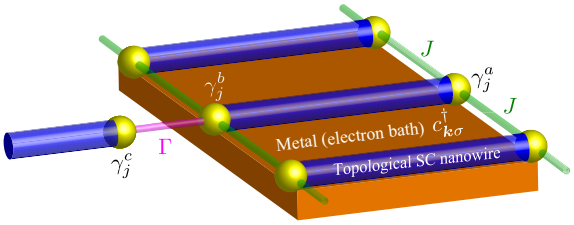

Figure 1: Schematics of Yang-Lee anyon system with Majorana quasiparticles.

References

[1] Y. Tanaka, T. Sanno, T. Mizushima, and S. Fujimoto: submitted.

[2] T. Sanno, M. G. Yamada, T. Mizushima, and S. Fujimoto: submitted.

Extension of susceptibilities, screened exchange and spin-fluctuation integrals into ultrasoft pseudopotentials

Mitsuaki KAWAMURA
Institute for Solid State Physics, University of Tokyo
Kashiwa-no-ha, Kashiwa, Chiba 277-8581

In the Eliashberg theory or density functional theory for superconductors (SCDFT) [1], where the electron-phonon, screened Coulomb, spin-fluctuation mediated interactions are included non-empilically, we need to compute the folowing product of two Kohn-Sham orbitals

$$\rho_{n\mathbf{k}n'\mathbf{k}'}(\mathbf{r}) = \varphi^*_{n\mathbf{k}}(\mathbf{r})\varphi_{n'\mathbf{k}'}(\mathbf{r}), \tag{1}$$

where n (n') and $\mathbf{k}$ ($\mathbf{k}'$) are the band index and Bloch wavenumber, respectively. To perform this product together with the ultrasoft pseudopotentials (USPP) or projector augumented waves (PAW) that are widely used because of the good accuracy and reasonable numerical costs [2], we need a correction term for the norm-conservation. Such a correction is originally proposed for the calculation of the susceptibility [3] as

$$\Delta\rho_{n\mathbf{k}n'\mathbf{k}'}(\mathbf{r}) = \sum_{\tau ii'} \langle\varphi_{n\mathbf{k}}|\beta_{\tau i'}\rangle\langle\beta_{\tau i}|\varphi_{n'\mathbf{k}'}\rangle Q_{\tau ii'}(\mathbf{r}), \tag{2}$$

where $\beta_{\tau i}$ is the projector dual to the atomic pseudo orbital $\psi^{PS}_{\tau i}$ at atom τ and orbital i, and the augumentation charge $Q_{\tau ii'}(\mathbf{r})$ is computed from the pseudo (PS) and all-electron (AE) atomic orbitals as follows:

$$Q_{\tau ii'}(\mathbf{r}) \equiv \psi^{AE*}_{\tau i}(\mathbf{r})\psi^{AE}_{\tau i'}(\mathbf{r}) - \psi^{PS*}_{\tau i}(\mathbf{r})\psi^{PS}_{\tau i'}(\mathbf{r}). \tag{3}$$

To utilise this correction to the calculation of the spin-fluctuation mediated interaction,

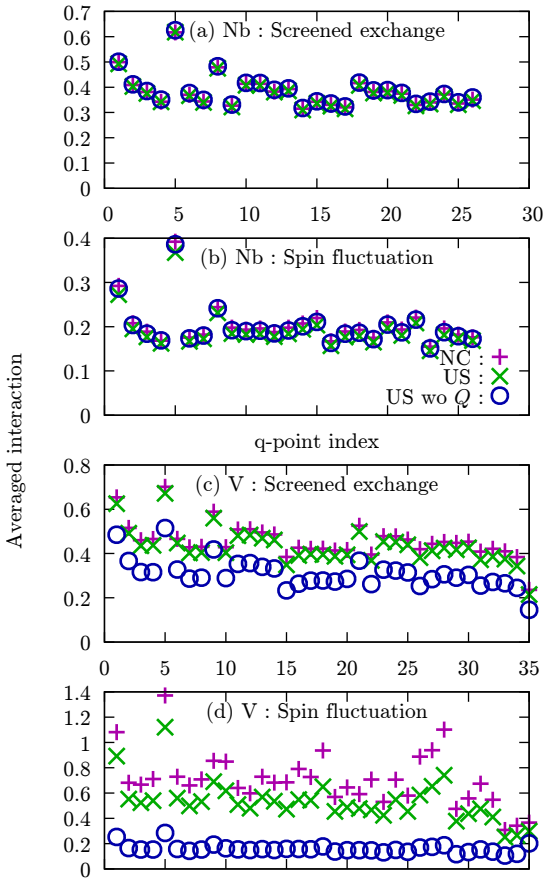

Figure 1: Spin-fluctuation mediated- (a, c) and screened exchange- (b, d) interactions averaged over the Fermi surface of Nb (a, b) and V (c, d). "+", "×", and "○" idicate results with norm-conserving (NC) ultrasoft (US) with and without augumentation charge $Q(\mathbf{r})$, respectivelly.

we implemented this formalism into our first-principles program package Superconducting-Toolkit [4] which is based on SCDFT.

Figure 1 shows the screened exchange and spin-fluctuation interactions averaged over the Fermi surface of Nb and V. In Nb, the effect of the augmentation charges Q is small because the USPP for this atom is almost norm-conserving. At the same time, V has a significant contribution from Q due to the nodeless 3d orbitals. In Fig. 1(d), we can see a deviation between the result by NC and US pseudopotential even if we include the correction. This deviation may be because the exchange-correlation kernel included in the spin-fluctuation is sensitive to the charge density in the vicinity of atoms.

We also performed the benchmark of the calculation of T_c for 15 materials, namely Al, V, Ta, In, Zn, Cd, Sn, ZrN, TaC, MgB_2, H_3S (at a pressure of 200 GPa), CaC_6, YNi_2B_2C, and V_3Si. Figure 2 shows the experimental, and calculated T_c; we performed four kind of calculations by changing superconducting density functional, namely the conventional plasmon-assisted [5], Sanna's Eliashberg-mimic (Sanna) [6], Sanna+Coulomb renormalization ($Z_\mathbf{C}$) [7], and Sanna + $Z_\mathbf{C}$ + Spin-fluctuation [9, 8] functional.

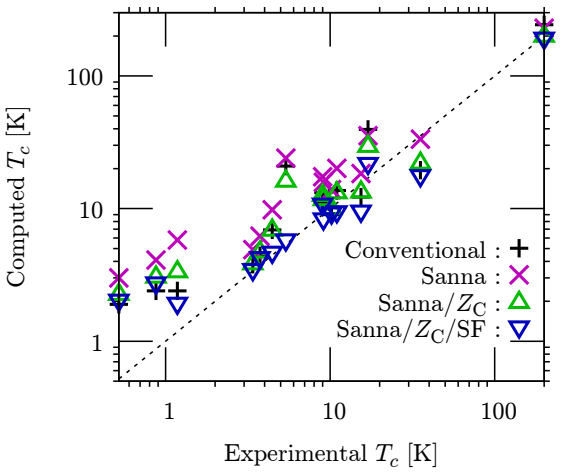

Figure 2: Computed- and experimental T_c. "+", "×", "△", and "▽" indicate result with conventional plasmon-assisted [5], Sanna's Eliashberg-mimic (Sanna) [6], Sanna+Coulomb renormalization ($Z_\mathbf{C}$) [7], and Sanna + $Z_\mathbf{C}$ + Spin-fluctuation [9, 8] functional, respectively.

References

[1] M. Lüders, M. A. L. Marques, N. N. Lathiotakis, A. Floris, G. Profeta, L. Fast, A. Continenza, S. Massidda, and E. K. U. Gross Phys. Rev. B **72**, 024545 (2005).

[2] G. Prandini, A. Marrazzo, I. E. Castelli, N. Mounet and N. Marzari: npj Computational Materials **4**, 72 (2018). https://materialscloud.org/sssp

[3] M. Gajdoš, K. Hummer, G. Kresse, J. Furthmüller and F. Bechstedt: Phys. Rev. B **73**, 045112 (2006).

[4] M. Kawamura, Y. Hizume, and T. Ozaki: Phys. Rev. B **101**, 134511 (2020). https://sctk.osdn.jp/index.html

[5] R. Akashi and R. Arita Phys. Rev. Lett. **111**, 057006 (2013).

[6] A. Sanna, C. Pellegrini, and E. K. U. Gross Phys. Rev. Lett. **125**, 057001 (2020).

[7] A. Davydov, A. Sanna, C. Pellegrini, J. K. Dewhurst, S. Sharma, and E. K. U. Gross Phys. Rev. B **102**, 214508 (2020).

[8] K. Tsutsumi, Y. Hizume, M. Kawamura, R. Akashi, and S. Tsuneyuki Phys. Rev. B **102**, 214515 (2020).

[9] F. Essenberger, A. Sanna, A. Linscheid, F. Tandetzky, G. Profeta, P. Cudazzo, and E. K. U. Gross Phys. Rev. B **90**, 214504 (2014).

Development of Algorithms for Ising Machines Based on Statistical Mechanics

Shu TANAKA
Department of Applied Physics and Physico-Informatics, Keio University
Hiyoshi, Yokohama, Kanagawa, 223-8522

Ising machines are a promising computational technique for highly efficient combinatorial optimization problems. Simulated annealing and quantum annealing are known as the internal algorithms of Ising machines, and a thorough investigation of the statistical dynamic properties of the Ising model is expected to improve the performance of Ising machines. In addition, investigating new ways of utilizing Ising machines is also an essential topic in the field of Ising machines. In this research project, we concentrated on the following two points.

(I) Dynamical properties of one-dimensional random Ising model with random transverse field [1]

Quantum annealing is a method of introducing an Ising Hamiltonian and Hamiltonian expressing noncommutative quantum fluctuations. We wish to search the ground state, and by varying the coefficients of each Hamiltonian with time, we eventually find the ground state of the Ising Hamiltonian. One of the factors that deteriorate the computational performance of quantum annealing is the reduction of the energy gap. The study of quantum phase transitions, where the energy gap systematically decreases with system size, is a common strategy for understanding the performance of quantum annealing from the perspective of statistical mechanics.

We considered an Ising model with random interactions defined as a one-dimensional chain. We investigate the system size dependence of the energy gap and the behavior of the dynamical critical exponent when a transverse magnetic field with randomness uncorrelated with the randomness of the interaction is applied and when a transverse magnetic field with randomness correlated with the randomness of the interaction is applied. As a result, it was found that there is a difference between the two cases.

(II) Black-box continuous optimization using Ising machines [2]

An Ising machine is a hardware that takes an Ising model or equivalent QUBO representation as input format and operates to search its ground state. Ising machines have been applied in various situations to combinatorial optimization problems that Ising models or QUBOs can represent. On the other hand, a method for utilizing Ising machines for black-box discrete optimization, i.e., discrete optimization problems for which the objective function is not explicitly given, was proposed by us in 2020 [3]. We extended it and proposed a method to perform black-box continuous optimization with Ising machines.

References

[1] T. Shirai and S. Tanaka: Ann. Phys. **435** (2021) 168483

[2] S. Izawa, K. Kitai, S. Tanaka, R. Tamura, and K. Tsuda: Phys. Rev. Res. **4** (2022) 023062.

[3] K. Kitai, J. Guo, S. Ju, S. Tanaka, K. Tsuda, J. Shiomi, and R. Tamura: Phys. Rev. Res. **2** (2020) 013319.

Numerical Study of One Dimensional Frustrated Quantum Spin Systems

Kazuo HIDA
Professor Emeritus, Division of Material Science,
Graduate School of Science and Engineering,
Saitama University, Saitama, Saitama 338-8570

We investigate the ground-state phases of mixed diamond chains with bond alternation described by the following Hamiltonian : [1]

$$\mathcal{H} = \sum_{l=1}^{L} \Big[(1+\delta)\boldsymbol{S}_l(\boldsymbol{\tau}_l^{(1)} + \boldsymbol{\tau}_l^{(2)}) + (1-\delta)(\boldsymbol{\tau}_l^{(1)} + \boldsymbol{\tau}_l^{(2)})\boldsymbol{S}_{l+1} + \lambda \boldsymbol{\tau}_l^{(1)}\boldsymbol{\tau}_l^{(2)} \Big], \quad (1)$$

where $\boldsymbol{S}_l, \boldsymbol{\tau}_l^{(1)}$ and $\boldsymbol{\tau}_l^{(2)}$ are spin operators with magnitudes $S_l = \tau_l^{(1)} = 1/2$ and $\tau_l^{(2)} = 1$. The number of unit cells is denoted by L, and the total number of sites is $3L$. Here, the parameters λ and δ control the frustration and bond alternation, respectively, as depicted in Fig. 1.

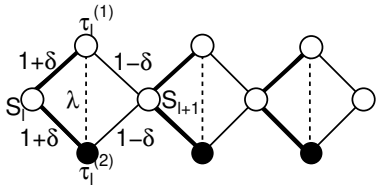

Figure 1: Structure of the diamond chain investigated in this work.

Defining the composite spin operators $\boldsymbol{T}_l$ as $\boldsymbol{T}_l \equiv \boldsymbol{\tau}_l^{(1)} + \boldsymbol{\tau}_l^{(2)}$, it is evident that $\forall l\ [\boldsymbol{T}_l^2, \mathcal{H}] = 0$. Thus, we have L good quantum numbers $\boldsymbol{T}_l^2 \equiv (T_l+1)T_l$ where $T_l = 1/2$ and $3/2$. The total Hilbert space of the Hamiltonian (1) consists of separated subspaces, each of which is specified by a definite set $\{T_l\}$.

For large λ, $\forall l\ T_l = 1/2$. Hence, for $\delta \neq 0$, the ground state is equivalent to that of the spin 1/2 chain with bond alternation δ. Therefore, the ground state is a gapped spin liquid.

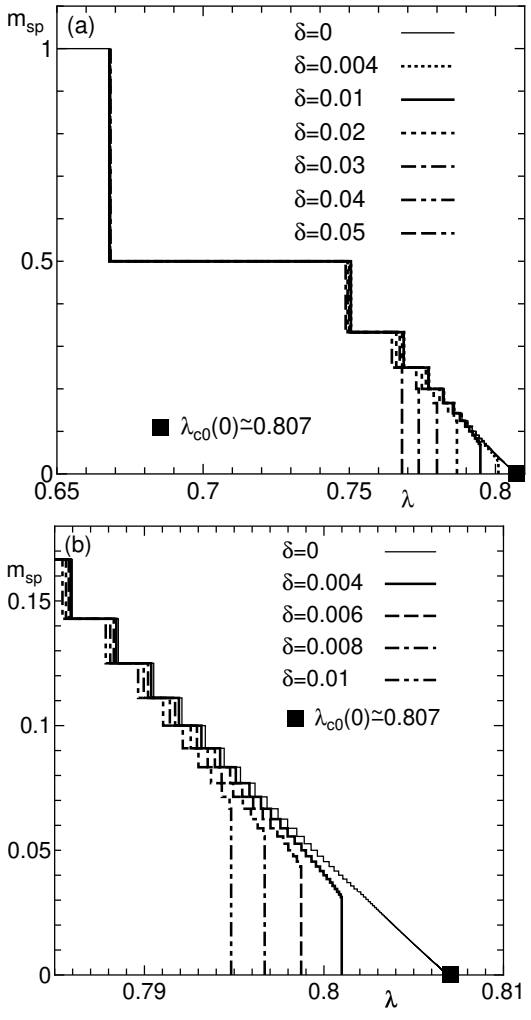

Figure 2: (a) λ-dependence of $m_{\rm sp}$ calculated by the infinite-size DMRG method. (b) Magnified figure around $\lambda \sim \lambda_{\rm c0}(0)$.

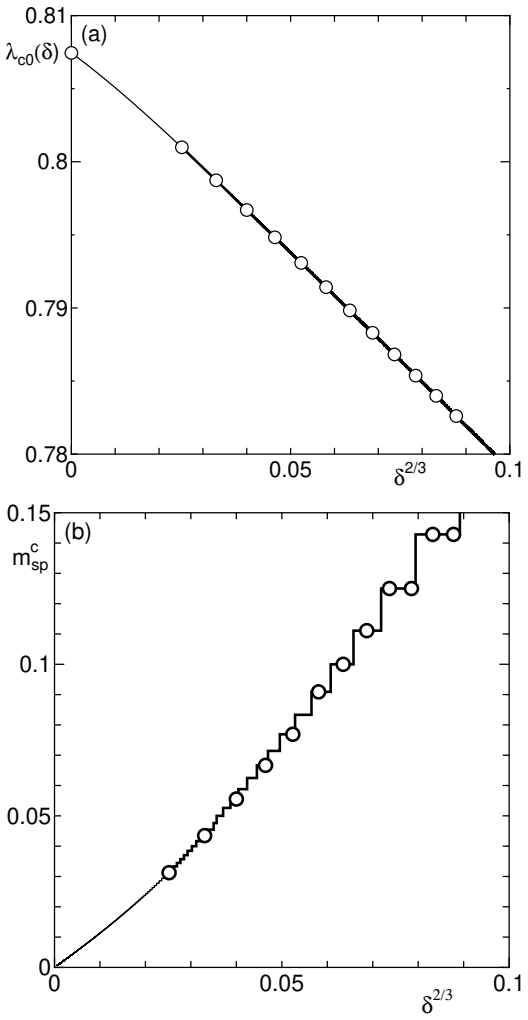

Figure 3: δ-dependence of (a) $\lambda_{\rm c0}(\delta)$ and (b) $m^{\rm c}_{\rm sp}$.plotted against $\delta^{2/3}$.

This energy gap vanishes for $\delta = 0$. For small λ, $\forall l$ $T_l = 3/2$. Hence, the ground state is equivalent to that of the spin 1/2-3/2 alternating chain. Therefore, the ground state is a ferrimagnetic phase with a spontaneous magnetization $m_{\rm sp} = 1$ per unit cell. Between these two phases, we carry out the infinite-size DMRG calculations for various configurations of $\{T_l\}$ to obtain the ground-state energy per unit cell. As a result, we find that the ground state undergoes a transition at $\lambda = \lambda_{\rm c0}(\delta)$ to a series of ferrimagnetic phases with $m_{\rm sp} = 1/p$ where p takes positive integer values. This transition is a first-order transition for $\delta \neq 0$ with a discontinuous change $m^{\rm c}_{\rm sp}$ in $m_{\rm sp}$, while no discontinuity is found for $\delta = 0$.[2]

The critical behaviors of $m^{\rm c}_{\rm sp}$ and $\lambda_{\rm c0}(\delta)$ around the critical point $(\delta, \lambda) = (0, \lambda_{\rm c0}(0))$ turned out to be

$$m^{\rm c}_{\rm sp} \propto \delta^{2/3}, \tag{2}$$

$$\lambda_{\rm c0}(\delta) - \lambda_{\rm c0}(0) \propto \delta^{2/3}. \tag{3}$$

These relations are also explained analytically.[1]

References

[1] K. Hida, J. Phys. Soc. Jpn. **91**, 024706 (2022).

[2] K. Hida, J. Phys. Soc. Jpn. **90**, 054701 (2021).

Quantum simulation using Ising models

Yuya SEKI

Graduate School of Science and Technology, Keio University, Kanagawa 223-8522

We have studied properties of factorization machine with annealing (FMA) [1] for quantum simulations. The FMA method approximates the Hamiltonian of the target system with Ising model through a machine learning model called factorization machine (FM) [2]. Instead of finding the low-energy states of the target system that is hard to analysis, we investigate low-energy states of the approximated Ising spin system. In FMA procedure, we use Monte Carlo methods to generate low-energy samples from the trained FM. In addition, the training process of FM includes the backpropagation method for updating the model parameters in FM, which requires a linear algebra library for calculation. These calculations were performed using multithreading to reduce the execution time. FMA includes various hyperparameters that should be optimized to achieve high accuracy solutions. To search for optimal hyperparameters efficiently, we performed the calculation in parallel by changing the parameters.

This year we developed a new method that combines FMA with integer-encoding methods. The developed method enables us to calculate the ground state of quantum systems approximately. As a benchmark problem, we consider the problem of finding the ground state of the hydrogen molecule, whose Hamiltonian consists of fermions. In this project, we used three encoding methods: binary encoding, one-hot encoding, and domain-wall encoding. To investigate performance for each encoding method, we calculate the distribution of the accuracy of solution of the developed method by running the developed method repeatedly. As a result, we obtained the optimal region of parameters where the developed method provides a solution that is close to the true ground state with a high probability for each encoding method. Adjusting the parameters, we obtain the ground-state of the hydrogen molecule where relative energy error is less than 10^{-5}. Also, we determined the proper encoding method from the obtained data. Among the encoding methods, one-hot encoding shows better performance than the others. This result indicates that the sparsity of data expression determines the performance of FMA.

References

[1] K. Kitai *et al.*: Phys. Rev. Research **2** (2020) 013319.

[2] S. Rendle: 2010 IEEE Int. Conf. Data Min. (2010) 995.

Large-scale molecular-dynamics simulation of silica melt and glass under high pressure with ANN potentials by active learning

Daisuke WAKABAYASHI

Photon Factory, Institute of Materials Structure Science,

High Energy Accelerator Research Organization (KEK), Tsukuba 305-0801

Silica is well known as an archetypal oxide and the compression behavior of silica glass and melt has attracted considerable attention in various research fields of physical sciences. Due to the strong covalent bonding, the melting point is extremely high. It is difficult to perform experiments on silica melt under high pressure, and theoretical calculations are a powerful research tool.

In contrast to crystalline materials, non-crystalline materials do not have long-range order, and therefore, in order to obtain reliable information, it is necessary to perform theoretical calculations on a system as large as possible. There is a limit to the size of the system which can be calculated by ab-initio methods. In this study, we have fitted the potential with a machine-learning technique (ANN potential) on the basis of the results of ab-initio calculations, and have applied it for the calculations with an extended system. However, in our previous projects, it has been observed that the large-scale calculations of melt were difficult to stabilize and quickly diverged, making them impossible to continue. In this project, we tested a new method of efficiently obtaining required training data through active learning.

An active-learning method can be roughly divided into three stages. First, multiple ANN potentials are decided for the same set of training data and MD simulations are made with each potential. Second, ab-initio calculations are made for the atomic arrangement corresponding to the steps for which the calculation results in the first stage differ significantly among the potentials. Finally, the ab-initio results are added as new training data for the next potential fitting.

The test calculations were performed for the solidification process of silica melt under high pressure. The ANN potential was determined by the machine-learning method with the potential, force, and stress data obtained by ab-initio calculations for a temperature range of 300-5,000 K at 60 GPa with 144 atoms. Active learning was performed three times to search for the conditions under which calculations on silica melt do not diverge at 60 GPa and 4,000 K for a system expanded to about 30,000 atoms.

The number of data was originally 15,000 and about 2,000 were added for each active

learning. Although there was improvement in the differences in calculation results between ANN potentials and in the number of steps at which divergence occurred in the expanded system up to the second active learning, there was almost no improvement after the third learning. This may be due to the fact that the active learning process increases the likelihood of mixing training data of unrealistic atomic arrangements. It was found that active learning enables us to delay, if not completely prevent, divergence.

Theoretical study of thermoelectric properties in doped Fe_2VAl: A weak-coupling approach

Kazutaka NISHIGUCHI
Graduate School of System Informatics, Kobe University
Rokkodai-cho, Nada-ku, Kobe 657-8501

1 Heusler compound Fe_2VAl

Heusler compound Fe_2VAl is one of the promising thermoelectric materials, which exhibits large power factor $P = \sigma S^2$ with σ and S being the electrical conductivity and Seebeck coefficient, respectively, although the thermal the dimensionless figure of merit $ZT = \sigma S^2 T/\kappa$ is not so large yet reflecting its large thermal conductivity κ.

Recently, it is experimentally observed in doped Fe_2VAl (i.e., $Fe_2V_{0.9}Cr_{0.1}Al_{0.9}Si_{0.1}$ and $Fe_{2.2}V_{0.8}Al_{1-y}Si_y$) as a weekly ferromagnetic material that ferromagnetic fluctuations enhance the thermoelectric properties such as S and P around the Curie temperature ($T_c = 285$ K). [1] It is not only a desirable property for practical use in realistic (room) temperatures, but also a fundamental and intriguing quantum phenomena where quantum fluctuations and thermoelectric effects are entangled by electron correlations.

Motivated above, we have studied electronic properties of Fe_2VAl using first-principles calculations based on the density functional theory (DFT) within the generalized gradient approximation (GGA). We performed DFT calculations with the Perdew–Burke–Ernzerhof (PBE) exchange-correlation functional and the projector augmented wave (PAW) method using The Vienna Ab Initio Simulation Package (VASP) [2] and QUANTUM ESPRESSO package. [3] One could observe from the band structure and density of states (DOS) are shown in Figure 1 that the Fe and V d-orbitals around the Fermi level mainly contribute to the low-energy electronic structures.

We have also considered the dopant effects on the doped Fe_2VAl to investigate its magnetic properties: the Cr and Fe substitution for V and the Si substitution for Si were taken into account by the $(2 \times 2 \times 2)$ supercell calculations. We could observe that the Cr and Fe substitution for V induce the spin-polarized states and the magnetic moment arises at the Cr and Fe, respectively, while the electronic structure for the Si substitution for Si is still paramagnetic state.

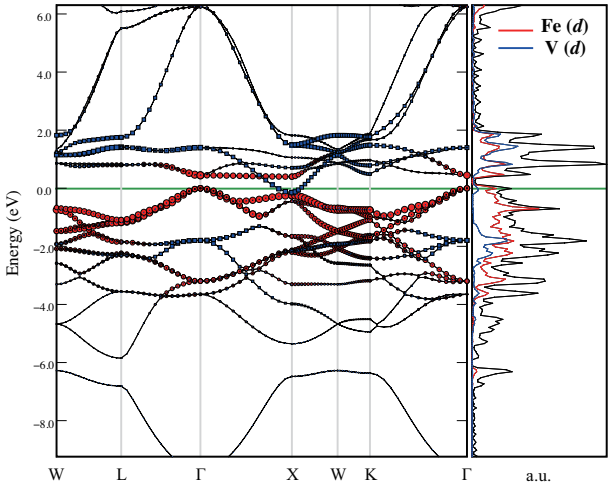

Figure 1: (Left) Band structure and (Right) DOS of Fe_2VAl. The energy is measured from the Fermi level. The components of Fe and V d-orbitals are projected (by red and blue), respectively.

Furthermore, we have constructed the first-principles effective model for Fe_2VAl using the maximally localized Wannier functions with Wannier90. [4] We here found that the effective model has to involve not only Fe and V d-orbitals mentioned above but also Al s- and p-orbitals in or-

der to reproduce the original band structure around the Fermi level since these orbitals highly entangle with each other and have large hybridization. Therefore, we adopted a 19-orbital effective model for Fe_2VAl: $5(Fe-d)\times 2+5(V-d)+4(Al-sp)$.

2 122 Zintl Phase Compound $CaZn_2X_2$ (X = As, P)

In order to search for high-performance thermoelectric materials, the possibility of n-type doping of $CaAl_2Si_2$-type Zintl phase compound $CaZn_2X_2$ (X = As, P) is explored using first-principles calculations based on DFT. [5] We consider n-type (electron carrier) doping of $CaZn_2X_2$ with the following two situations: interstitial-site doping of alkaline earth metals AE (= Mg, Ca, Sr, Ba) and group 3 elements G3 (= Sc, Y, La), and G3 substitutional doping for the Ca site.

To see this, the defect formation energy of these charged states is evaluated within GGA using the supercell approach. Among the considered possibilities, the interstitial-site doping of AE = Ca, Mg or G3 = Sc, Y, and the G3 = La, Y substitutional doping for the Ca have been found to have relatively small formation energies. In particular, the formation energy of the La substitutional doping is found to be negative for both $CaZn_2As_2$ and $CaZn_2P_2$ (Figure 2). This suggests that La can substitute the Ca site spontaneously and hence provide electron carriers, as far as these calculation results are concerned. We have also found that the formation energies of the defects are smaller for $CaZn_2As_2$ than for $CaZn_2P_2$, which suggests that n-type doping is relatively easier for the former than for the latter.

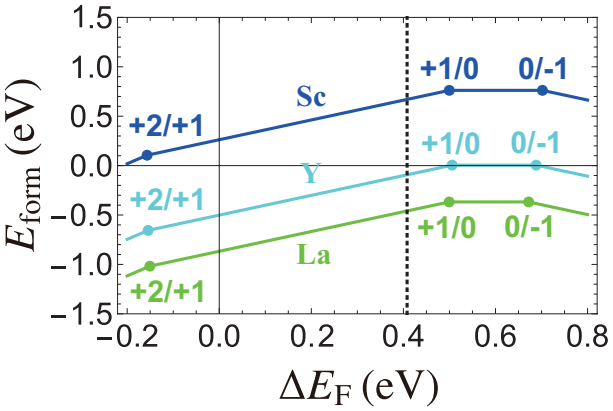

Figure 2: The formation energy of the G3 substitutional doping for the Ca site $E_{\rm form}$ against the Fermi energy $\Delta E_{\rm F} = E_{\rm F} - E_{\rm V}$ for $CaZn_2As_2$. The group 3 elements G3 (= Sc, Y, La) are chosen as dopant D. The dotted line denotes the position of the conduction band minimum ($E_{\rm F}$ = 0.408 eV).

References

[1] N. Tsujii, A. Nishide, J. Hayakawa, and T. Mori: Sci. Adv. **5** (2019) eaat5935.

[2] G. Kresse *et. al.*: Phys. Rev. B **47** (1993) 558; Phys. Rev. B **49** (1994) 14251; Computational Materials Science **6** (1996) 15; Phys. Rev. B **54** (1996) 11169.

[3] P. Giannozzi *et. al.*: J. Phys.: Condens. Matter **21** (2009) 395502; J. Phys.: Condens. Matter **29** (2017) 465901; J. Chem. Phys. **152** (2020) 154105.

[4] I. Souza, N. Marzari, and D. Vanderbilt: Phys. Rev. B **65** (2001) 035109; A. A. Mostofi *et. al.*: Comput. Phys. Commun. **178** (2008) 685; A. A. Mostofi *et. al.*: Comput. Phys. Commun. **185** (2014) 2309; G. Pizzi *et. al.*: J. Phys.: Condens. Matter **32** (2020) 165902.

[5] K. Nishiguchi, M. Ochi, C. H. Lee, and K. Kuroki: J. Phys. Soc. Jpn. (to be published).

Spontaneous formation of multiple-Q orders in inversion-symmetric Hubbard Models

Takashi UCHIDA
Hokkaido University of Science
4-1, 7-15, Maeda, Teine-ku, Sapporo 006-8585

In the last decade, multiple-Q orders in magnetic systems have attracted attention because they sometimes reveal topologically protected magnetic structures such as magnetic skyrmions. Typically, these structures are realized in the Dzyaloshinskii-Moriya (DM) interaction driven systems under magnetic field. The multiple-Q orders can also be realized in inversion-symmetric systems where the DM interaction is absent [1, 2]. In the present work, we have attempted to explore theoretically the possibility of multiple-Q orders in the inversion-symmetric systems in the absence of external magnetic field. For this purpose, we have applied the molecular spin dynamics (MSD) method [3] to the triangular-lattice single-band Hubbard model.

The MSD method is based on the functional integral method for the spin fluctuation theories and the isothermal molecular dynamics method. The method allows us to find automatically the magnetic structure of a large system with thousands of atoms in a unit cell at finite temperatures. Starting from the Hamiltonian expressed in terms of the locally rotated coordinates and by adopting the static approximation to the functional integral technique, the MSD method reduces to the generalized Hartree-Fock approximation at the ground state.

In the numerical calculations the most time-consuming process is the magnetic force calculation at each time step, where the local electronic structures are calculated in real space by means of the recursion method. We have adopted the automatic parallel calculation scheme and found it effective in saving both computing time and CPU resources.

We have performed magnetic structure calculations on a hexagonal supercell with 972 lattice points, which is embedded in a large cluster consisting of 6 such supercells, each of which are connected by the periodic boundary condition. Under zero magnetic field and the fixed value of the temperature $T/t = 0.0005$, we have explored the magnetic structures changing the Coulomb interaction strength U/t ($U/t = 3.0 \sim 8.0$) and the electron number n ($n = 1.10 \sim 1.60$) along the antiferromagnetic-ferromagnetic boundary. We have found that for $U/t \sim 3.5$ and $n = 1.48 \sim 1.53$ the dominant state is 3Q-structure with $\boldsymbol{Q}_1 = (0.3889, -0.2245)2\pi/a$, $\boldsymbol{Q}_2 = (0.3889, 0.2245)2\pi/a$, and $\boldsymbol{Q}_3 = (0.0, 0.4491)2\pi/a$ (with a being the lattice constant), which is superimposed with satellite 3Q structures with the Q vectors pointing in the same direction (in the direction of three axes of the triangular lattice).

References

[1] T. Okubo, S. Chung, and H. Kawamura: Phys. Rev. Lett. **108** (2012) 017206

[2] Y. Kakehashi: J. Phys. Soc. Jpn. **89** (2020) 094710.

[3] Y. Kakehashi, S. Akbar, and N. Kimura: Phys. Rev. B**57** (1998) 8354.

Molecular Dynamics Simulations of Reversibly Cross-linked Rubbers

Yusuke Yasuda

Research Center for Computational Design of Advanced Functional Materials.

National Institute for Advanced Industrial Science and Technology, Ibaraki 305-8568.

Reversibly cross-linked rubbers, whose cross-links are made of reversible bonds, such as hydrogen bonds, ionic bonds, and dynamic covalent bonds, have self-healing property and toughness. Though many researchers have studied those materials, the molecular mechanisms of these properties are still unclear due to the difficulty of the observations of molecular dynamics. To understand those materials, it is needed to study the relationship between structure, dynamics, and properties of these rubbers from several research methods.

In this work, we constructed coarse-grained model for reversibly cross-linked rubbers based on Kremer-Grest model [1], by introducing associating and dissociating condition (Fig.(a)) changing bond dissociation energy and bond potential shape. Calculation was conducted using molecular dynamics simulation software packages OCTA and LAMMPS on ISSP Supercomputer System. From equilibrium simulation, we found that association constants and bond lifetime are controlled by bond dissociation energy and bond potential shape. Mechanical simulation was conducted via loading-unloading test conducted in the range of elongation ratio λ= 1 – 4. From loading-unloading simulation, stress-extension rate curve shows stress retardation and specific hysteresis (Mullins effect, Fig.(b)) which is observed experimentally in reversibly cross-linked elastomer. We also found that the dynamic bonds dissociate by elongation, and that dissociation synchronizes to stress retardation. Self-healing test was conducted via equilibrium calculation at high temperature after loading and unloading. In the elongation after equilibrium, stress recovered completely, and our model can reproduce the feature of self-healing. (Fig.(b)) From these results, we have succeeded in constructing coarse-grained model of reversibly cross-linked rubbers.

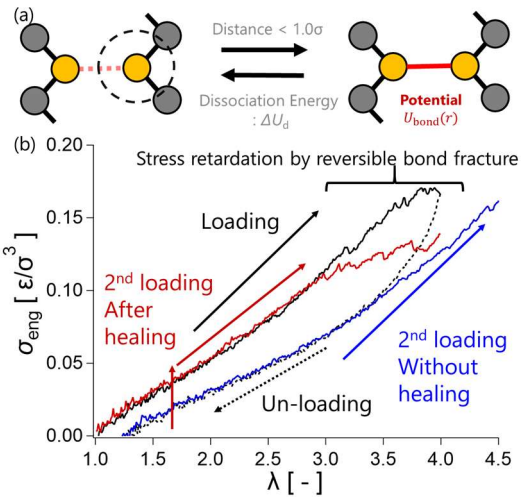

Fig. (a) The schematic illustration of coarse-grained dynamic bonds, (b) loading-unloading curves of the model.

References [1] K, Kremer, G. S. Grest; J. Chem. Phys., **92**, (1990) 5057.

Acknowledgement This work is partially supported by a project JPNP18016, commissioned by the New Energy and Industrial Technology Development Organization(NEDO).

Development of integrated interface of eigensolvers Rokko and application to quantum spin systems

Tatsuya Sakashita
Center for Quantum Information and Quantum Biology, Osaka University
1-2 Machikaneyamachō, Toyonaka, Osaka 560-0043

To establish universal exact diagonalization package for quantum lattice models including the Heisenberg-Kitaev model, we focused on developing integrated interfaces for eigensolvers, "Rokko"[1].

In Rokko, we implemented the integrated interfaces for the following types:

- Serial solvers for dense matrices (Eigen3, LAPACK)
- MPI parallelized solvers for dense matrices (EigenExa[2], ELPA[3], Elemental[4], ScaLAPACK)
- MPI parallelized solvers for sparse matrices (Anasazi in Trilinos[5], SLEPc[6]) to cover matrix representations below:
  - CRS (Compressed Row Storage)
  - Matrix-free method (the method to give matrix-vector product routines to solvers)

Rokko has the following features:

- Integrated interfaces for eigensolvers and matrices, independent of individual eigensolver libraries
- Rokko's interfaces are implemented by utilizing factory. It enables the user to dynamically select a solver.
- C, Fortran, and Python bindings of Rokko
- Automatically detecting libraries by using CMake in building Rokko
- Unit and integrated test programs by GoogleTest
- Install scripts of eigensolvers for various architectures

We prepare a paper to report design policy, software structure, and usage examples of Rokko.

References

[1] T. Sakashita, R. Igarashi, Y. Motoyama, T. Okubo, and S. Todo. Repository of Rokko. `https://github.com/t-sakashita/rokko.git`, 2012.

[2] T. Imamura, T. Hirota, and T. Fukaya. EigenExa web page. `https://www.r-ccs.riken.jp/labs/lpnctrt/projects/eigenexa/`, 2021.

[3] ELPA Consortium. ELPA (Eigenvalue soLvers for Petaflop Applications web page). `http://elpa.rzg.mpg.de`, 2013.

[4] J. Poulson. Distributed-memory dense linear algebra Elemental web page. `https://github.com/elemental/Elemental`, 2013.

[5] M. A. Heroux, R. A. Bartlett, and V. E. Howle. Trilinos Project web page. `https://trilinos.github.io`, 2003.

[6] V. Hernandez, J. E. Roman, and V. Vidal. SLEPc web page. `http://slepc.upv.es`, 2002.

Molecular dynamics analyses of ion migration at grain boundaries in solid state electrolyte

Ryo KOBAYASHI

Department of Applied Physics, Nagoya Institute of Technology,

Gokiso-cho, Showa-ku, Nagoya, Aichi 466-8555

All-solid-state battery (ASSB) is considered as a candidate of next generation Li-ion batteries because it uses a solid-state electrolyte instead of liquid-state electrolytes that are used in conventional Li-ion batteries. The key to achieve high-performance in ASSB is to reduce/control the resistivities at interfaces such as electrode/electrolyte interface and grain boundary (GB) inside electrolyte. For this purpose, we need deeper understandings about the atomic structure and precise mechanisms of ion migration of the GBs, and the goal of this project is to obtain new insights about them by using large-scale molecular dynamics (MD) simulation.

In order to obtain atomistic insights on Li-ion migration mechanism at GBs, we performed non-equilibrium MD simulation of large-scale poly-crystalline Li2Zr(PO4)3 (LZP) system containing half a million atoms and extracted local ion flux information around GBs. From the simulation and local ion-flux analyses[1], we showed that, in poly-crystalline materials, the ions migrate towards the lower reaches of grain and go through spots at GBs, and the high-flux spots contain migration paths as low energy as the bulk ones.

In this study, we have developed a new technique to obtain local ion-flux information from non-equilibrium MD implemented in our own code, nap[2]. And several MD simulation runs and the local-ion flux analyses were performed on the ISSP supercomputers.

.

References

[1] R. Kobayashi, K. Nakano, M. Nakayama, Acta Materialia, 226 (2022) 117596.

[2] Nagoya Atomistic-simulation Package (nap) http://github.com/ryokbys/nap

Electronic structure in mismatched multilayer systems: evaluation and application of the modeling scheme

Toshikaze KARIYADO

International Center for Materials Nanoarchitectonics,

National Institute for Materials Science, Tsukuba, Ibaraki 305-0044

After the report of superconductivity in twisted bilayer graphene, artificially stacked two-dimensional (2D) materials with moiré pattern induced by some mismatches between the layers attracts much attention. Generically, the moiré pattern affects the electronic band structure, and can be used to realize unique band structures. Then, designing interesting band structures in artificially stacked systems is a current urgent topic to explore.

In this project, we have analyzed electronic structures of twisted bilayer GeSe, where the anisotropic band flattening is expected. Here, the anisotropic band flattening means that originally 2D band dispersion is squeezed into quasi 1D one in twisted bilayers. To analyze the band structure, we derived an effective model for twisted bilayer GeSe. There are multiple important quantities in the effective model such as the effective mass for each layer or the effective interlayer tunneling. We obtain these quantities making use of the first-principles calculations. Our analysis clarifies the relation between the crystal structure of GeSe and the anisotropy in the effective interlayer tunneling, which gives us an intuitive understanding of the physics behind the anisotropic band flattening.

The first-principles calculations have been done using Quantum Espresso package, which is adapted to the parallel computation and suitable to use the supercomputing resources efficiently.

Not only calculating electronic band structures itself, we also tried to extract some characteristic response tied to the unique band structure, focusing on the orbital magnetic susceptibility. For that, we first derived a new formula to calculate the orbital magnetic susceptibility, and numerically tested its validity using several types of toy models by our homemade program [2]. In order to access the low temperature regime, we need fine mesh in k-point sampling, where the parallelization by MPI is applied in our homemade program.

References

[1] M. Fujimoto and T. Kariyado: Phys. Rev. B **104** (2021) 125427.

[2] T. Kariyado, H. Matsuura, and M. Ogata: J. Phys. Soc. Jpn. **90** (2021) 124708.

Compact spin qubits using the common gate structure of fin field-effect transistors

Tetsufumi Tanamoto
Department of Information and Electronic Engineering, Teikyo University
Utsunomiya 320-8511, Japan.

By using the ISSP supercomputer, we numerically investigate a transport properies of the compact spin-qubit system embedded into the common multi-gate FinFET transistors [1], where all gates are electrically tied togther as the common gate. The quantum dots (QDs) as qubits are coupled with their nearest Fin conducting channels. The Hamiltonian of the QDs and the channel is given by the tunneling Hamiltonian:

$$
\begin{aligned}
H_0 = {} & E_2 d_{2s}^\dagger d_{2s} + E_4 d_{4s}^\dagger d_{4s} + \sum_{i=1,3,5}\sum_{k_i,s} E_{k_i} c_{k_i s}^\dagger c_{k_i s} \\
& + \sum_{k_1}[V_{k_1} c_{k_1 s}^\dagger d_{2s} + V_{k_1}^* d_{2s}^\dagger c_{k_1 s}] \\
& + \sum_{k_3}[V_{k_3} c_{k_3 s}^\dagger (d_{2s} + d_{4s}) + V_{k_3}^* (d_{2s}^\dagger + d_{4s}^\dagger) c_{k_3 s}] \\
& + \sum_{k_5}[V_{k_5} c_{k_5 s}^\dagger d_{4s} + V_{k_5}^* d_{4s}^\dagger c_{k_5 s}], \qquad (1)
\end{aligned}
$$

where the channels are numbered as 1, 3, and 5, and the two QDs are numbered as 2 and 4. d_{is} and $c_{k,s}$ are the annihilation operators of the QD i and the conducting electrons in the channel, respectively. The qubit states are detected by the channel currents. The conductance $g_{yy}(\omega)$ is calculated from the Kubo formula given by $g_{yy}(\omega) = -\frac{1}{i\omega}[\Phi^{\rm R}_{yy}(\omega) - \Phi^{\rm R}_{yy}(0)]$, $\Phi^{\rm R}_{yy}[t] = -\frac{i}{\hbar V}\theta(t)\langle J_y(t)J_y(0) - J_y(0)J_y(t)\rangle$. The current operator J_y^i of the ith channel is given by $J_y^i = (e\hbar/(m^*L))\sum_{k_i} k_i c_{k_i s}^\dagger c_{k_i s}$, where L is the channel length and the summation of k_i is carried out over the channel. The expression for $g_{yy}^{(3)}$ is

$$
g_{yy}^{(3)} = \frac{2e^2}{h} k_d \frac{4[\Delta^2 + \delta^2]^2}{[(\Delta^2 - 2s_{33}\Delta - \delta^2)^2 + 4\Delta^2\Gamma_3^2]^2}, \qquad (2)
$$

where $k_1 = 1$, $k_2 = \pi n_{e2} W^2$, $\Delta = (2E_{k_F} - E_{SL} - E_{SR} - s_{11} - s_{55})/2$, and $\delta = E_{SL} - E_{SR}$. n_{e2} is the number of the carriers per nm^2, and $s_{ij} \equiv \int |V_{\rm tun}(k_i)|^2/(E_{k_i} - E_{k_j})$ is the self-energy. $\Gamma_i \approx 2\pi|V_{\rm tun}(k_i)|^2\rho_F$ (ρ_F is the density of state at Fermi energy E_F, and $V_{\rm tun}$ is the overlap of wave functions between the channel and the QDs in the tunneling Hamiltonian).

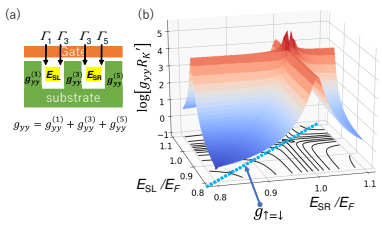

Figure 1: (a) Three current lines. (b)g_{yy} as functions of energy levels of two quantum dots.

Figure 1(b) shows the conductance g_{yy} of the summation of the three current lines $g_{yy}^{(i)}$ ($i \in 1, 3, 5$) as a function of the energy levels of the two QDs, where E_{SL} and E_{SR} are either $E_{S\downarrow}$ or $E_{S\uparrow}$. We can observe a double-peak structure around the Fermi energy where E_{SL} is close to E_{SR} but $E_{SL} \neq E_{SR}$. The symmetric case $\delta = 0$ gives the conventional resonant tunneling form $g = 4/[(\Delta - 2s_{33})^2 + 4\Gamma_3^2]^2$.

References

[1] T. Tanamoto and K. Ono, AIP Advances 11 (4), 045004 (2021).

Change in period of ordinary earthquakes due to the interaction with slow earthquakes

Takehito SUZUKI
Dept. Phys. Sci., Aoyama Gakuin University
5-10-1, Fuchinobe, Chuo-ku, Sagamihara, Kanagawa 252-5258

Two qualitatively different behaviors of earhtquakes have been known. One is the ordinary earthquake, which we feel naturally. The other one is slow earthquakes, which generate negligible seismic waves. Although the slow earthquakes are not disastrous, they are considered to sometimes change to the ordinary earthquakes after several repetitions. Whether this transition occurs or not is a fatal problem to the human society, and we should clarify the condition for the transition to occur.

The fault rocks can be considered as poroelastic media, including pores inside it. The pores are usually considered to be filled with water. If the dynamic earthquake slip (frictional slip) occurs, we can consider the interaction among heat, fluid pressure, and porosity [1, 2]. The slip is interpreted as the deformation around the contact area, called slip zone, which has a finite width. During the dynamic slip, the generation of pores [frictional heating] reduces [raises] the fluid pressure in the slip zone, inducing the increase [reduction] in the friction stress and the reduction [increase] in the slip velocity [1, 2]. Therefore, the slow and ordinary earthquakes are dominated by the generation of pores and the frictional heating, respectively.

The spring-block model and the interaction between three quantities are employed to analyze the slow-ordinary transition. The single block is assumed here. The upper substrate is drived with the constant speed V_p, and it also loads the block via a spring whose spring constant is k_p. As widely known, this system repeats the dynamic slip and cessation. The healing of pores in the cessation time is also taken into account. However, the choice of the healing law does not induce qualitative changes in the result below.

We neglect the heat and fluid diffusions during the dynamic slips. The governing equations for the fluid pressure, porosity, and temperature in the slip zone during the dynamic slip are given by

$$\dot{p} = C_1 \dot{T} - M_0 \dot{\phi}, \tag{1}$$

$$\dot{\phi} = \alpha_0 \dot{u} \left(1 - \frac{\phi}{\phi_\infty} \right), \tag{2}$$

$$\dot{T} = -C_2 (\sigma_n^0 + p) \dot{u}, \tag{3}$$

respectively, where C_1 and C_2 are positive constants. From here and below, quantities not explained are summarized in Ref. [2]. From Eq. (2), we obtain

$$\phi = \phi_\infty - (\phi_\infty - \phi_0) e^{-\alpha_0 u / \phi_\infty}, \tag{4}$$

where ϕ_0 is the porosity at the intant of the slip onset. Note that this value need not equal to the value at time $t = 0$. Additionally, from Eqs. (1)–(4), we obtain

$$\dot{p} = \left(-C_1 C_2 (\sigma_n^0 + p) - M_0 \left(1 - \frac{\phi_0}{\phi_\infty} \right) \alpha_0 e^{-\alpha_0 u / \phi_\infty} \right) \dot{u}, \tag{5}$$

where $\gamma = C_1 C_2 > 0$. From this representation, we can write p in terms of u to obtain

$$p = \left(\sigma_n^0 + p_0 - \frac{M_0' \alpha_0}{\frac{\alpha_0}{\phi_\infty} - \gamma} \right) e^{-\gamma u} + \frac{M_0' \alpha_0}{\frac{\alpha_0}{\phi_\infty} - \gamma} e^{-\alpha_0 u / \phi_\infty} - \sigma_n^0, \tag{6}$$

where $M_0' \equiv M_0(1-\phi_0/\phi_\infty)$ and p_0 is the fluid pressure at the instant of slip onset.

We now consider the energy conservation law. First, note that the loading stress from the upper substrate must be equal to the macroscopic static friction stress at the instant of the slip onset, which leads to

$$k_p V_p t_i = -\mu_{\rm stat}(\sigma_n^0 + p_0), \tag{7}$$

where t_i is the time when the slip initiated. Using Eq. (7), the energy stored in the upper spring just before the dynamic slip is given by

$$E_1 = \frac{1}{2}k_p(V_p t_i)^2 = \frac{1}{2}\frac{\mu_{\rm stat}^2}{k_p}(\sigma_n^0 + p_0)^2. \tag{8}$$

Moreover, the energy stored in the upper spring after the cessation is written as (we assume that the upper spring does not move during the dynamic slip)

$$\begin{aligned} E_2 &= \frac{1}{2}k_p(V_p t_i - u_f)^2 \\ &= \frac{1}{2}k_p\left(-\frac{\mu_{\rm stat}}{k_p}(\sigma_n^0 + p_0) - u_f\right)^2, \end{aligned} \tag{9}$$

where u_f is the final slip distance for the single slip. Furthermore, the work done to the block by the friction stress during the dynamic slip is obtained using Eq. (6):

$$\begin{aligned} E_{\rm fric} &= \int_0^{u_f}\Big(-\mu_{\rm slid}(\sigma_n^0 + p)\Big)\,du \\ &= -\mu_{\rm slid}\int_0^{u_f}\left[\left(\sigma_n^0 + p_0 - \frac{M_0\alpha_0}{\frac{\alpha_0}{\phi_\infty}-\gamma}\right)e^{-\gamma u} + \frac{M_0\alpha_0}{\frac{\alpha_0}{\phi_\infty}-\gamma}e^{-\alpha_0 u/\phi_\infty}\right]du \\ &= -\mu_{\rm slid}\left[\frac{1}{\gamma}\left(\sigma_n^0 + p_0 - \frac{M_0\alpha_0}{\frac{\alpha_0}{\phi_\infty}-\gamma}\right)(1-e^{-\gamma u_f}) + \frac{M_0\phi_\infty}{\frac{\alpha_0}{\phi_\infty}-\gamma}(1-e^{-\alpha_0 u_f/\phi_\infty})\right]. \end{aligned} \tag{10}$$

Therefore, from the energy conservation law, we found an equation which u_f must satisfy:

$$\begin{aligned} &\frac{1}{2}k_p u_f^2 + \mu_{\rm stat}(\sigma_n^0 + p_0)u_f \\ &-\mu_{\rm slid}\left[\frac{1}{\gamma}\left(\sigma_n^0 + p_0 - \frac{M_0'\alpha_0}{\frac{\alpha_0}{\phi_\infty}-\gamma}\right)(1-e^{-\gamma u_f}) + \frac{M_0'\phi_\infty}{\frac{\alpha_0}{\phi_\infty}-\gamma}(1-e^{-\alpha_0 u_f/\phi_\infty})\right] = 0. \end{aligned} \tag{11}$$

We define $F(u_f)$ as the left hand side of Eq. (11). The condition $F(u_f) = 0$ corresponds to the condition where the elastic energy change is equal to the energy loss due to the friction during the single slip. It is also important that $F(u_f)$ includes p_0 and ϕ_0. As mentioned, these initial values are not values at $t = 0$, but the values at the slip onset of each slip.

Notably, $F(u_f)$ is the double-well form, and the first well is much shallower than the second one. If $F(u_f) = 0$ has a solution between the wells, the slow earthquakes occur because we can consider that the slip is inhibited. On the other hand, if $F(u_f) = 0$ does not have a solution there, the solution jumps to almost two orders larger one. This behavior is interpreted as the first-order phase change. The slow-ordinary earthquake transition can be understood as the first-order phase change. Additionally, we can conclude that this phase change is governed by p_0 and ϕ_0.

The analytical result described here was confirmed by ISSP supercomputer. The numerical study can treat the BK model with several blocks, and we confirmed that the results here can give useful implications to such a several-block case. Detailed and comprehensive numerical treatments will be a potential future work.

References

[1] T. Suzuki, and T. Yamashita: J. Geophys. Res. **119** (2014)

[2] T. Suzuki: Phys. Rev. E **96** (2017)